particles

MDPI

Review

Forward & Far-Forward Heavy Hadrons with JETHAD: A High-Energy Viewpoint

Francesco Giovanni Celiberto

Departamento de Física y Matemáticas, Campus Universitario, Universidad de Alcalá (UAH), Alcalá de Henares, E-28805 Madrid, Spain; francesco.celiberto@uah.es

Abstract: Inspired by recent findings that semi-inclusive detections of heavy hadrons exhibit fair stabilization patterns in high-energy resummed distributions against (missing) higher-order corrections, we review and extend our studies on the hadroproduction of light and heavy hadrons tagged in forward and far-forward rapidity ranges. We analyze the NLL/NLO$^+$ behavior of rapidity rates and angular multiplicities via the JETHAD method, where the resummation of next-to-leading energy logarithms and beyond is consistently embodied in the collinear picture. We explore kinematic regions that are within LHC typical acceptances, as well as novel sectors accessible thanks the combined tagging of a far-forward light or heavy hadron at future Forward Physics Facilities and a of central particle at LHC experiments via a precise timing-coincidence setup.

Keywords: heavy flavor; QCD resummation; LHC phenomenology; forward physics facilities; hadron detections

1. Introduction

New paths in the exploration of fundamental interactions by next-generation colliders [1–32] mark the turn of a new era in particle physics. Venturing into uncharted kinematic territories permits stringent analyses of the Standard Model (SM) and direct or indirect quests for deviations from its predictions. The strong-interaction sector presents significant challenges within the SM. Here, the interplay between perturbative and nonperturbative aspects of Quantum ChromoDynamics (QCD) gives rise to unresolved puzzles regarding fundamental questions, including the origin of hadron mass and spin, as well as the behavior of QCD observables in critical kinematic regimes.

Precise examinations of the dynamics underlying strong interactions rely on two essential components. Firstly, the ability to perform increasingly accurate calculations of high-energy parton scatterings through higher-order perturbative QCD techniques. Secondly, the understanding of proton structure, dictated by the motion and spin interactions among constituent partons. A series of successes in describing data for hadron, lepton, and lepton-hadron reactions have been achieved through collinear factorization [33,34], where partonic cross sections, computed within pure perturbative QCD, are convoluted with collinear Parton Distribution Functions (PDFs).

These PDFs encode information about the likelihood of finding a parton inside the struck hadron with a specific longitudinal momentum fraction, x. They evolve according to the Dokshitzer–Gribov–Lipatov–Altarelli–Parisi (DGLAP) equation [35–39]. Collinear PDFs are well-suited for describing inclusive or semi-inclusive observables weakly sensitive to low-transverse momentum regimes. Similarly, collinear Fragmentation Functions (FFs) portray the production mechanism of identified hadrons, detailing the probability of generating a specific final-state hadron with momentum fraction z from an outgoing collinear parton with longitudinal fraction, $\zeta \equiv x/z$.

However, by relying on collinear PDFs only, one overlooks information about the transverse-space distribution and motion of partons. Thus, the description provided by

check for updates

Citation: Celiberto, F.G. Forward & Far-Forward Heavy Hadrons with JETHAD: A High-Energy Viewpoint. *Particles* **2024**, *7*, 502–542. https://doi.org/10.3390/particles7030029

Academic Editor: Armen Sedrakian

Received: 15 May 2024
Revised: 12 June 2024
Accepted: 14 June 2024
Published: 24 June 2024

Copyright: © 2024 by the authors. Licensee MDPI, Basel, Switzerland. This article is an open access article distributed under the terms and conditions of the Creative Commons Attribution (CC BY) license (https://creativecommons.org/licenses/by/4.0/).

collinear factorization can be seen as a one-dimensional mapping of hadron properties. Achieving an accurate portrayal of low-transverse-momentum observables necessitates embracing a three-dimensional perspective, which permits the capture of intrinsic effects stemming from the transverse motion and spin of partons, and their interaction with the polarization state of the parent hadron. Such a tomographic representation of hadrons is naturally provided by the Transverse-Momentum-Dependent (TMD) factorization (see Refs. [40,41] and reference therein).

Furthermore, given the nonperturbative nature of parton densities and fragmentation functions, they must be extracted from data through *global fits* encompassing various hadronic processes. Despite the significant successes of the collinear approach, certain kinematic regions demand a departure from the fixed-order, DGLAP-driven description. Enhanced logarithmic contributions, which enter the perturbative expansion of the strong running coupling α_s with increasingly higher powers, must be included to all orders to restore the convergence of the perturbative series. These logarithms, depending on the kinematic regimes, necessitate specific all-order *resummation* techniques.

For instance, accurately describing the differential distributions for inclusive hadron, boson, or Drell–Yan (DY) lepton production at low $|\vec{q}_T|$ demands employing Transverse-Momentum (TM) resummation techniques [42–49]. TM-resummed predictions have been recently extended to various reactions, including hadroproduction of photons [50–53], Higgs bosons [54], W-boson pairs [55], boson-jet [56,57], Z-photon systems [58], as well as DY and Higgs spectra [59–65]. Moreover, almost back-to-back final states lead to Sudakov-type logarithms, which should be resummed as well [66–70].

Conversely, when a physical observable is defined and/or measured close to its phase space edges, Sudakov effects originating from soft and collinear gluon emissions near *threshold* become significant and require appropriate resummation techniques. Various approaches exist in the literature for achieving threshold resummation for inclusive rates [71–89]. Recent studies have also addressed resummation for rapidity distributions [79–83,85,86].

The standard fixed-order description of cross sections has been enhanced by incorporating threshold resummation for numerous processes, including DY [90–97], scalar and pseudo-scalar Higgs production [90,92,94,96,98–111], bottom annihilation [96,112,113], Deep-Inelastic Scattering (DIS) [105,114–116], electron-positron Single-Inclusive Annihilation (SIA) [105], and spin-2 boson production [117,118]. Additionally, a combined TM-plus-threshold resummation for TM distributions of colorless final states has been developed [119].

From a partonic perspective, the threshold regime corresponds to the large-x limit. Prime determinations of large-x improved collinear PDFs were achieved in Ref. [120]. Additionally, as x approaches one, the impact of *target-mass* power corrections becomes significant. These corrections have been studied extensively in the literature [121–129], particularly in the context of large-x DIS events [130].

Another crucial kinematic regime, sensitive to logarithmic enhancements, is the *semi-hard* (or Regge–Gribov) sector [131–134], characterized by the scale hierarchy $\sqrt{s} \gg \{Q\} \ll \Lambda_{\rm QCD}$, with $\sqrt{s}$ being the center-of-mass energy, $\{Q\}$ one or a set of process-characteristic energy scales, and $\Lambda_{\rm QCD}$ the QCD hadronization scale. Here, large energy logarithms of the form $\ln(s/Q^2)$ compensate for the narrowness of α_s, potentially spoiling the perturbative-series convergence.

Like in previous cases, these logarithms must be resummed to all orders. The Balitsky–Fadin–Kuraev–Lipatov (BFKL) formalism is the most powerful tool for such resummations [135–139]. BFKL resummation accounts for contributions proportional to $\alpha_s^n \ln(s/Q^2)^n$ up to the Leading Logarithmic (LL) level, and terms proportional to $\alpha_s^{n+1} \ln(s/Q^2)^n$ at the Next-to-Leading Logarithmic (NLL) level.

In the BFKL framework, the imaginary part of amplitudes (and also cross sections of inclusive processes, via to the *optical theorem* [140]) takes the form of a high-energy factorization, where TM-dependent functions play a key role [141–143]. Specifically, the BFKL

amplitude is a convolution between two singly off-shell emission functions (also known in the BFKL jargon as forward-production *impact factors*), describing the transition from each parent particle to the outgoing objects in its fragmentation region, and a Green's function, which evolves according to the BFKL integral equation. The kernel of this equation has been computed with Next-to-Leading Order (NLO) accuracy for forward scatterings [144–150] and partially at next-to-NLO [151–156].

Conversely, emission functions are sensitive to the given final state. They are also $\{Q\}$-dependent, but s-independent. Thus, they represent the most intricate piece of a BFKL computation, and only few of them are currently known at NLO. We mention: (a) collinear-parton functions [157,158], which are needed to compute (b) forward-jet [159–164] and (c) light-hadron [165], (d) virtual photon to light vector meson [166], (e) light-by-light [167–172], and (f) forward-Higgs boson in the infinite top-mass limit [173,174] (see also Refs. [175,176]) emission functions. Considering the Leading Order (LO) only, one has DY pairs [177,178], heavy-quark pairs [179–181], and low-$|\vec{q}_T|$ J/ψ [182–185] impact factors.

A primary category of processes that act as probe channels for high-energy resummation involves single forward emissions. In these cases, the cross section for an inclusive process follows the typical BFKL-factorized structure. Specifically, when at least one hadron participates in the initial state, the impact factor governing the production of the forward identified particle is convoluted with the BFKL Green's function and a nonperturbative quantity known as the hadron impact factor. The sub-convolution of the last two components provides an operational definition of the BFKL Unintegrated Gluon Distribution (UGD).

The hadron impact factor serves as the initial-scale UGD, while the Green's function governs its low-x evolution. Given the forward kinematics, the struck parton is predominantly a gluon with a small longitudinal-momentum fraction. Hence, in this context, high-energy resummation effectively amounts to low-x resummation. A similar high-energy factorization formula applies to the imaginary part of the amplitude for exclusive single forward processes. This is feasible because, in the forward limit, skewness effects are suppressed, allowing for the use of the same UGD. In more general off-forward configurations, one would consider low-x enhanced GPDs [186–189].

An intriguing subset of inclusive forward reactions involves proton-initiated processes. Here, a hybrid high-energy and collinear factorization is employed, where the forward object originates from a fast parton with a moderate x, described by a collinear PDF, while the other proton is characterized by the UGD. Studies on the BFKL UGD trace back to the growing interest in forward physics at HERA. Investigations of DIS structure functions at low x were undertaken in Refs. [190,191].

Subsequently, different UGD models were scrutinized against HERA data for exclusive light vector-meson electroproduction in references [192–198]. Evidence of low-x dynamics is expected to emerge from ρ-meson studies at the Electron-Ion Collider (EIC) [199–203]. Similarly, insights are sought from the photoemission of quarkonium states [204–216]. Forward DY and single inclusive b-quark tags at the Large Hadron Collider (LHC) serve as hadronic probes for the UGD [178,217–220].

Besides single forward emissions, the low-x QCD sector can also be probed via gluon-induced single central productions. In these processes, the cross sections are formulated in a pure high-energy factorized form, involving a convolution between two BFKL UGDs and a central-production impact factor, embodying a doubly off-shell coefficient function. Due to its doubly off-shell nature (involving virtual gluons g^*g^*), with gluon virtualities determined by their transverse momenta, computing the coefficient function is considerably more intricate compared to the forward-case scenarios. To our knowledge, the coefficient function depicting the inclusive emission of a central, light-flavored jet is the only one known at NLO [221].

A very powerful formalism aimed at enhancing standard fixed-order computation of central processes via the low-x resummation is the Altarelli–Ball–Forte (ABF) scheme [222–228], where κ_T-factorization theorems [141–143,229,230] permits to combine DGLAP and BFKL

inputs. The high-energy series is stabilized by imposing consistency conditions based on duality aspects, symmetrizing the BFKL kernel in (anti-)collinear regions of the phase space, and encoding such contributions to the running coupling.

Significant progress has been achieved in small-x studies within the ABF formalism, particularly in the context of inclusive central emissions. Notable advancements include investigations into the inclusive central emissions of Higgs bosons in gluon-gluon fusion [231–234] and higher-order corrections to top-quark pair emissions [235]. Applications ABF to resummed inclusive or differential distributions for Higgs-boson and heavy-flavor hadroproductions were done by means of the High Energy Large Logarithms (HELL) method [84,236,237]. Moreover, this framework has been instrumental in extracting low-x enhanced collinear PDFs for the first time [238–240]. Subsequently, the information from these collinear PDFs was utilized to constrain the parameters of initial-scale unpolarized and helicity gluon TMD PDFs [241].

Another class of processes serving as promising channel whereby unveiling the onset of high-energy QCD dynamics, is represented by inclusive hadroproductions of two particles emitted with transverse momenta well above $\Lambda_{\rm QCD}$ and strongly separated in rapidity (high-energy effects were also seen in photon-initiated processes, such as the $(\gamma^*\gamma^*)$ reaction [242–244], the exclusive di-meson leptoproduction [245–247], and the semi-inclusive heavy-quark pair photodetection [179]). Contrarily to single forward and central processes, forward-plus-backward two-particle hadroproduction rates are sensitive to enhanced energy logarithms even at moderate values of x, due to the peculiar kinematic ranges in transverse momentum and rapidity currently covered by acceptances of LHC detectors.

Thus, on the one hand, a collinear treatment still holds here. On the other hand, however, high rapidity intervals (ΔY) correspond to large TM exchanges in the t-channel, leading to the emergence of energy logarithms. In such cases, a high-energy factorization treatment is needed, and it is inherently provided by the BFKL formalism. Consequently, another form of hybrid high-energy and collinear factorization is established [248–254] (see Refs. [255–261] for a close-in-spirit formalism), wherein high-energy resummed partonic cross sections are derived directly from BFKL and subsequently convoluted with collinear PDFs. This approach allows for a comprehensive description of processes occurring in kinematic regimes characterized by both large rapidity intervals and transverse momenta.

The "mother" reaction of forward-plus-backward inclusive hadroproductions is the Mueller–Navelet [262] tagging of two light jets at large momenta and ΔY, for which a series of phenomenological studies have appeared so far [69,162,248,263–277] and they have been compared with CMS data at $\sqrt{s} = 7$ TeV [278,279]. Exploring further observables that are sensitive to more exclusive final states offers additional avenues for uncovering clues about the onset of BFKL dynamics. These channels complement the insights provided by Mueller–Navelet channels and offer a deeper understanding of the underlying processes.

By studying such observables, we can gain a more comprehensive view of how BFKL dynamics manifest across various exclusive final states, thereby enriching our understanding of high-energy QCD phenomena. We can mention: light-flavored di-hadron [280–284], hadron-plus-jet [249,285–289], multi-jet [290–302] and Drell–Yan [303] angular distributions, Higgs-jet rapidity and transverse-momentum distributions [250,304–307], heavy-flavored jet [251,308] and hadron [179–182,253,309–320] distributions.

Analyses on angular correlations for light-jet and/or light-hadron detections have played a crucial role in distinguishing between high-energy resummed and fixed-order calculations. By employing asymmetric TM ranges, we have been able to decisively discriminate between these approaches, shedding light on the underlying dynamics of high-energy QCD processes [249,269,270]. However, these studies have also revealed significant challenges associated with higher-order BFKL corrections.

Specifically, NLL contributions have been found to be comparable in magnitude to LL terms but with opposite signs, leading to instability in the high-energy series. This sensitivity to the variations of renormalization (μ_R) and factorization (μ_F) scales, aimed

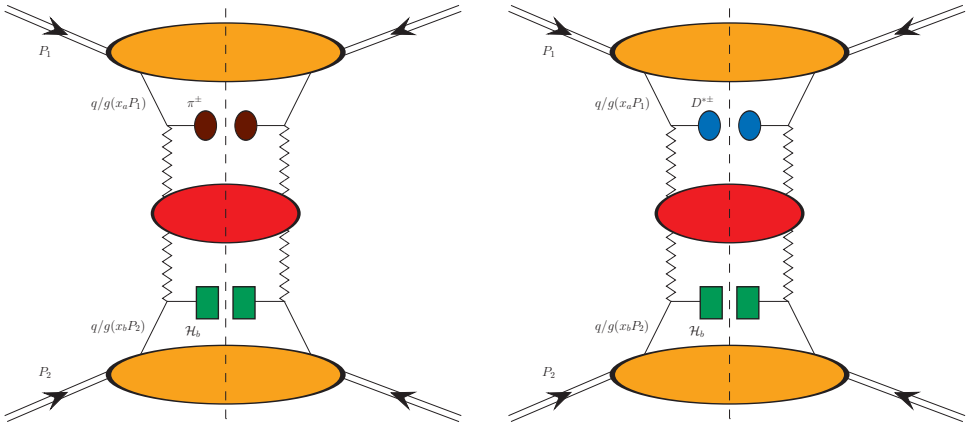
at gauging the size of Missing Higher-Order Uncertainties (MHOUs), poses a significant obstacle to achieving reliable theoretical predictions.

Efforts to address these challenges have included the adoption of scale-optimization methods such as the Brodsky–Lepage–Mackenzie (BLM) optimization [242,321–323] in its semi-hard oriented version [271]. While this approach has shown some success in partially mitigating instabilities in azimuthal correlations, it has proven ineffective for cross sections. In particular, the optimal scales obtained using this method have often been much larger than the natural scales dictated by kinematics [249], resulting in a substantial and unphysical reduction in statistical precision. As a result, achieving precision in the study of inclusive forward-backward light-flavored objects has remained elusive despite these efforts.

Recent studies have provided corroborating indication of a stabilization of the high-energy resummation under higher-order corrections and MHOUs studies, particularly in the context of semi-hard Higgs-boson inclusive emissions [134,250,324–330]. This stabilization trend has been observed also in analyses focusing on semi-inclusive emissions of Λ_c baryons [309] or singly bottomed hadrons at the LHC [310].

A key observation is a clear signature of stabilization, which is directly linked to the distinctive behavior exhibited by Variable-Flavor Number-Scheme (VFNS) [331–333] collinear FFs governing the production of these singly heavy-flavored particles at high transverse momentum. These findings mark a significant advancement in our understanding of high-energy QCD processes and offer promising prospects for future precision studies in this area. Subsequent analyses on vector quarkonia [253,254,334,335], B_c mesons [314,317], and $X_{Qq\bar{Q}\bar{q}}$ tetraquarks [318], confirmed that this remarkable feature, known as *natural stability* of the BFKL resummation [312], comes out as basic property connected to the inclusive emission of any given heavy-flavored particle.

In this review, we will provide predictions for rapidity-interval rates and angular distributions for a novel selection of forward-plus-backward two-particle semi-hard reactions. These processes involve final states characterized by identified hadrons only (see Figure 1). Specifically, the first hadron can be a charged pion or a charged D^* meson. The second hadron singly b-flavored particle, i.e., and inclusive state consisting of the sum of fragmentation channels to noncharmed B mesons and Λ_b^0 baryons.



(**a**) $\pi^{\pm} + \mathcal{H}_b$ (**b**) $D^{*\pm} + \mathcal{H}_b$

Figure 1. Diagrammatic representation of the hybrid factorization at work for the $\pi^{\pm} + \mathcal{H}_b$ (**a**, left) and $D^{*\pm} + \mathcal{H}_b$ (**b**, right) channels. The big yellow ovals denote collinear PDFs. Maroon (navy blue) blobs stand for $\pi^{\pm}$ ($D^{*\pm}$ meson collinear FFs, while green rectangles depict $\mathcal{H}_b$ hadron collinear FFs. The high-energy Green's function (red oval blob) is connected to singly off-shell coefficient functions by Reggeon zigzag lines.

Comparing predictions from the BFKL-driven approach with those from a high-energy fixed-order treatment will help gauge the impact of high-energy resummation on top of the DGLAP approach. To this end, a numerical tool for calculating NLO cross sections for the inclusive production of two identified hadrons widely separated in rapidity in proton collisions would be needed and crucial for a systematic high-energy versus DGLAP analysis. While the LO limit for such reactions can be extracted from higher-order works [336–341], it currently cannot be compared with calculations based on our hybrid factorization due to kinematic constraints. Two-particle LO computations without resummation typically result in a back-to-back final state, which is incompatible with the asymmetric windows for observed transverse momenta in our calculations.

Therefore, to assess the weight of the NLL resummation on top of the DGLAP approach, we will compare BFKL predictions with the corresponding ones obtained from a high-energy fixed-order treatment, firstly developed to address light-flavored di-jet [269,270] and hadron-plus-jet [249] studies. It builds upon truncating of the high-energy series up to the NLO level, so that we can reconstruct the high-energy signal of a pure NLO computation.

We will consider two different rapidity configurations. The first one is a standard LHC tagging, where both particles ($\pi^{\pm}$ or $D^{*\pm}$ and the b-hadron) are detected by a current LHC detector, say CMS or ATLAS. This selection provides symmetric rapidity windows for both particles, making it an ideal channel for further testing high-energy QCD dynamics, akin to previous investigations into two-particle semi-hard processes. In the second scenario, we consider the tag of the pion or the D meson in a far-forward rapidity range accessible at future Forward Physics Facilities (FPFs), while the bottomed hadron is simultaneously detected in the barrel of a current LHC detector. Our exploration fairly takes inspiration for a prospective FPF + ATLAS study [252,315] proposed in the context of the FPF program [1,2] (see Refs. [342–349] for related work).

The simultaneous tag of a far-forward object and a central one results in an asymmetric configuration between the longitudinal fractions x of the two struck partons. One parton has a large x, while the other assumes more moderate x values. Thus, a coincidence between the FPF and a LHC detector give us a faultless chance to unravel not only the high-energy dynamics arising from to the very large rapidity intervals accessed, but also the connection between BFKL and threshold resummations. This interplay can shed light on the dynamics of parton interactions in this kinematic regime, providing valuable insights into the underlying physics.

The impact of double BFKL-plus-threshold logarithms for central Higgs-bosons inclusive rates is small at ongoing LHC energies, but it becomes quite relevant at the nominal ones of the Future Circular Collider (FCC) [28–32]. On the other side, the high-energy resummed TM rates for the Higgs-plus-jet hadroproduction already deviate from the fixed-order background at current LHC energies [250]. Thus, our two-particle observables are expected to be very sensitive to the co-action of the two resummations.

Future analyses at FPFs will be crucial for deepening our understanding of perturbative QCD and the structure of protons and nuclei in previously unexplored regimes. The sensitivity of FPF detectors to far-forward production of light hadrons and charmed mesons will allow us to investigate BFKL effects and gluon-recombination dynamics. Additionally, TeV-scale neutrino-induced DIS experiments at FPFs will serve as valuable probes of proton structure and the production mechanisms of heavy or light decaying hadrons. Our work on light mesons at the FPF via hybrid factorization can provide a common framework for describing the production and decays of these particles.

QCD studies are fundamental components of the multi-frontier research program at FPFs. Searches for long-lived particles, indirect detection of dark matter, sterile neutrinos, as well as investigations into the muon puzzle, lepton universality, and the connection between high-energy particle physics and modern astroparticle physics, all depend on a deep understanding of the Standard Model. Progress towards precision QCD in the

kinematic sectors reachable at FPFs will be essential for driving scientific interest towards new and compelling directions.

This review is organized as follows: highlights on the NLL/NLO$^+$ hybrid factorization for our reference processes are given in Section 2; the phenomenological analysis is discussed in Section 3; conclusions and outlook are drawn in Section 4.

2. Hybrid Factorization at Work

In this Section we presents basic features of the NLL/NLO$^+$ hybrid factorization well-adapted to the description of our reactions. After a brief introduction of the process kinematics (Section 2.1), we give details of the NLL resummed cross section (Section 2.2). Choices for collinear PDFs and FFs are explained later (Section 2.3).

2.1. Kinematics of the Process

We consider the two following processes (Figure 1)

$$\begin{aligned} p(P_1) + p(P_2) &\to \pi^{\pm}(q_\pi, y_\pi, \phi_\pi) + \mathcal{X} + \mathcal{H}_b(q_b, y_b, \phi_b) \,, \\ p(P_1) + p(P_2) &\to D^{*\pm}(q_D, y_D, \phi_D) + \mathcal{X} + \mathcal{H}_b(q_b, y_b, \phi_b) \,. \end{aligned} \tag{1}$$

The upper equation of (1) says that a $\pi^{\pm}$ meson with mass $M_\pi = 139.57$ MeV, four-momentum q_π, rapidity y_π, and azimuthal angle ϕ_π is emitted in association with a singly bottomed hadron $\mathcal{H}_b$ with four-momentum q_b, rapidity y_b, and azimuthal angle ϕ_b. In the lower equation the pion is replaced by a $D^{*\pm}$ meson with mass $M_D = 1.968$ GeV, four-momentum q_D, rapidity y_D, and azimuthal angle ϕ_D. The $\mathcal{H}_b$ particle is given by an inclusive sum of all noncharmed B mesons and Λ_b baryons.

Initial-state partons posses four-momentum $x_a P_1$ and $x_b P_2$, where $P_{1,2}$ are the momenta of the incoming protons. The $\mathcal{X}$ system in Equation (1) depicts all the final-state inclusively irradiated gluons. One can take $P_{1,2}$ as Sudakov vectors satisfying $P_1^2 = P_2^2 = 0$ and $2P_1 \cdot P_2 = s$, to decompose the final-state four momenta as

$$q_{\mathcal{M},b} = x_{\mathcal{M},b} P_{1,2} - \frac{\vec{q}^{\,2}_{\perp_{\mathcal{M},b}}}{x_{\mathcal{M},b}} \frac{P_{2,1}}{s} + q_{\perp_{\mathcal{M},b}} \,, \qquad q^2_{\perp_{\mathcal{M},b}} = -\vec{q}^{\,2}_{T_{\mathcal{M},b}} \,, \tag{2}$$

where the $\mathcal{M}$ subscript inclusively refer to π or D. The outgoing-object longitudinal momentum fractions, $x_{\mathcal{M},b}$, can be calculated by inverting the relation

$$y_{\mathcal{M},b} = \pm \ln\left(\frac{x_{\mathcal{M},b}}{|\vec{q}_{T_{\mathcal{M},b}}|} \sqrt{s} \right) , \tag{3}$$

so that

$$\mathrm{d}y_{\mathcal{M},b} = \pm \frac{\mathrm{d}x_{\mathcal{M},b}}{x_{\mathcal{M},b}} \,. \tag{4}$$

The semi-hard nature of our reactions follows (i) from the size of final-state transverse momenta, which are taken to respect the hierarchy $\Lambda_{\mathrm{QCD}} \ll |\vec{q}_{T_{\mathcal{M},b}}| \ll \sqrt{s}$, and (ii) from imposing a large rapidity distance $\Delta Y = y_{\mathcal{M}} - y_b$ between the $\mathcal{M}$ meson and the b-hadron. Furthermore, to ensure the validity of a VFNS description for heavy-hadron production [331–333], $|\vec{q}_{T_{\mathcal{M},b}}|$ ranges must remain sufficiently above the thresholds for DGLAP evolution determined by the charm and bottom masses.

2.2. NLO Cross Section Resummed at NLL and Beyond

Following a pure QCD collinear vision for the LO cross section of our processes (Equation (1)), one would take a one-dimensional convolution between the partonic hard subprocess, incoming proton PDFs and tagged hadron FFs

$$\frac{\mathrm{d}\sigma^{[p+p\to\mathcal{M}+\mathcal{H}_b+\mathcal{X}]}_{\mathrm{LO,\,collinear}}}{\mathrm{d}x_{\mathcal{M}}\mathrm{d}x_b\mathrm{d}^2\vec{q}_{T_{\mathcal{M}}}\mathrm{d}^2\vec{q}_{T_b}} = \sum_{i,j=q,\bar{q},g}\int_0^1\mathrm{d}x_a\int_0^1\mathrm{d}x_b\, f_i(x_a,\mu_F)f_j(x_b,\mu_F) \times\int_{x_{\mathcal{M}}}^1\frac{\mathrm{d}\zeta_1}{\zeta_1}\int_{x_b}^1\frac{\mathrm{d}\zeta_2}{\zeta_2}D_i^{\mathcal{M}}\left(\frac{x_{\mathcal{M}}}{\zeta_1},\mu_F\right)D_j^b\left(\frac{x_b}{\zeta_2},\mu_F\right)\frac{\mathrm{d}\hat{\sigma}_{i,j}(\hat{s},\mu_F,\mu_R)}{\mathrm{d}x_{\mathcal{M}}\mathrm{d}x_b\mathrm{d}^2\vec{q}_{T_{\mathcal{M}}}\mathrm{d}^2\vec{q}_{T_b}}\,. \tag{5}$$

Here the i,j indices run over all the parton species except for the top quark which does not hadronize, with $f_{i,j}(x_{1,2},\mu_F)$ being proton PDFs and $D_{i,j}^{\mathcal{M},b}(x_{\mathcal{M},b}/\zeta_{1,2},\mu_F)$ standing for $\mathcal{M}$ meson and b-hadron FFs. Then, $x_{1,2}$ are longitudinal-momentum fractions for the partons initiation the hard scattering and $\zeta_{1,2}$ the ones for partons fragmenting to detected hadrons. The hard factor $\hat{\sigma}_{i,j}(\hat{s},\mu_F,\mu_R)$ depends on the squared center-of-mass energy of the partonic collision, $\hat{s}\equiv x_a x_b s$, and on factorization (μ_F) and renormalization (μ_R) scales.

Vice versa, to construct differential observables in our NLL/NLO$^+$ hybrid formalism one first performs the high-energy resummation of logarithms connected to transverse-momentum exchanges in the t-channel. Subsequently, one adds collinear ingredients, namely PDFs and FFs. The NLL/NLO$^+$ differential cross section can be rewritten as a Fourier sum of angular coefficients

$$\frac{\mathrm{d}\sigma^{[p+p\to\mathcal{M}+\mathcal{X}+\mathcal{H}_b]}_{\mathrm{NLL/NLO^+}}}{\mathrm{d}y_{\mathcal{M}}\,\mathrm{d}y_b\,\mathrm{d}|\vec{q}_{T_{\mathcal{M}}}|\,\mathrm{d}|\vec{q}_{T_b}|\,\mathrm{d}\phi_{\mathcal{M}}\,\mathrm{d}\phi_b} = \frac{1}{(2\pi)^2}\left[\mathcal{C}_0+2\sum_{n=1}^{\infty}\cos(n\varphi)\,\mathcal{C}_n\right], \tag{6}$$

where $\varphi=\phi_{\mathcal{M}}-\phi_b-\pi$ is the distance between the azimuthal angles of the light and the heavy hadron. The angular coefficients $\mathcal{C}_n$ are calculated within the BFKL framework and they embody the resummation of energy logarithms. A NLL-consistent formula obtained in the Modified Minimal Subtraction ($\overline{\mathrm{MS}}$) renormalization scheme [350] is cast as follows (for details on the derivation see, e.g., Ref. [162])

$$\begin{aligned}\mathcal{C}_n^{\mathrm{NLL/NLO^+}} &= \int_0^{2\pi}\mathrm{d}\phi_{\mathcal{M}}\int_0^{2\pi}\mathrm{d}\phi_b\,\cos(n\varphi)\,\frac{\mathrm{d}\sigma^{[p+p\to\mathcal{M}+\mathcal{X}+\mathcal{H}_b]}_{\mathrm{NLL/NLO^+}}}{\mathrm{d}y_{\mathcal{M}}\,\mathrm{d}y_b\,\mathrm{d}|\vec{q}_{T_{\mathcal{M}}}|\,\mathrm{d}|\vec{q}_{T_b}|\,\mathrm{d}\phi_{\mathcal{M}}\,\mathrm{d}\phi_b}\\ &= \frac{e^{\Delta Y}}{s}\int_{-\infty}^{+\infty}\mathrm{d}\nu\, e^{\Delta Y\bar{\alpha}_s(\mu_R)\chi^{\mathrm{NLL}}(n,\nu)}\alpha_s^2(\mu_R)\\ &\times\left[c_{\mathcal{M}}^{\mathrm{NLO}}(n,\nu,|\vec{q}_{T_{\mathcal{M}}}|,x_{\mathcal{M}})\,[c_b^{\mathrm{NLO}}(n,\nu,|\vec{q}_{T_b}|,x_b)]^*+\bar{\alpha}_s^2(\mu_R)\,\Delta Y\frac{\beta_0}{4N_c}\chi(n,\nu)\,\mathcal{F}(\nu)\right],\end{aligned} \tag{7}$$

with $\bar{\alpha}_s(\mu_R)\equiv\alpha_s(\mu_R)N_c/\pi$, N_c the number of colors and β_0 the QCD β-function leading coefficient. The $\chi^{\mathrm{NLL}}(n,\nu)$ stands for the NLL high energy kernel:

$$\chi^{\mathrm{NLL}}(n,\nu)=\chi(n,\nu)+\bar{\alpha}_s(\mu_R)\left[\bar{\chi}(n,\nu)+\frac{\beta_0}{8N_c}\chi(n,\nu)\left[-\chi(n,\nu)+\frac{10}{3}+2\ln\frac{\mu_R^2}{|\vec{q}_{T_{\mathcal{M}}}||\vec{q}_{T_b}|}\right]\right], \tag{8}$$

where

$$\chi(n,\nu)=2\left\{\psi(1)-\mathrm{Re}\left[\psi\left(i\nu+\frac{n+1}{2}\right)\right]\right\} \tag{9}$$

is its eigenvalue at LL and $\psi(z)=\Gamma'(z)/\Gamma(z)$. The $\hat{\chi}(n,\nu)$ NLO term was calculated in Refs. [351,352] and can be found in the Appendix A. The $c_h^{\mathrm{NLO}}(n,\nu,|\vec{q}_T|,x)$ emission function describe the forward inclusive emission of a given hadron, labeled as h. It was obtained in Ref. [165] in the light-quark cases and embodies collinear inputs. It also can be employed for heavy hadrons within a VFNS scheme, provided that observed transverse momenta $|\vec{q}_{T_b}|$ are sufficiently higher than the charm (for a D meson) or bottom (for a b hadron) masses. One has

$$c_h^{\mathrm{NLO}}(n,\nu,|\vec{q}_T|,x)=c_h(n,\nu,|\vec{q}_T|,x)+\alpha_s(\mu_R)\,\hat{c}_h(n,\nu,|\vec{q}_T|,x)\,, \tag{10}$$

with

$$c_h(n,\nu,|\vec{q}_T|,x) = 2\sqrt{\frac{C_F}{C_A}}|\vec{q}_T|^{2i\nu-1}\int_x^1 \frac{\mathrm{d}\zeta}{\zeta}\left(\frac{\zeta}{x}\right)^{2i\nu-1}\left[\frac{C_A}{C_F}f_g(\zeta)D_g^h\left(\frac{x}{\zeta}\right)+\sum_{i=q,\bar{q}} f_i(\zeta)D_i^h\left(\frac{x}{\zeta}\right)\right] \tag{11}$$

its LO limit and $\hat{c}_h(n,\nu,|\vec{q}_T|,x)$ its NLO correction (see Appendix B). The $\mathcal{F}(\nu)$ function in Equation (7) embodies the logarithmic derivative of the two LO emission functions

$$\mathcal{F}(\nu) = \frac{i}{2}\frac{\mathrm{d}}{\mathrm{d}\nu}\ln\left(\frac{c_{\mathcal{M}}(n,\nu,|\vec{q}_{T_b}|,x_{\mathcal{M}})}{[c_b(n,\nu,|\vec{q}_{T_b}|,x_b)]^*}\right)+\ln\left(|\vec{q}_{T_{\mathcal{M}}}||\vec{q}_{T_b}|\right). \tag{12}$$

From Equations (7)–(14), we gather the implementation of our hybrid factorization approach. The cross section is expressed as a factorized formula reminiscent of the BFKL formalism. In this formulation, the Green's function read as a high-energy convolution between the emission functions of the two tagged hadrons. These functions are further expressed as collinear convolutions between PDFs and FFs, along with the hard-scattering term. The '+' label indicates that our representation for angular coefficients in Equation (7) encode terms beyond the NLL accuracy generated by the cross product of the NLO emission functions, $\hat{c}_{\mathcal{M}}(n,\nu,|\vec{q}_{T_{\mathcal{M}}}|,x_{\mathcal{M}})\,[\hat{c}_b(n,\nu,|\vec{q}_{T_b}|,x_b)]^*$.

Expanding and truncating to the $\mathcal{O}(\alpha_s^3)$ order the NLL/NLO$^+$ angular coefficients in Equation (7), one gets the high-energy fixed-order (HE-NLO$^+$) counterpart of the BFKL-resummed cross section [249,269,270,288,309]). It is sensitive to the leading-power asymptotic dynamics of a pure NLO DGLAP computation and discards factors suppressed by inverse powers of $\hat{s}$. Our HE-NLO$^+$ expression for angular coefficients in the $\overline{\mathrm{MS}}$ scheme [350] reads

$$\mathcal{C}_n^{\text{HE-NLO}^+} = \frac{e^{\Delta Y}}{s}\int_{-\infty}^{+\infty}\mathrm{d}\nu\,\alpha_s^2(\mu_R)\,c_{\mathcal{M}}^{\text{NLO}}(n,\nu,|\vec{q}_{T_{\mathcal{M}}}|,x_{\mathcal{M}})\,[c_b^{\text{NLO}}(n,\nu,|\vec{q}_{T_b}|,x_b)]^*[1+\bar{\alpha}_s(\mu_R)\Delta Y\chi(n,\nu)]\,. \tag{13}$$

In our approach, an expansion up to contributions proportional to $\alpha_s(\mu_R)$ takes over the BFKL exponentiated kernel. Analogous to Equation (7), our fixed-order formula at high energies is denoted as HE-NLO$^+$, meaning contributions the beyond NLL accuracy arise from the cross product of NLO emission functions.

Then, we can obtain a genuine LL/LO formula by simply discarding all the NLO contributions, thus having

$$\mathcal{C}_n^{\text{LL/LO}} = \frac{e^{\Delta Y}}{s}\int_{-\infty}^{+\infty}\mathrm{d}\nu\,e^{\Delta Y\bar{\alpha}_s(\mu_R)\chi(n,\nu)}\,\alpha_s^2(\mu_R)\,c(n,\nu,|\vec{q}_{T_{\mathcal{M}}}|,x_{\mathcal{M}})\,[c(n,\nu,|\vec{q}_{T_b}|,x_b)]^*\,. \tag{14}$$

In our phenomenological analysis (see Section 3) we compare observables built in terms of NLL/NLO$^+$, HE-NLO$^+$, and LL/LO angular coefficients. We fix $\mu_{R,F}$ scales at the *natural* energies given by kinematics, thus having $\mu_R = \mu_F = \mu_N \equiv m_{\perp_{\mathcal{M}}} + m_{\perp_b}$, with $m_{h\perp} = \sqrt{m_h^2+|\vec{q}_{T_h}|^2}$ being the transverse mass of the specific hadron h. To assess the impact of MHOUs, scales will be varied from 1/2 to 2 times their natural values, as specified by the C_μ parameter (see Section 3.2).

We employ a two-loop QCD-coupling setup with $\alpha_s(M_Z) = 0.11707$ and five quark flavors active. In the $\overline{\mathrm{MS}}$ renormalization scheme [350], we write

$$\alpha_s(\mu_R) \equiv \alpha_s^{\overline{\mathrm{MS}}}(\mu_R) = \frac{\pi}{\beta_0\,\lambda_R}\left(4-\frac{\beta_1}{\beta_0^2}\frac{\ln\lambda_R}{\lambda_R}\right) \tag{15}$$

with

$$\lambda_R(\mu_R) = \ln\frac{\mu_R^2}{\Lambda_{\text{QCD}}^2}\,,\qquad \beta_0 = 11-\frac{2}{3}n_f\,,\qquad \beta_1 = 102-\frac{38}{3}n_f\,. \tag{16}$$

We emphasize that in our approach, energy scales are inherently tied to the transverse masses of observed particles. Consequently, they consistently fall within the perturbative regime, obviating the need for any infrared enhancement of the running coupling (see, for instance, Ref. [353]). Moreover, the utilization of large-scale values shields us from a regime where the significance of the *diffusion pattern* (see, for instance, Refs. [354–356]) becomes pronounced.

2.3. Choice of Collinear PDFs and FFs

As we already mentioned, due to the moderate parton x values, we build our framework upon standard collinear inputs, at NLO while the high-energy resummation is performed via BFKL at NLL. As for proton PDFs, make us of the novel `NNPDF4.0` NLO determination [357,358].

When considering charged pions, there is a broad array of NLO FFs available for potential use. The `NNFF1.0` FFs [359,360], derived from SIA data using a neural-network approach, feature NLO gluon FFs. On the other hand, `DEHSS14` sets [361] were obtained from a combination of SIA, Semi-Inclusive Deep-Inelastic Scattering (SIDIS), and proton-proton collision data. They assume a partial $SU(2)$ isospin symmetry, resulting in specific relations among the different flavor components. Meanwhile, `JAM20` determinations [362] incorporate datasets from both SIA and SIDIS and are determined concurrently with collinear PDFs in DIS and fixed-target Drell-Yan measurements. These FFs adhere to a full $SU(2)$ isospin symmetry.

Recently, `MAPFF1.0` functions [363,364] have been derived from SIA and SIDIS data using neural-network techniques. Notably, these FFs allow for a deviation from isospin symmetry, with separate parametrizations for $D_u^{\pi^+}$ and $D_{\bar{d}}^{\pi^+}$, which varies with the momentum fraction z. Gluon FFs are generated at NLO, although the data are collected at lower energies, where the gluon distribution has a more pronounced impact. Moreover, the methodology employed for extracting `MAPFF1.0` FFs has been extended to study the fragmentation of the $\Xi^-/\bar{\Xi}^+$ octet baryon [365] and to establish a new FF set for describing unidentified charged light hadrons, both from SIA and SIDIS data [366]. In our phenomenological analysis, we make use of two pion NLO FF determinations: `NNFF1.0` and `MAPFF1.0`.

As regards heavy hadrons, we employ the `KKKS08` NLO set [367–370] to describe parton fragmentation into Λ_c baryons. These FFs were extracted from OPAL and Belle data for SIA and mainly rely on a Bowler-like description [371] for charm and bottom flavors. We depict emissions of b flavored hadrons in terms of the `KKSS07` parametrization [372] based on data of the inclusive B-meson production in SIA events at CERN LEP1 and SLAC SLC and portrayed by a simple, three-parameter power-like function [373] for heavy-quark species. The `KKSS19` and `KKSS07` determinations use the VFNS. We remark that the employment of given VFNS PDFs or FFs is admitted in our approach, provided that typical energy scales are much larger than thresholds for the DGLAP evolution of charm and bottom quarks. As highlighted in Section 3.3, this requirement is always fulfilled (for further studies on D-meson, Λ_c-baryon and b-hadron VFNS fragmentation, see Refs. [374–378], [372,379–385], and [368,386,387], respectively).

We note that `KKSS08` and `KKSS07` FF sets do not carry any quantitative information regarding the extraction uncertainty. Future investigations incorporating potential new parametrizations of Λ_c and $\mathcal{H}_b$ fragmentation functions, including uncertainties, are essential to supplement our analysis of systematic errors in high-energy distributions.

3. Heavy Hadrons with JETHAD

All predictions presented in this review were generated using JETHAD, a hybrid code that consistently integrates both PYTHON- and FORTRAN-based modules. JETHAD is specifically designed for computing, managing, and processing physical distributions defined within various formalisms [249,252,254,319]. Numeric calculations of differential distributions were primarily performed using FORTRAN 2008 modular routines within

JETHAD, while the built-in PYTHON 3.0 analyzer was utilized for final data analysis and interpretation. All computation of observables are conducted within the $\overline{\text{MS}}$ scheme [350].

Section 3.1 briefly introduces core elements of the `v0.5.2` version of JETHAD. Our strategy to gauge systematic uncertainties is discussed in Section 3.2. Final-state kinematic ranges can be found in Section 3.3. Predictions rapidity-interval rates and angular multiplicities are discussed in Sections 3.4 and 3.5, respectively.

3.1. Highlights of JETHAD `v0.5.2`

The inception of the JETHAD project dates back to late 2017, driven by the necessity for precise predictions of semi-hard hadron [280,282] and jet [269,272,285] sensitive final states at the LHC. Phenomenological analyses of such reactions, proposed as probe channels for high-energy resummation in QCD, required the development of a reference numerical framework dedicated to computing and analyzing high-energy related distributions.

The initial named version, JETHAD `v0.2.7`, provided us with a first, quantitative BFKL-versus-DGLAP examination within the context of semi-inclusive hadron-plus-jet emissions at the LHC [249]. Subsequent iterations introduced new functionalities, such as selecting forward heavy-quark pair observables (`v0.3.0` [181]), enabling studies on Higgs emissions and transverse-momentum distributions (`v0.4.2` [250]), and integrating the PYTHON analyzer with the FORTRAN core supermodule (`v0.4.3` [251]).

Advancements continued with the ability to analyze heavy-flavored hadrons via VFNS FFs at NLO (`v0.4.4` [309]). The Δυναμις (DYNAMIS) work package, dedicated to the forward DY dilepton reaction [219], became part of JETHAD in `v0.4.5`. Integration with the LEXA modular code enabled exploration of proton content at low-x through small-x TMD densities in `v0.4.6` [199].

Version `v0.4.7` [253] introduced quarkonium-sensitive reactions from NRQCD leading-twist fragmentation. Novel features in `v0.5.0` [254] and `v0.5.1` [317] encompass an enhanced system for MHOU-related studies, an expanded list of observables with a focus on singly- and doubly-differential transverse-momentum production rates [276,289,317], and support for *matching* procedures with collinear factorization [324–327,329]. The most significant update of `v0.5.2` is `symJETHAD`, a MATHEMATICA plugin devoted to symbolical calculations for high-energy QCD and the proton structure.

From the fundamental core to service modules and routines, JETHAD has been designed to dynamically achieve high levels of computational performance. The multidimensional integrators within JETHAD support extensive parallel computing to actively choose the most suitable integration algorithm based on the shape of the integrand.

Any process implemented in JETHAD can be dynamically selected through an intuitive, *structure* based smart-management interface. Physical final-state particles are represented by *object* prototypes within this interface, where particle objects encapsulate all pertinent information about their physical counterparts, ranging from mass and charge to kinematic ranges and rapidity tags. These particle objects are initially loaded from a master database using a dedicated *particle generation* routine, and custom particle generation is also supported. Then, these objects are *cloned* into a final-state vector and *injected* from the integrand routine to the corresponding, process-specific module by a dedicated *controller*.

The flexibility in generating the physical final states is accompanied by a range of options for selecting the initial state. A unique *particle-ascendancy* structure attribute enables JETHAD to rapidly learn whether an object is hadroproduced, electroproduced, photoproduced, etc. This dynamic feature ensures that only relevant modules are initialized, optimizing computing-time efficiency.

JETHAD is structured as an *object-based* interface that is entirely independent of the specific reaction under investigation. While originally inspired by high-energy QCD and TMD factorization phenomenology, the code's design allows for easy encoding of different approaches by simply implementing novel, dedicated (super)modules. These can be straightforwardly linked to the core structure of the code by means of a natively-equipped *point-to-routine* system, making JETHAD a versatile, particle-physics oriented environment.

With the aim of providing the Scientific Community with a standard computation technology tailored for the management of diverse processes (described by distinct formalisms), we envision releasing the first public version of JETHAD in the medium-term future.

3.2. Uncertainty Estimation

A commonly adopted approach to assess the impact of MHOUs involves examining the sensitivity of our observables to variations in the renormalization scale and the factorization scale around their natural values. It is widely acknowledged that MHOUs significantly contribute to the overall uncertainty [252]. To gauge their influence, we simultaneously vary μ_R and μ_F around $\mu_N/2$ and $2\mu_N$, with the C_μ parameter in the figures of Section 3 denoted as $C_\mu \equiv \mu_F/\mu_N = \mu_R/\mu_N$.

Another potential source of uncertainty arises from proton PDFs. Recent analyses of high-energy production rates suggest that selecting different PDF parametrizations and members within the same set has minimal effect [249,252,285,310]. Hence, our observables will be computed using only the central member of the `NNPDF4.0` parametrization.

Additional uncertainties may stem from a *collinear improvement* of the NLO kernel, which entails incorporating renormalization-group (RG) terms to align the BFKL equation with the DGLAP one in the collinear limit, or from changes in the renormalization scheme [388–394]. The impact of collinear-improvement techniques on semi-hard rapidity-differential rates is observed to be encapsulated within the error bands generated by MHOUs [252].

Furthermore, the $\overline{\text{MS}}$ [350] to MOMentum (MOM) [395,396] renormalization-scheme transition was assessed in Ref. [252], resulting in systematically higher MOM results for rapidity distributions. However, these outcomes remain within the MHOUs bands. Notably, a proper MOM analysis should be grounded on MOM-evolved PDFs and FFs, which are presently unavailable.

To establish uncertainty bands for our distributions, we combine MHOUs with the numerical errors arising from multidimensional integration (see Section 3.3). The latter is consistently kept below 1% owing to the integrators employed in JETHAD.

3.3. Final-State Kinematic Ranges

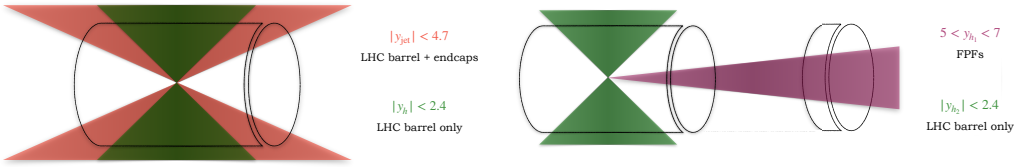
By making use of formulæ of Equations (7), (13) and (14), we construct physical observables as functions of angular coefficients *integrated* over the final-state phase-space variables, while the rapidity separation $\Delta Y = y_{\mathcal{M}} - y_b$ between the two observed particles is kept fixed. Thus, we have

$$C_n(\Delta Y, s) = \int_{q_{T_{\mathcal{M}}}^{\min}}^{q_{T_{\mathcal{M}}}^{\max}} \mathrm{d}|\vec{q}_{T_{\mathcal{M}}}| \int_{q_{T_b}^{\min}}^{q_{T_b}^{\max}} \mathrm{d}|\vec{q}_{T_b}| \int_{y_{\mathcal{M}}^{\min}}^{y_{\mathcal{M}}^{\max}} \mathrm{d}y_{\mathcal{M}} \int_{y_b^{\min}}^{y_b^{\max}} \mathrm{d}y_b \; \delta(\Delta Y - (y_{\mathcal{M}} - y_b)) \; \mathcal{C}_n \,. \quad (17)$$

The C_n terms inclusively represents all the NLL/NLO$^+$, HE-NLO$^+$, and LL/LO integrated angular coefficients. This approach allows us to impose and investigate various windows in transverse momenta and rapidities, based on realistic kinematic configurations employed in current and future experimental studies at the LHC. In particular, we will focus on the following two kinematic ranges.

3.3.1. Standard LHC Tagging

We delve into the emission dynamics of both hadrons within the standard detection acceptances of CMS or ATLAS barrel calorimeters. Unlike the Mueller–Navelet channel, which extends into the end-cap region (as illustrated in panel (*a*) of Figure 2), allowing for jet tagging with $|y_{\text{jet}}| < 4.7$, hadron detection is confined to the barrel regions. A realistic proxy for the rapidity range of hadron tags at the LHC can be derived from recent CMS analyses on Λ_b particles [397], yielding $|y_{\Lambda_b}| < 2$. For our study, we adopt a slightly broader range, matching the coverage of the CMS barrel detector, $|y_{\mathcal{M},b}| < 2.4$.



(**a**) LHC hadron-jet tagging (**b**) FPF + LHC coincidence

Figure 2. (**a**): A typical forward-backward hadron-jet tag in standard LHC rapidity ranges. (**b**): concurrent detection of a far-forward hadron at FPFs [1,2] and a central one at an LHC experiment thanks a narrow timing coincidence.

Following precedent studies [282,288,309], we set a $10 < |\vec{q}_{T_{\mathcal{M}}}|/\text{GeV} < 20$ window for the transverse momentum of the $\mathcal{M}$ hadron. In contrast, we select a wider and disjoint transverse momentum range for the b-hadron, specifically $20 < |\vec{q}_{T_b}|/\text{GeV} < 60$, as recently suggested in studies of high-energy b-flavored emissions [310,317]. This selection ensures the robustness of our treatment within the VFNS framework, as energy scales consistently exceed the thresholds for DGLAP evolution of heavy-quark FFs (we refer to Section 2.3 for further details).

On the one hand, the symmetric tagging in rapidity of both light and heavy particles enables us to rigorously apply our formalism in a well-defined regime, allowing for stringent tests of the NLL/NLO$^+$ hybrid factorization. On the other hand, as highlighted in Ref. [249], the use of disjoint transverse momentum intervals amplifies effects of additional, undetected gluon radiation by suppressing the Born contribution. This accentuates the signatures of the high-energy resummation over the fixed-order background.

Furthermore, asymmetric $|\vec{q}_T|$-windows mitigate potential instabilities arising in NLO calculations [398,399], as well as violations of energy-momentum at NLL [400]. However, the achievable ΔY values with standard LHC tagging may not be sufficiently large to unambiguously discriminate between BFKL and fixed-order signals. This challenge can be addressed by exploring *far-forward* emissions of one of the two particles, as proposed in Section 3.3.2.

3.3.2. FPF + LHC Coincidence

Expanding upon the standard detection regime outlined in Section 3.3.1, we advocate for the simultaneous identification of an *far-forward* particle (our choice falls into the $\mathcal{M}$ hadron) alongside a more centrally located one (the $\mathcal{H}_b$ hadron, as depicted in panel (*b*) of Figure 2).

Once the planned FPF [1,2] becomes operational, this novel configuration might be achievable by coordinating FPF detectors with ATLAS. Integrating information from both ATLAS and the FPF hinges on the capability to trigger ATLAS events using far-forward signatures, necessitating precise timing protocols and influencing FPF detector design. Technical specifics regarding a possible FPF + ATLAS tight timing synchronization are detailed in Section VI E of Ref. [1].

As a preliminary investigation, we examine the emission of a $\mathcal{M}$ meson within the far-forward range given by $5 < y_{\mathcal{M}} < 7$. While greater rapidities could be explored, we adopt a conservative approach, opting for a rapidity interval disjoint from and more forward than that accessible by end-caps of standard LHC detector. Investigations into larger rapidity ranges are deferred to future endeavors. The meson is paired with a b-hadron detected by the LHC barrel calorimeter within the standard rapidity spectrum, $|y_{\mathcal{H}}| < 2.4$. The transverse momenta of both final-state hadrons remain consistent with those specified in Section 3.3.1.

The combined FPF + LHC tagging strategy yields a hybrid and markedly asymmetric range selection, presenting an excellent avenue for disentangling clear high-energy signals from collinear backgrounds. However, as highlighted in Refs. [251,288] and mentioned

previously, the joint detection of an far-forward particle alongside a central one results in an asymmetric configuration between the longitudinal momentum fractions of the corresponding incoming partons. This configuration significantly suppresses the contribution of undetected gluon radiation at LO and has a notable impact at NLO.

This kinematic constraint leads to an incomplete cancellation between virtual and real contributions from gluon emissions, resulting in the emergence of large threshold logarithms in the perturbative series. Given that the BFKL framework encompasses the resummation of energy-type single logarithms while systematically neglecting threshold ones, we anticipate a partial degradation in the convergence of our resummed calculation in this FPF + LHC coincidence setup compared to the LHC standard scenario. Despite these challenges, these features motivate future developments aimed at incorporating the threshold resummation into our framework [71–89].

In conclusion, explorations via a FPF + LHC coincidence method offer an unparalleled opportunity for rigorous and in-depth examinations of strong interaction dynamics in the high-energy regime. In this regard, the advent of the planned FPF [1,2] may complement the capabilities of the ATLAS detector, enabling us to (*i*) assess the feasibility of precision analyses using hybrid high-energy and collinear factorization, and (*ii*) explore potential commonalities among distinct resummation techniques.

3.4. Rapidity-Interval Rates

We delve into the analysis of ΔY-rates for our studied processes, as illustrated in Figure 1. These distributions represent φ-summed, ΔY-differential cross sections. We note that clues of a *natural stabilization* of these observables are strongly expected when a standard LHC tagging is considered, while they are awaited in a FPF + LHC coincidence setup. Observing such stability would not only be a further reliability test for the NLL/NLO$^+$ factorization, but it also would mark a milestone toward future precision analyses.

Stabilization effects can manifest at various levels. Firstly, the involve the ability to study ΔY-distributions for all considered final states around the natural energy scales prescribed by kinematics. This prerequisite is essential for claiming evidence of stability, a feat unattainable when considering light hadrons and/or jets [249,265,267,282]. In such cases, large NLL contributions, of similar magnitude but opposite sign to their LL counterparts, can lead to unphysical ΔY-distributions, sometimes even resulting in negative values for large ΔY. Another sign of instability arises in the analysis of mean values of cosines of multiples of the azimuthal-angle distance, $\langle \cos(n\phi) \rangle$, which can exceed one. Secondly, achieving a substantial reduction in the discrepancy between pure LL calculations and NLL-resummed ones would push natural stability to a higher level.

To assess the impact of our resummed calculations on fixed-order predictions, we contrast LL/LO and NLL/NLO$^+$ results with the corresponding ones derived using our HE-NLO$^+$ formula (Equation (13)), which effectively mimics the high-energy signal of a pure NLO computation. Given a dedicated numerical tool for higher-order perturbative calculations of cross sections for semi-hard hadroproduction of two identified hadrons is not yet available, our HE-NLO$^+$ approach remains the most valid and efficient method for a BFKL versus fixed-order comparison.

Plots of Figure 3 depict the ΔY-rate for inclusive $\pi^{\pm} + \mathcal{H}_b$ productions at the LHC (left panels) and at FPF + LHC (right panel). Analogously, plots of Figure 4 refer to the inclusive $D*^{\pm} + \mathcal{H}_b$ detections. Uncertainty bands are constructed considering the combined effect of MHOUs from energy-scale variation and numerical multi-dimensional integration over the final-state phase space, with the former being significantly dominant. Upon inspection, our ΔY-distributions generally exhibit favorable statistics, lying in the range 10^{-1} to 5×10^2 nb.

The observed reflects the typical dynamics of our hybrid factorization. While the BFKL resummation predicts an increase in the partonic hard-scattering cross section with energy, its convolution with collinear PDFs and FFs leads to a decrease with ΔY for LL/LO, NLL/NLO$^+$, and NLL/NLO$^+$ results. This decrease is more pronounced for LHC kinematic configurations and appears smoother in the FPF + LHC case. The noncontiguous

rapidity ranges covered by the FPF and current LHC detectors may contribute to this smoother shape, compensating for the increment with ΔY of the available phase space by the absence of detected events in the interval between $y_{\rm FPF}^{\rm min}$ and $y_{\rm LHC}^{\rm max}$.

A similar pattern was also noted in a complementary configuration, namely the CMS + CASTOR setup (see Figure 10 of Ref. [249]). Results for rapidity-interval rates obtained with different pion FF parametrizations (upper versus lower panels of Figure 3) exhibit qualitatively similar trends, with their differences remaining significant, beyond a factor of three.

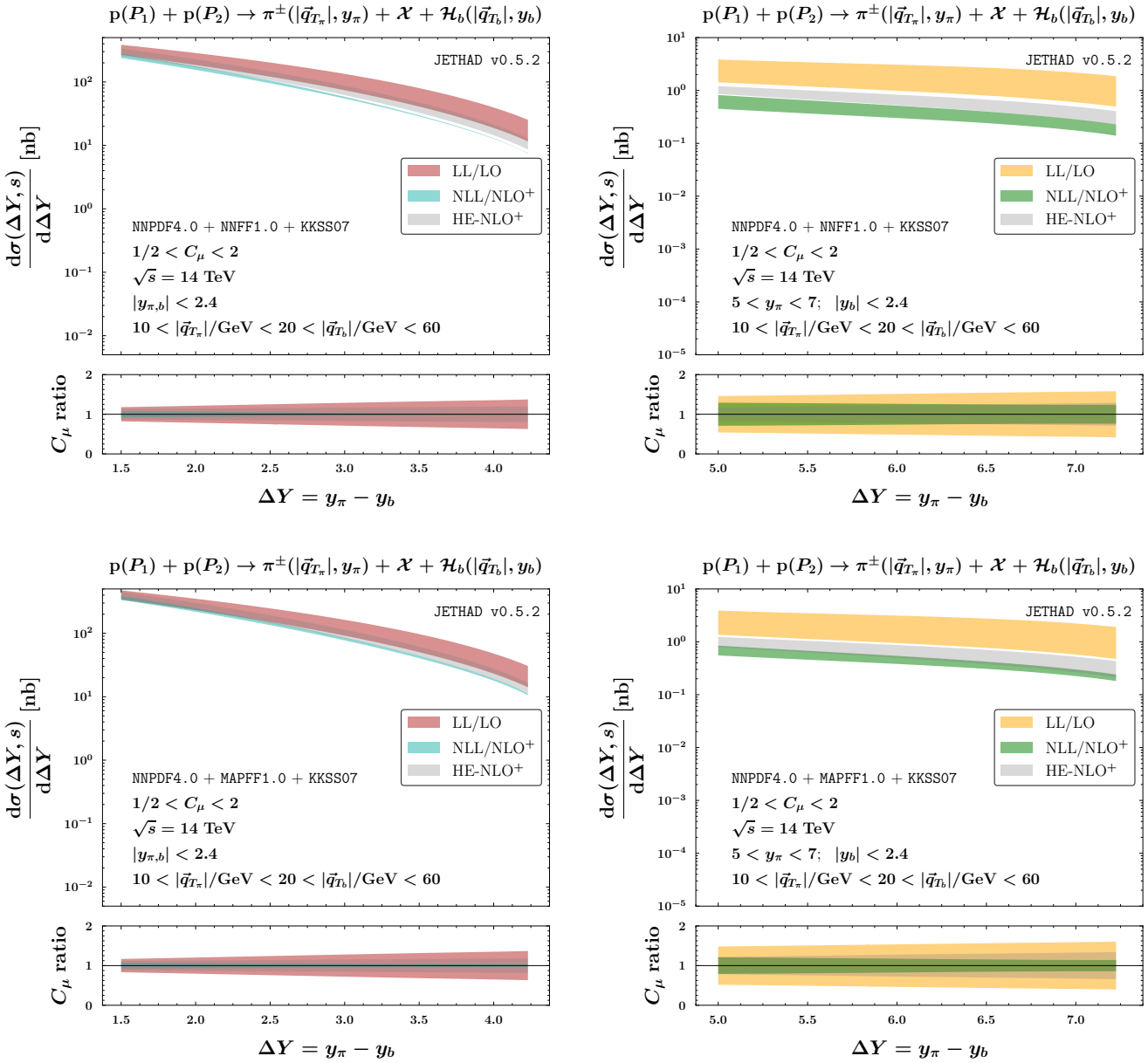


Figure 3. Rapidity-interval rate for the inclusive $\pi^{\pm} + \mathcal{H}_b$ production at $\sqrt{s} = 14$ TeV LHC (**left**) and FPF + LHC (**right**). Upper (lower) plots were obtained by using `NNFF1.0` (`MAPFF1.0`) pion NLO FFs together with `KKSS07` b-hadron NLO FFs, and `NNPDF4.0` NLO proton PDFs.

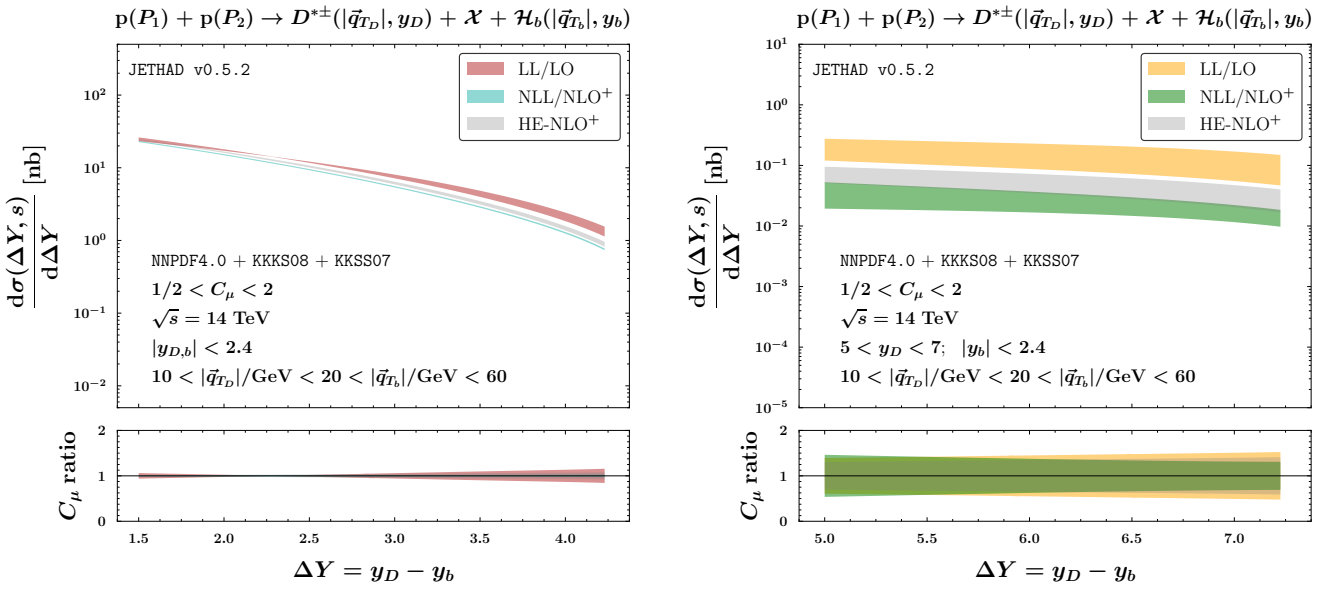


Figure 4. Rapidity-interval rate for the inclusive $D^{*\pm} + \mathcal{H}_b$ production at $\sqrt{s} = 14$ TeV LHC (**left**) and FPF + LHC (**right**). Plots were obtained by using KKKS08 D-meson NLO FFs together with KKSS07 b-hadron NLO FFs, and NNPDF4.0 NLO proton PDFs.

We observe the emergence of clear and natural stabilization effects in the high-energy series when standard LHC cuts are applied. The ΔY-distributions for all the channels in Figure 1 feature NLL/NLO$^+$ bands that are partially or entirely nested within LL/LO bands for small and moderate values of ΔY. However, as the rapidity interval increases, NLL/NLO corrections become increasingly negative, causing NLL/NLO$^+$ predictions to become smaller than pure LL/LO ones. NLL/NLO and HE-NLO$^+$ uncertainty bands are generally narrower than NLL/NLO and HE-NLO$^+$ ones. Furthermore, their width generally diminishes in the large ΔY range, where high-energy effects dominate over pure DGLAP ones. These observations are consistent with previous analyses on heavy-flavored emissions at CMS [253,309,310], highlighting the convergence of the energy-resummed series thanks to the natural stabilizing effect of VFNS FFs, which accurately describe the hadronization mechanisms of the detected heavy-flavor species.

The high-energy stabilizing pattern is also evident in the FPF + LHC coincidence setup, although its effects are less pronounced (see right panels of Figures 5–7). While our required condition for asserting evidence of stability is met, allowing for precision studies of cross sections around the natural energy scales provided by kinematics, it is notable that FPF + LHC NLL/NLO$^+$ predictions consistently remain below LL/LO results. Additionally, NLL/NLO$^+$ uncertainty bands are narrower than LL/LO ones, but slightly wider than NLL/NLO$^+$ bands for the same channels investigated in the standard LHC configurations. Furthermore, LL/LO results consistently exceed HE-NLO$^+$ ones, while NLL/NLO$^+$ results are smaller. Although further dedicated studies are required to determine if the observed natural-stability signals degrade when the FPF rapidity acceptances are expanded beyond those imposed in our analysis, an explanation for the increased sensitivity of ΔY-rates to the resummation accuracy can be provided based on our current understanding of the dynamics behind other resummation mechanisms.

We stress that the semi-hard nature of the final states considered leads to high energies but not necessarily to small-x dynamics. This is particularly evident in the FPF + LHC coincidence setup, where the strongly asymmetric final-state rapidity ranges result in one of the two parton longitudinal fractions being consistently large, while the other takes more moderate values. As highlighted in Section 3.3.2, our approach does not capture large-x logarithms, whose inclusion would be performed via an appropriate resummation mechanism, the aforementioned threshold resummation. A significant finding from Ref. [340] on

inclusive di-hadron detections in hadronic collisions is that incorporating NLL threshold resummation on top of pure NLO calculations leads to a notable increase in cross sections. Remarkably, this increase is comparable to the gap between our LL/LO and NLL/NLO$^+$ high-energy predictions for ΔY-distributions in FPF + LHC configurations.

Recent works [88,401] have demonstrated how NLL instabilities arising from forward hadron hadroproduction, described within the saturation framework [402], can be substantially mitigated when threshold logarithms are incorporated into these calculations. Considering these findings, we contend that the natural stability observed in our high-energy studies is not compromised by the adoption of FPF + LHC coincidence setups. It remains robust and provides a satisfactory description of ΔY-rates at natural scales. The discrepancy between LL/LO and NLL/NLO$^+$ predictions could come from those large-x, threshold logarithms, which are currently not accounted for by our hybrid factorization. Incorporating the large-x resummation represents a crucial step toward enhancing the description of the considered observables. Therefore, it should be pursued as the next logical step to evaluate the feasibility of precision studies of ΔY-distributions at FPF + LHC.

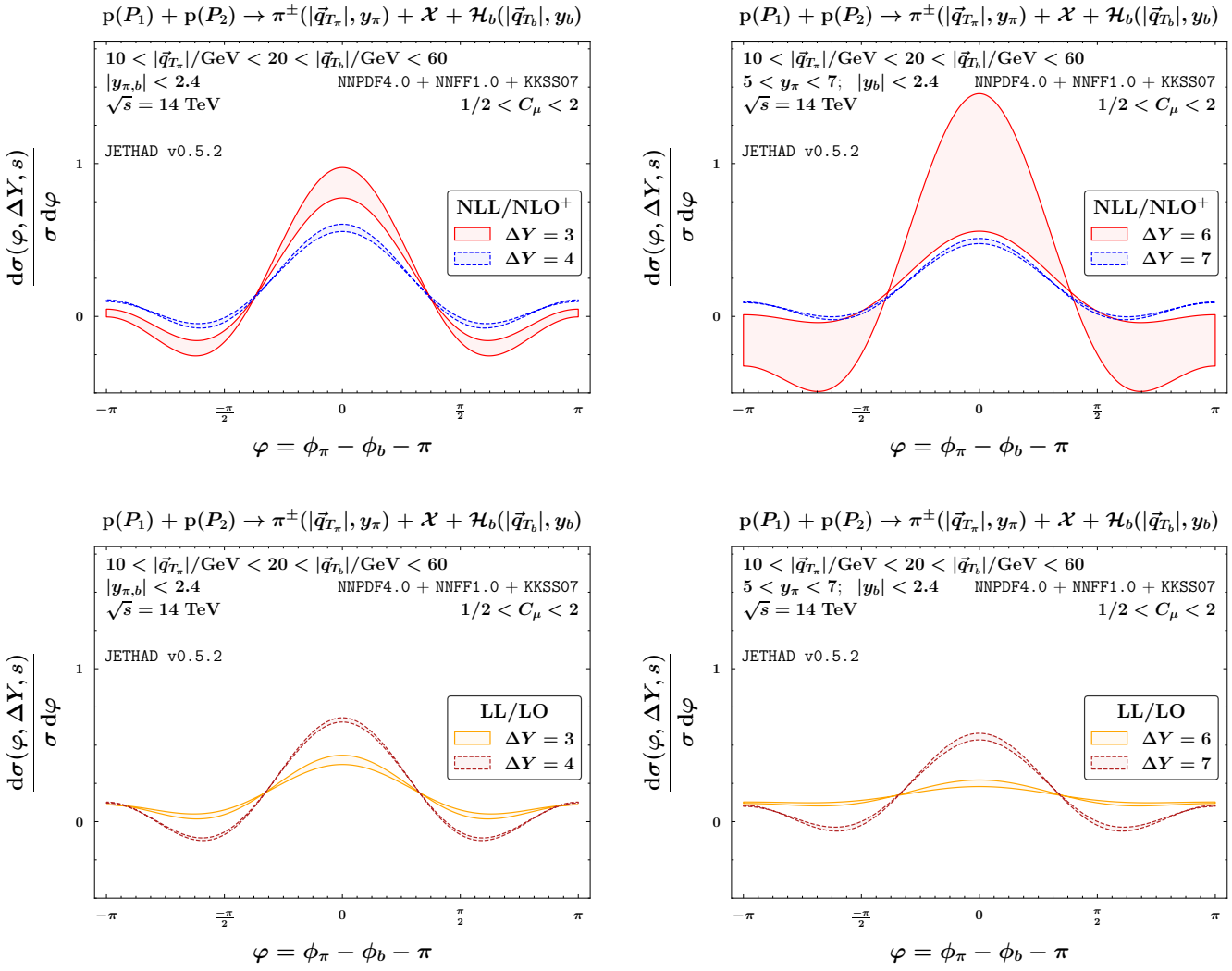


Figure 5. Angular multiplicity for the inclusive $\pi^{\pm} + \mathcal{H}_b$ production at $\sqrt{s} = 14$ TeV LHC (**left**) and FPF + LHC (**right**). Upper (lower) panels are for the NLL/NLO$^+$ (LL/LO) case. Plots were obtained by using `NNFF1.0` pion NLO FFs together with `KKSS07` b-hadron NLO FFs, and `NNPDF4.0` NLO proton PDFs.

The analysis presented in this section underscores that light-meson plus heavy-flavor production processes offer a promising avenue for stabilizing the high-energy resummation,

as anticipated. ΔY-distributions emerge as particularly promising observables for detecting signals of high-energy dynamics and potentially discriminating between BFKL-driven and fixed-order computations. Further exploration of these distributions holds significant potential for delving into the interplay between high-energy QCD dynamics and other resummations, particularly the large-x threshold effects. By probing these aspects in greater detail, we can gain deeper insights into the underlying mechanisms governing semi-hard phenomenology and refine our understanding of QCD dynamics in the high-energy regime.

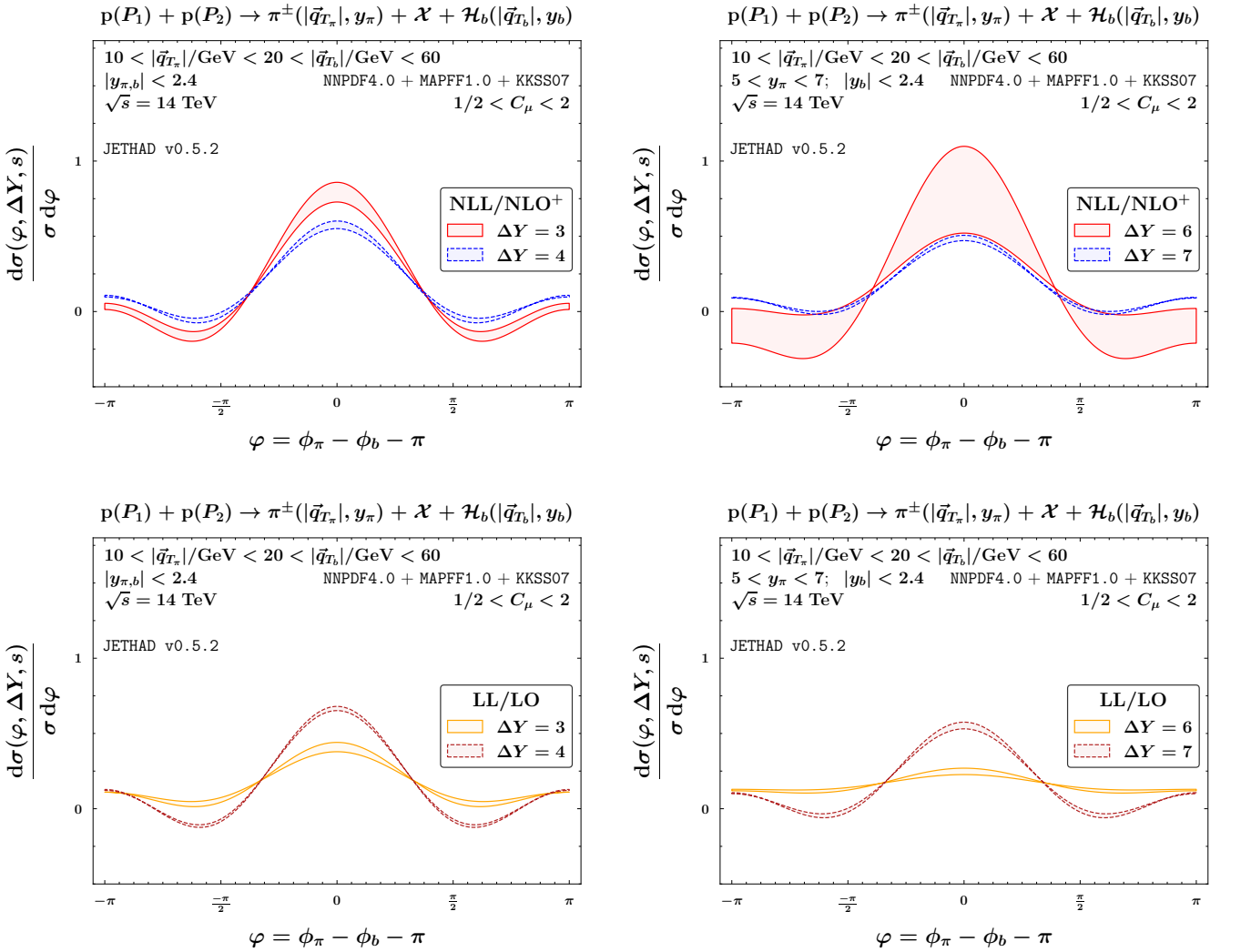


Figure 6. Angular multiplicity for the inclusive $\pi^{\pm} + \mathcal{H}_b$ production at $\sqrt{s} = 14$ TeV LHC (**left**) and FPF + LHC (**right**). Upper (lower) panels are for the NLL/NLO$^+$ (LL/LO) case. Plots were obtained by using `MAPFF1.0` pion NLO FFs together with `KKSS07` b-hadron NLO FFs, and `NNPDF4.0` NLO proton PDFs.

3.5. Angular Multiplicities

Semi-hard phenomenology delves into observables that become increasingly sensitive to final-state rapidity intervals. When these observables are also differential in azimuthal angles, it exposes a core aspect of high-energy QCD. In the context of two-particle hadroproduction reactions, significant insights into the onset of BFKL dynamics emerge when large rapidity distances (ΔY) enhance the weight of undetected gluons strongly ordered in rapidity. These gluon emissions, resummed as energy logarithms, induce a growing-with-ΔY decorrelation on the azimuthal plane of the outgoing particles.

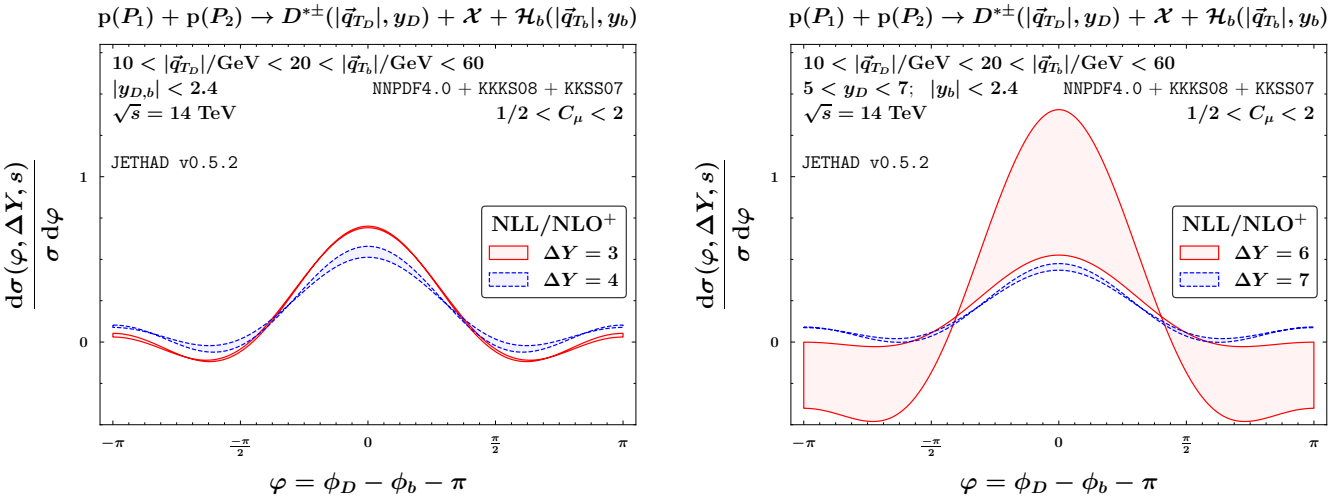


Figure 7. Angular multiplicity for the inclusive $D^{*\pm} + \mathcal{H}_b$ production at $\sqrt{s} = 14$ TeV LHC (**left**) and FPF + LHC (**right**). Upper (lower) panels are for the NLL/NLO$^+$ (LL/LO) case. Plots were obtained by using `KKKS08` D-meson NLO FFs together with `KKSS07` b-hadron NLO FFs, and `NNPDF4.0` NLO proton PDFs.

The angular decorrelation was initially observed through the ΔY dependence of cross-section azimuthal moment [248,264,265,267,403], defined as the ratios $R_{n0} \equiv C_n / C_0$ between a specific azimuthal coefficient ($C_{n\geq 1}$) and the φ-summed C_0 coefficient, which genuinely corresponds to the ΔY rate of Section 3.4. The R_{10} ratio effectively measures the azimuthal decorrelation between the two outgoing particles, akin to the mean value of $\langle \cos\varphi \rangle$. The R_{n0} ratios represent the higher moments $\langle \cos(n\varphi) \rangle$, while further probes of BFKL were proposed through ratios between azimuthal moments, $R_{nm} \equiv C_n / C_m = \langle \cos(n\varphi) \rangle / \langle \cos(m\varphi) \rangle$, in earlier studies [404,405].

NLL-resummed predictions for angular correlations of Mueller–Navelet jets exhibited satisfactory agreement with LHC data at $\sqrt{s} = 7$ TeV, particularly for symmetric $|\vec{q}_T|$-windows [264,265,267]. However, due to instabilities affecting the NLL series for processes involving the emission of two light-flavored particles, comparisons between theory and experiment had to be conducted at energy scales optimized via different procedures [264,267,271].

Recent investigations into inclusive hadroproductions of heavy-flavored hadrons have revealed that the stabilizing effects associated with the use of heavy-flavor VFNS FFs are less pronounced when a heavy hadron is emitted alongside a light jet, as opposed to another heavy object [309,310]. Consequently, only a partial reduction in instabilities for azimuthal moments is observed.

As recently shown [253,276], starting from the angular coefficients, we can construct a more stable observable that contains signals of high-energy dynamics coming from all azimuthal modes. We refer to the *angular multiplicity*

$$\frac{1}{\sigma}\frac{\mathrm{d}\sigma}{\mathrm{d}\varphi}(\varphi, \Delta Y, s) = \frac{1}{2\pi}\left[1 + 2\sum_{n=1}^{\infty} \cos(n\varphi)\langle \cos(n\varphi)\rangle\right] = \frac{1}{2\pi}\left[1 + 2\sum_{n=1}^{\infty} \cos(n\varphi)\, R_{n0}(\Delta Y, s)\right], \tag{18}$$

with $\varphi \equiv \phi_{\mathcal{M}} - \phi_b - \pi$. This observable, initially proposed in Ref. [263] within the framework of Mueller–Navelet analyses, was further examined with NLL precision in Ref. [264] for the same process (the Fourier coefficients $R_{n0}(\Delta Y, s)$ in Equation (18) can be also employed to describe the azimuthal anisotropy of long-range correlations in heavy-ion collisions (see, e.g., Refs. [406–413] and references therein)). Exploring its characteristics holds significant advantages from both theoretical and experimental standpoints. On the one hand, it collects signals of high-energy dynamics from all azimuthal modes, rendering it one of the most robust observables for spotting BFKL effects.

As a normalized distribution, i.e., a *multiplicity*, its sensitivity to uncertainties arising from uncertainties propagating from PDFs and/or FFs, as well as those from different replicas within the same set, is notably diminished. This allows for a focused examination of uncertainties intrinsic to high-energy resummation, facilitating stringent BFKL tests. On the other hand, experimental detector acceptances typically do not cover the entire (2π) azimuthal-angle range. Thus, comparing φ-dependent observables, like our azimuthal distribution, with experimental data is considerably more straightforward than for R_{nm} correlation moments.

From a numerical standpoint, ensuring reliable predictions for our φ-distribution necessitates computing a large number of C_n coefficients. We assessed the numerical stability of our calculations by progressively increasing the effective upper bound of the n sum in Equation (18), achieving satisfactory convergence at $n_{[\text{bound}]} \simeq 20$.

Results for angular multiplicities as functions of φ and for two different sets of values for the rapidity interval, $\Delta Y = 3,4$ (LHC) or $\Delta Y = 6,7$ (FPF + LHC), are shown in Figures 5–7. Panels in these figures are structured as follows. Upper (lowers) plots refer to NLL/NLO$^+$ (LL/LO) rates. Standard LHC tagging and the FPF + LHC coincidence setups are used in left and right plots, respectively. Figures 5 and 6 refer to pion channels described via `NNFF1.0` and `MAPFF1.0` pion collinear FFs, whereas Figure 7 show results for D-meson channels depicted by means of `KKKS08` FF determinations.

The prominent feature shared among all the depicted multiplicities is the emergence of a peak centered at $\varphi = 0$, corresponding of the physical configuration where the $\mathcal{M}$ meson and the $\mathcal{H}_b$ hadron are emitted (almost) back-to-back. With increasing ΔY, a characteristic trend emerges: the NLL/NLO$^+$ peak height decreases while its width expands. This trend stems from the heightened number of secondary gluons emitted with substantial rapidity separation, as predicted by the BFKL equation. Consequently, the correlation in the azimuthal plane between the two tagged particles diminishes, leading to a decrease in the number of nearly back-to-back events.

Conversely, LL/LO distributions exhibit an opposing pattern: the peak grows while its width decreases with increasing ΔY. This behavior generates from the connection between the strongly asymmetric transverse-momentum windows at which the two hadrons are tagged (see Section 3.3) and the corresponding longitudinal-momentum fractions. This bring to a reduction in the combinations of these fractions for the given ΔY. However, this results in an unphysical recorrelation pattern in the azimuthal plane for LL/LO distributions, contradicting the expected loss of correlation due to the weight of rapidity-ordered gluons forming the inclusive system $\mathcal{X}$. The correct behavior is reinstated when full NLL corrections are considered.

Additionally, the size of uncertainty bands due to scale variations sensibly diminishes as ΔY increases. This becomes strongly manifest in FPF + LHC selections. Multiplicities taken at lower reference values of the rapidity interval exhibit two symmetric minima at $|\varphi| \gtrsim \pi/2$, which extend to unphysical values beyond zero, whereas no negative values are observed for larger ΔY values. This indicates a natural stabilization of the high-energy series in the large rapidity-interval regime, as as expected.

Upon qualitative comparison of our predictions with corresponding results studied in other semi-hard channels, novel features emerge. As an example, angular distributions for our reactions appear less peaked compared to vector quarkonium + jet distributions (Figure 6 of Ref. [253]). They exhibit similarities with light-hadron or jet rates (Figures 17 and 18 of Ref. [249]).

In summary, multiplicities for $\mathcal{M}$-meson plus b-hadron productions within the hybrid factorization at NLL/NLO$^+$ allow for stringent tests of high-energy QCD dynamics. The natural stabilization of the high-energy resummation becomes significant in its expected applicability domain, particularly in the large ΔY sector. This makes azimuthal distributions easily measurable in current LHC experimental configurations and future analyses facilitated by the FPF + LHC coincidence methods, this enhances our ability to conduct rigorous analyses of high-energy QCD dynamics.

4. Toward Precision Studies of High-Energy QCD

By employing the hybrid high-energy and collinear factorization approach at NLL/NLO$^+$, we have investigated the inclusive detection of pion or a D meson, in association with a singly-bottomed hadron, at current LHC energies and kinematic configurations. Additionally, we explored configurations accessible via a FPF + LHC tight timing-coincidence setup.

Our analysis of distributions differential in the observed rapidity interval (ΔY) or in the azimuthal-angle distance (ϕ) between the two tagged objects has corroborated the remarkable property of *natural stability* of the high-energy resummation. This feature, recently uncovered in the context of heavy-flavor studies in forward directions [253,309,310,314,318], enables a reliable description of the considered observables around the natural values of energy scales dictated by process kinematics. This stability is a prerequisite and an initial stride toward precision investigations of high-energy QCD through inclusive di-hadron system emissions in proton collisions.

We have demonstrated that ΔY-rates effectively discriminate between the high-energy signal from the fixed-order background. On the other hand, φ-distributions exhibit robust stability in the large ΔY regime, offering a means to identify new and distinctive high-energy features. The promising statistical outcomes of our observables in the FPF + LHC configuration underscore the interest of the FPF Community [1,2] in exploring the intriguing prospect of enabling FPF and LHC detectors to operate in coincidence. Achieving this will necessitate extremely precise timing procedures, the technical feasibility of which should be actively pursued and complemented by positive feedback from the theoretical domain.

A striking conclusion from our recent investigation into the interplay between BFKL and DGLAP in inclusive semi-hard emissions of light jets and hadrons at the LHC [249] is the imperative for a *multi-lateral* formalism. Such a framework would entail the simultaneous and consistent incorporation of several distinct resummation mechanisms, serving as a fundamental element for conducting precision studies of high-energy QCD. The sensitivity of FPF + LHC results presented in this study to both high-energy and threshold resummation underscores the urgency of developing such a unified description as a top priority in the medium-term future.

As a first prospect, we will complement our investigation on $\mathcal{M}$ mesons emitted in FPF-like kinematic configurations, where heavy particles are detected by LHC detectors, by examining the opposite configuration. In this setup, a far-forward heavy-flavored hadron is tagged at the FPF while another central object remains within LHC cuts. Subsequently, we will explore the high-energy behavior of observables sensitive to single inclusive emissions of heavy hadrons reconstructed by FPF detectors. Our aim is to gain access to the proton content in far-forward (very low-x) regimes provided by FPF cuts. Here, our hybrid factorization framework could serve as a theoretical common basis for exploring production mechanisms and decays of heavy-flavored particles.

Then, by making use of estimates for differential cross sections of heavy-quark spectra at the particle-generated level, such as the ones provided via the `FONLL` method [414–417], it will be possible to make JETHAD work with parameters tuned for current high-energy hadron-hadron and lepton-hadron colliders which can produce heavy hadrons in forward directions of rapidity.

Mapping the proton structure in the very low-x regime will hinge on a comprehensive exploration of the connections among different approaches. Specifically, we aim to investigate the interplay between our hybrid factorization, which permits the description of cross sections for single forward emissions in terms of a κ_T-factorization between off-shell matrix elements and the UGD and the ABF formalism which, as mentioned before, allowed us to obtain low-x enhanced collinear PDFs (see also Section 6.1.2 of Ref. [2]).

Then, as highlighted by model studies of leading-twist gluon TMD PDFs [241,418] (see also Refs. [419–432]), the distribution of linearly-polarized gluons can induce spin effects even in collisions of unpolarized hadrons. The latters, collectively known as the Boer–Mulders effect, were first observed in the case of quark polarization [433–436]). The gluon Boer–Mulders density can be readily accessed via inclusive emissions of heavy-flavored

objects in hadron collisions, such as those that can be studied at FPFs (see Section 6.1.7 of Ref. [2]). Considering these insights, we aim to utilize FPF kinematic ranges as a tool to elucidate the connection between the BFKL UGD and the (un)polarized gluon TMDs.

Further progress will also hinge on connecting our program with NLO investigations of far-forward semi-inclusive emissions within the framework of gluon saturation [437–451]. In this context, the influence of soft-gluon radiation on angular asymmetries in emissions of far-forward di-jet or di-hadron systems might be relevant [452–457]. Higher-order saturation permits to explore of the (un)polarized gluon content of protons and nucleons at low-x [458–463]. Studies in Refs. [464–468] consider into heavy-hadron emissions in proton-proton and proton-nucleus collisions while accounting for low-x effects. Prospective inquiries of exclusive emission of heavy flavors in far-forward rapidity directions will unravel the connection between of our NLL/NLO$^+$ hybrid factorization NLO saturation [469,470].

We view the analyses presented in this work as a significant step forward toward conducting precision studies of high-energy QCD. Our hybrid factorization framework, potentially enhanced via the integration of additional resummation techniques, offers a systematic approach to reducing uncertainties stemming from both perturbative calculations of high-energy scatterings and from collinear inputs. This serves a dual purpose: it provides a benchmark for SM measurements and establishes a shared foundation for the exploration of Beyond-the-Standard-Model (BSM) physics.

Funding: This research was funded by the Atracción de Talento Grant n. 2022-T1/TIC-24176 of the Comunidad Autónoma de Madrid, Spain.

Acknowledgments: Feynman diagrams in Figure 1 were realized via the `JaxoDraw 2.0` code [471].

Conflicts of Interest: The author declares no conflict of interest.

Abbreviations

ABF	Altarelli–Ball–Forte
BFKL	Balitsky–Fadin–Kuraev–Lipatov
BLM	Brodsky–Lepage–Mackenzie
BSM	Beyond-the-Standard-Model
DGLAP	Dokshitzer–Gribov–Lipatov–Altarelli–Parisi
DIS	Deep-Inelastic Scattering
DY	Drell–Yan
EIC	Electron-Ion Collider
FCC	Future Circular Collider
FFs	Fragmentation Functions
FPFs	Forward Physics Facilities
`HELL`	High Energy Large Logarithms
LHC	Large Hadron Collider
LL	Leading Logarithmic
LO	Leading Order
MOM	MOMentum
$\overline{\text{MS}}$	Modified Minimal Subtraction
MHOUs	Missing Higher-Order Uncertainties
NLL	Next-to-Leading Logarithmic
NLO	Next-to-Leading Order
PDFs	Parton Distribution Functions
QCD	Quantum ChromoDynamics
SIA	Single-Inclusive Annihilation
SIDIS	Semi-Inclusive Deep-Inelastic Scattering
SM	Standard Model
TM	Transverse-Momentum

TMD	Transverse-Momentum-Dependent
UGD	Unintegrated Gluon Distribution
VFNS	Variable-Flavor Number-Scheme

Appendix A. High-Energy Kernel at NLL

The characteristic function encoded in the NLL correction to the high-energy kernel of Equation (8) is

$$\bar{\chi}(n,\nu) = -\frac{1}{4}\Bigg\{\frac{\pi^2-4}{3}\chi(n,\nu) - 6\zeta(3) - \frac{\mathrm{d}^2\chi}{\mathrm{d}\nu^2} + 2\,\phi(n,\nu) + 2\,\phi(n,-\nu) \tag{A1}$$

$$+\frac{\pi^2\sinh(\pi\nu)}{2\,\nu\,\cosh^2(\pi\nu)}\left[\left(3+\left(1+\frac{n_f}{N_c^3}\right)\frac{11+12\nu^2}{16(1+\nu^2)}\right)\delta_{n0} - \left(1+\frac{n_f}{N_c^3}\right)\frac{1+4\nu^2}{32(1+\nu^2)}\delta_{n2}\right]\Bigg\},$$

where

$$\phi(n,\nu) = -\int_0^1 \mathrm{d}x\,\frac{x^{-1/2+i\nu+n/2}}{1+x}\Bigg\{\frac{1}{2}\left(\psi'\left(\frac{n+1}{2}\right)-\zeta(2)\right) + \mathrm{Li}_2(x) + \mathrm{Li}_2(-x) \tag{A2}$$

$$+\ln x\left[\psi(n+1)-\psi(1)+\ln(1+x)+\sum_{k=1}^{\infty}\frac{(-x)^k}{k+n}\right] + \sum_{k=1}^{\infty}\frac{x^k}{(k+n)^2}\left[1-(-1)^k\right]\Bigg\}$$

$$= \sum_{k=0}^{\infty}\frac{(-1)^{k+1}}{k+(n+1)/2+i\nu}\Big\{\psi'(k+n+1)-\psi'(k+1)$$

$$+(-1)^{k+1}\left[\Xi_\psi(k+n+1)+\Xi_\psi(k+1)\right] - \frac{\psi(k+n+1)-\psi(k+1)}{k+(n+1)/2+i\nu}\Bigg\},$$

$$\Xi_\psi(z) = \frac{1}{4}\left[\psi'\left(\frac{z+1}{2}\right)-\psi'\left(\frac{z}{2}\right)\right], \tag{A3}$$

and

$$\mathrm{Li}_2(x) = -\int_0^x \mathrm{d}\zeta\,\frac{\ln(1-\zeta)}{\zeta}. \tag{A4}$$

Appendix B. Forward-Hadron Emission Function at NLO

The NLO correction to the forward-hadron singly off-shell emission function can be written as [165]

$$\hat{\mathcal{J}}_h(n,\nu,|\vec{q}_T|,x) = \frac{1}{\pi}\sqrt{\frac{C_F}{C_A}}\left(|\vec{q}_T|^2\right)^{i\nu-\frac{1}{2}}\int_x^1\frac{\mathrm{d}\zeta}{\zeta}\int_{\frac{x}{\zeta}}^1\frac{\mathrm{d}\vartheta}{\vartheta}\left(\frac{\zeta\vartheta}{x}\right)^{2i\nu-1} \tag{A5}$$

$$\times\left[\frac{C_A}{C_F}f_g(\zeta)D_g^h\left(\frac{x}{\zeta\vartheta}\right)\mathcal{C}_{gg}(\zeta,\vartheta) + \sum_{i=q\bar{q}}f_i(\zeta)D_i^h\left(\frac{x}{\zeta\vartheta}\right)\mathcal{C}_{qq}(\zeta,\vartheta)\right.$$

$$\left.+\,D_g^h\left(\frac{x}{\zeta\vartheta}\right)\sum_{i=q\bar{q}}f_i(\zeta)\mathcal{C}_{qg}(\zeta,\vartheta) + \frac{C_A}{C_F}f_g(\zeta)\sum_{i=q\bar{q}}D_i^h\left(\frac{x}{x\vartheta}\right)\mathcal{C}_{gq}(\zeta,\vartheta)\right].$$

Here, the $\mathcal{C}_{ij}$ parton coefficients read

$$\mathcal{C}_{gg}(\zeta,\vartheta) = 2P_{gg}(\vartheta)\left(1+\vartheta^{-2\gamma}\right)\ln\left(\frac{|\vec{q}_T|\zeta\vartheta}{\mu_F x}\right) - \beta_0\ln\left(\frac{|\vec{q}_T|\zeta\vartheta}{\mu_R x}\right) \tag{A6}$$

$$+\delta(1-\vartheta)\Big[C_A\ln\Big(\frac{s_0\,\zeta^2}{|\vec{q}_T|^2\,x^2}\Big)\chi(n,\gamma)-C_A\Big(\frac{67}{18}-\frac{\pi^2}{2}\Big)+\frac{5}{9}n_f$$
$$+\frac{C_A}{2}\Big(\psi'\Big(1+\gamma+\frac{n}{2}\Big)-\psi'\Big(\frac{n}{2}-\gamma\Big)-\chi^2(n,\gamma)\Big)\Big]+C_A\Big(\frac{1}{\vartheta}+\frac{1}{(1-\vartheta)_+}-2+\vartheta\bar{\vartheta}\Big)$$
$$\times\Big(\chi(n,\gamma)(1+\vartheta^{-2\gamma})-2(1+2\vartheta^{-2\gamma})\ln\vartheta+\frac{\bar{\vartheta}^2}{\vartheta^2}\mathcal{I}_2\Big)$$
$$+2\,C_A(1+\vartheta^{-2\gamma})\Big(\Big(\frac{1}{\vartheta}-2+\vartheta\bar{\vartheta}\Big)\ln\bar{\vartheta}+\Big(\frac{\ln(1-\vartheta)}{1-\vartheta}\Big)_+\Big)\,,$$

$$\mathcal{C}_{gq}(\zeta,\vartheta)=2P_{qg}(\vartheta)\Big(\frac{C_F}{C_A}+\vartheta^{-2\gamma}\Big)\ln\Big(\frac{|\vec{q}_T|\zeta\vartheta}{\mu_F x}\Big) \tag{A7}$$
$$+2\,\vartheta\bar{\vartheta}\,T_R\,\Big(\frac{C_F}{C_A}+\vartheta^{-2\gamma}\Big)+\,P_{qg}(\vartheta)\,\Big(\frac{C_F}{C_A}\,\chi(n,\gamma)+2\vartheta^{-2\gamma}\,\ln\frac{\bar{\vartheta}}{\vartheta}+\frac{\bar{\vartheta}}{\vartheta}\mathcal{I}_3\Big)\,,$$

$$\mathcal{C}_{qg}(\zeta,\vartheta)=2P_{gq}(\vartheta)\Big(\frac{C_A}{C_F}+\vartheta^{-2\gamma}\Big)\ln\Big(\frac{|\vec{q}_T|\zeta\vartheta}{\mu_F x}\Big) \tag{A8}$$
$$+\vartheta\Big(C_F\vartheta^{-2\gamma}+C_A\Big)+\,\frac{1+\bar{\vartheta}^2}{\vartheta}\Big[C_F\vartheta^{-2\gamma}(\chi(n,\gamma)-2\ln\vartheta)+2C_A\ln\frac{\bar{\vartheta}}{\vartheta}+\frac{\bar{\vartheta}}{\vartheta}\mathcal{I}_1\Big]\,,$$

and

$$\mathcal{C}_{qq}(x,\vartheta)=2P_{qq}(\vartheta)\Big(1+\vartheta^{-2\gamma}\Big)\ln\Big(\frac{|\vec{q}_T|\zeta\vartheta}{\mu_F x}\Big)-\beta_0\ln\Big(\frac{|\vec{q}_T|\zeta\vartheta}{\mu_R x}\Big) \tag{A9}$$
$$+\delta(1-\vartheta)\Big[-C_A\ln\Big(\frac{s_0\,\zeta^2}{|\vec{q}_T|^2\,x^2}\Big)\chi(n,\gamma)+C_A\Big(\frac{85}{18}+\frac{\pi^2}{2}\Big)-\frac{5}{9}n_f-8\,C_F$$
$$+\frac{C_A}{2}\Big(\psi'\Big(1+\gamma+\frac{n}{2}\Big)-\psi'\Big(\frac{n}{2}-\gamma\Big)-\chi^2(n,\gamma)\Big)\Big]+\,C_F\,\bar{\vartheta}\,(1+\vartheta^{-2\gamma})$$
$$+\Big(1+\vartheta^2\Big)\Big[C_A(1+\vartheta^{-2\gamma})\frac{\chi(n,\gamma)}{2(1-\vartheta)_+}+\Big(C_A-2\,C_F(1+\vartheta^{-2\gamma})\Big)\frac{\ln\vartheta}{1-\vartheta}\Big]$$
$$+\Big(C_F-\frac{C_A}{2}\Big)\Big(1+\vartheta^2\Big)\Big[2(1+\vartheta^{-2\gamma})\Big(\frac{\ln(1-\vartheta)}{1-\vartheta}\Big)_+\,+\frac{\bar{\vartheta}}{\vartheta^2}\mathcal{I}_2\Big]\,,$$

with $T_R=1/2$. The s_0 scale is an addition energy scale that we set to $s_0=\mu_C$. Furthermore, one has $\bar{\vartheta}\equiv 1-\vartheta$ and $\gamma\equiv-\frac{1}{2}+i\nu$. The LO DGLAP kernels $P_{ij}(\vartheta)$ are given by

$$\begin{aligned}
P_{gq}(z) &= C_F\frac{1+(1-z)^2}{z}\,, \\
P_{qg}(z) &= T_R\Big[z^2+(1-z)^2\Big]\,, \\
P_{qq}(z) &= C_F\Big(\frac{1+z^2}{1-z}\Big)_+=C_F\Big[\frac{1+z^2}{(1-z)_+}+\frac{3}{2}\delta(1-z)\Big]\,, \\
P_{gg}(z) &= 2C_A\Big[\frac{1}{(1-z)_+}+\frac{1}{z}-2+z(1-z)\Big]+\Big(\frac{11}{6}C_A-\frac{n_f}{3}\Big)\delta(1-z)\,,
\end{aligned} \tag{A10}$$

whereas the $\mathcal{I}_{2,1,3}$ functions read

$$\mathcal{I}_2=\frac{\vartheta^2}{\bar{\vartheta}^2}\Big[\vartheta\Big(\frac{{}_2F_1(1,1+\gamma-\frac{n}{2},2+\gamma-\frac{n}{2},\vartheta)}{\frac{n}{2}-\gamma-1}-\frac{{}_2F_1(1,1+\gamma+\frac{n}{2},2+\gamma+\frac{n}{2},\vartheta)}{\frac{n}{2}+\gamma+1}\Big) \tag{A11}$$
$$+\vartheta^{-2\gamma}\Big(\frac{{}_2F_1(1,-\gamma-\frac{n}{2},1-\gamma-\frac{n}{2},\vartheta)}{\frac{n}{2}+\gamma}-\frac{{}_2F_1(1,-\gamma+\frac{n}{2},1-\gamma+\frac{n}{2},\vartheta)}{\frac{n}{2}-\gamma}\Big)$$

$$+\left(1+\vartheta^{-2\gamma}\right)\left(\chi(n,\gamma)-2\ln\bar{\vartheta}\right)+2\ln\vartheta\Big]\,,$$

$$\mathcal{I}_1=\frac{\bar{\vartheta}}{2\vartheta}\mathcal{I}_2+\frac{\vartheta}{\bar{\vartheta}}\left[\ln\vartheta+\frac{1-\vartheta^{-2\gamma}}{2}\left(\chi(n,\gamma)-2\ln\bar{\vartheta}\right)\right]\,, \tag{A12}$$

and

$$\mathcal{I}_3=\frac{\bar{\vartheta}}{2\vartheta}\mathcal{I}_2-\frac{\vartheta}{\bar{\vartheta}}\left[\ln\vartheta+\frac{1-\vartheta^{-2\gamma}}{2}\left(\chi(n,\gamma)-2\ln\bar{\vartheta}\right)\right]\,, \tag{A13}$$

with ${}_2F_1$ the Gauss hypergeometric function. The *plus-prescription* in Equations (A6) and (A9) act as

$$\int_\zeta^1 \mathrm{d}\zeta\frac{f(\zeta)}{(1-\zeta)_+}=\int_\zeta^1 \mathrm{d}\zeta\frac{f(\zeta)-f(1)}{(1-\zeta)}-\int_0^\zeta \mathrm{d}\zeta\frac{f(1)}{(1-\zeta)} \tag{A14}$$

on any function $f(\zeta)$ regular at $\zeta=1$.

References

1. Anchordoqui, L.A.; Ariga, A.; Ariga, T.; Bai, W.; Balazs, K.; Batell, B.; Boyd, J.; Bramante, J.; Campanelli, M.; Carmona, A.; et al. The Forward Physics Facility: Sites, experiments, and physics potential. *Phys. Rep.* **2022**, *968*, 1–50. [CrossRef]
2. Feng, J.L.; Kling, F.; Reno, M.H.; Rojo, J.; Soldin, D.; Anchordoqui, L.A.; Boyd, J.; Ismail, A.; Harland-Lang, L.; Kelly, K.J.; et al. The Forward Physics Facility at the High-Luminosity LHC. *J. Phys. G* **2023**, *50*, 030501. [CrossRef]
3. Hentschinski, M.; Royon, C.; Peredo, M.A.; Baldenegro, C.; Bellora, A.; Boussarie, R.; Celiberto, F.G.; Cerci, S.; Chachamis, G.; Contreras, J.G.; et al. White Paper on Forward Physics, BFKL, Saturation Physics and Diffraction. *Acta Phys. Polon. B* **2023**, *54*, 2. [CrossRef]
4. Accardi, A.; Albacete, J.L.; Anselmino, M.; Armesto, N.; Aschenauer, E.C.; Bacchetta, A.; Boer, D.; Brooks, W.K.; Burton, T.; Chang, N.-B.; et al. Electron Ion Collider: The Next QCD Frontier: Understanding the glue that binds us all. *Eur. Phys. J. A* **2016**, *52*, 268. [CrossRef]
5. Abdul Khalek, R.; Accardi, A.; Adam, J.; Adamiak, D.; Akers, W.; Albaladejo, M.; Al-bataineh, A.; Alexeev, M.G.; Ameli, F.; Antonioli, P.; et al. Science Requirements and Detector Concepts for the Electron-Ion Collider: EIC Yellow Report. *Nucl. Phys. A* **2022**, *1026*, 122447. [CrossRef]
6. Abdul Khalek, R.; D'Alesio, U.; Arratia, M.; Bacchetta, A.; Battaglieri, M.; Begel, M.; Boglione, M.; Boughezal, R.; Boussarie, R.; Bozzi, G.; et al. Snowmass 2021 White Paper: Electron Ion Collider for High Energy Physics. *arXiv* **2022**, arXiv:2203.13199.
7. Acosta, D.; Barberis, E.; Hurley, N.; Li, W.; Colin, O.M.; Wood, D.; Zuo, X. The Potential of a TeV-Scale Muon-Ion Collider. *J. Instrum.* **2022**, *18*, P09025. [CrossRef]
8. Aryshev, A.; Behnke, T.; Berggren, M.; Brau, J.; Craig, N.; Freitas, A.; Gaede, F.; Gessner, S.; Gori, S.; Grojean, C.; et al. The International Linear Collider: Report to Snowmass 2021. *arXiv* **2022**, arXiv:2203.07622.
9. Brunner, O.; Burrows, P.N.; Calatroni, S.; Lasheras, N.C.; Corsini, R.; D'Auria, G.; Doebert, S.; Faus-Golfe, A.; Grudiev, A.; Latina, A.; et al. The CLIC project. *arXiv* **2022**, arXiv:2203.09186.
10. Arbuzov, A.; Bacchetta, A.; Butenschoen, M.; Celiberto, F.G.; D'Alesio, U.; Deka, M.; Denisenko, I.; Echevarria, M.G.; Efremov, A.; Ivanov, N.Y.; et al. On the physics potential to study the gluon content of proton and deuteron at NICA SPD. *Prog. Part. Nucl. Phys.* **2021**, *119*, 103858. [CrossRef]
11. Abazov, V.M.; Abramov, V.; Afanasyev, L.G.; Akhunzyanov, R.R.; Akindinov, A.V.; Akopov, N.; Alekseev, I.G.; Aleshko, A.M.; Alexakhin, V.Y.; Alexeev, G.D.; et al. Conceptual design of the Spin Physics Detector. *arXiv* **2021**, arXiv:2102.00442.
12. Bernardi, G.; Brost, E.; Denisov, D.; Landsberg, G.; Aleksa, M.; d'Enterria, D.; Janot, P.; Mangano, M.L.; Selvaggi, M.; Zimmermann, F.; et al. The Future Circular Collider: A Summary for the US 2021 Snowmass Process. *arXiv* **2022**, arXiv:2203.06520.
13. Amoroso, S.; Apyan, A.; Armesto, N.; Ball, R.D.; Bertone, V.; Bissolotti, C.; Bluemlein, J.; Boughezal, R.; Bozzi, G.; Britzger, D.; et al. Snowmass 2021 whitepaper: Proton structure at the precision frontier. *Acta Phys. Polon. B* **2022**, *53*, A1. [CrossRef]
14. Celiberto, F.G.; Fucilla, M.; Ivanov, D.Y.; Mohammed, M.M.A.; Papa, A. High-energy QCD at colliders: Semi-hard reactions and unintegrated gluon densities: Letter of Interest for SnowMass 2021. In Proceedings of the 2022 Snowmass Summer Study, Seattle, WA, USA, 17–26 July 2022. Available online: https://inspirehep.net/literature/1841481 (accessed on 18 June 2024).
15. Adam, J.; Aidala, C.; Angerami, A.; Audurier, B.; Bertulani, C.; Bierlich, C.; Blok, B.; Brandenburg, J.D.; Brodsky, S.; Bylinkin, A.; et al. New opportunities at the photon energy frontier. *arXiv* **2020**, arXiv:2009.03838.
16. Canepa, A.; D'Onofrio, M. Future Accelerator Projects: New Physics at the Energy Frontier. *Front. Phys.* **2023**, *10*, 916078. [CrossRef]
17. De Blas, J.; Buttazzo, D.; Capdevilla, R.; Curtin, D.; Franceschini, R.; Maltoni, F.; Meade, P.; Meloni, F.; Su, S.; Vryonidou, E.; et al. The physics case of a 3 TeV muon collider stage. *arXiv* **2022**, arXiv:2203.07261.
18. Aimè, C.; Apyan, A.; Mahmoud, M.A.; Bartosik, N.; Bertolin, A.; Bonesini, M.; Bottaro, S.; Buttazzo, D.; Capdevilla, R.; Casarsa, M.; et al. Muon Collider Physics Summary. *arXiv* **2022**, arXiv:2203.07256.

19. Bartosik, N.; Krizka, K.; Griso, S.P.; Aimè, C.; Apyan, A.; Mahmoud, M.A.; Bertolin, A.; Braghieri, A.; Buonincontri, L.; Calzaferri, S.; et al. Simulated Detector Performance at the Muon Collider. *arXiv* **2022**, arXiv:2203.07964.
20. Accettura, C.; Adams, D.; Agarwal, R.; Ahdida, C.; Aimè, C.; Amapane, N.; Amorim, D.; Andreetto, P.; Anulli, F.; Batsch, F.; et al. Towards a muon collider. *Eur. Phys. J. C* **2023**, *83*, 864; Erratum in *Eur. Phys. J. C 2024*, **84**, 36. [CrossRef]
21. Vignaroli, N. Charged resonances and MDM bound states at a multi-TeV muon collider. *J. High Energy Phys.* **2023**, *2023*, 121. [CrossRef]
22. Black, K.M.; Jindariani, S.; Li, D.; Maltoni, F.; Meade, P.; Stratakis, D.; Acosta, D.; Agarwal, R.; Agashe, K.; Aimè, C.; et al. Muon Collider Forum report. *J. Instrum.* **2024**, *19*, T02015. [CrossRef]
23. Dawson, S.; Meade, P.; Ojalvo, I.; Vernieri, C.; Adhikari, S.; Abu-Ajamieh, F.; Alberta, A.; Bahl, H.; Barman, R.; Basso, M.; et al. Report of the Topical Group on Higgs Physics for Snowmass 2021: The Case for Precision Higgs Physics. *arXiv* **2022**, arXiv:2209.07510.
24. Bose, T.; Boveia, A.; Doglioni, C.; Griso, S.P.; Hirschauer, J.; Lipeles, E.; Liu, Z.; Shah, N.R.; Wang, L.-T.; Agashe, K.; et al. Report of the Topical Group on Physics Beyond the Standard Model at Energy Frontier for Snowmass 2021. *arXiv* **2022**, arXiv:2209.13128.
25. Begel, M.; Hoeche, S.; Schmitt, M.; Lin, H.-W.; Nadolsky, P.M.; Royon, C.; Lee, Y.-J.; Mukherjee, S.; Baldenegro, C.; Campbell, J.; et al. Precision QCD, Hadronic Structure & Forward QCD, Heavy Ions: Report of Energy Frontier Topical Groups 5, 6, 7 submitted to Snowmass 2021. *arXiv* **2022**, arXiv:2209.14872.
26. Abir, R.; Akushevich, I.; Altinoluk, T.; Anderle, D.P.; Aslan, F.P.; Bacchetta, A.; Balantekin, B.; Barata, J.; Battaglieri, M.; Bertulani, C.A.; et al. The case for an EIC Theory Alliance: Theoretical Challenges of the EIC. *arXiv* **2023**, arXiv:2305.14572.
27. Accardi, A.; Achenbach, P.; Adhikari, D.; Afanasev, A.; Akondi, C.S.; Akopov, N.; Albaladejo, M.; Albataineh, H.; Albrecht, M.; Almeida-Zamora, B.; et al. Strong Interaction Physics at the Luminosity Frontier with 22 GeV Electrons at Jefferson Lab. *arXiv* **2023**, arXiv:2306.09360.
28. Mangano, M.L.; Zanderighi, G.; Aguilar Saavedra, J.A.; Alekhin, S.; Badger, S.; Bauer, C.W.; Becher, T.; Bertone, V.; Bonvini, M.; Boselli, S.; et al. Physics at a 100 TeV pp Collider: Standard Model Processes. *arXiv* **2016**, arXiv:1607.01831. [CrossRef]
29. Abada, A.; Abbrescia, M.; AbdusSalam, S.S.; Abdyukhanov, I.; Abelleira Fernandez, J.; Abramov, A.; Aburaia, M.; Acar, A.O.; Adzic, P.R.; Agrawal, P.; et al. FCC Physics Opportunities: Future Circular Collider Conceptual Design Report Volume 1. *Eur. Phys. J. C* **2019**, *79*, 474. [CrossRef]
30. Abada, A.; Abbrescia, M.; AbdusSalam, S.S.; Abdyukhanov, I.; Abelleira Fernandez, J.; Abramov, A.; Aburaia, M.; Acar, A.O.; Adzic, P.R.; Agrawal, P.; et al. FCC-ee: The Lepton Collider: Future Circular Collider Conceptual Design Report Volume 2. *Eur. Phys. J. Spec. Top.* **2019**, *228*, 261–623. [CrossRef]
31. Abada, A.; Abbrescia, M.; AbdusSalam, S.S.; Abdyukhanov, I.; Abelleira Fernandez, J.; Abramov, A.; Aburaia, M.; Acar, A.O.; Adzic, P.R.; Agrawal, P.; et al. FCC-hh: The Hadron Collider: Future Circular Collider Conceptual Design Report Volume 3. *Eur. Phys. J. Spec. Top.* **2019**, *228*, 755–1107. [CrossRef]
32. Abada, A.; Abbrescia, M.; AbdusSalam, S.S.; Abdyukhanov, I.; Abelleira Fernandez, J.; Abramov, A.; Aburaia, M.; Acar, A.O.; Adzic, P.R.; Agrawal, P.; et al. HE-LHC: The High-Energy Large Hadron Collider: Future Circular Collider Conceptual Design Report Volume 4. *Eur. Phys. J. Spec. Top.* **2019**, *228*, 1109–1382. [CrossRef]
33. Collins, J.C.; Soper, D.E.; Sterman, G.F. Factorization of Hard Processes in QCD. *Adv. Ser. Direct. High Energy Phys.* **1989**, *5*, 1–91. [CrossRef]
34. Sterman, G.F. Partons, factorization and resummation, TASI 95. *arXiv* **1995**, arXiv:hep-ph/9606312.
35. Gribov, V.; Lipatov, L. Deep inelastic e p scattering in perturbation theory. *Sov. J. Nucl. Phys.* **1972**, *15*, 438–450.
36. Gribov, V.N.; Lipatov, L.N. e+ e- pair annihilation and deep inelastic e p scattering in perturbation theory. *Sov. J. Nucl. Phys.* **1972**, *15*, 675–684.
37. Lipatov, L.N. The parton model and perturbation theory. *Yad. Fiz.* **1974**, *20*, 181–198.
38. Altarelli, G.; Parisi, G. Asymptotic Freedom in Parton Language. *Nucl. Phys. B* **1977**, *126*, 298–318. [CrossRef]
39. Dokshitzer, Y.L. Calculation of the Structure Functions for Deep Inelastic Scattering and e+ e- Annihilation by Perturbation Theory in Quantum Chromodynamics. *Sov. Phys. JETP* **1977**, *46*, 641–653.
40. Collins, J.C.; Soper, D.E. Back-To-Back Jets in QCD. *Nucl. Phys. B* **1977**, *193*, 381; Erratum in *Nucl. Phys. B* **1983**, *213*, 545. [CrossRef]
41. Collins, J. Foundations of perturbative QCD. *Camb. Monogr. Part Phys. Nucl. Phys. Cosmol.* **2011**, *32*, 1–624.
42. Catani, S.; de Florian, D.; Grazzini, M. Universality of nonleading logarithmic contributions in transverse momentum distributions. *Nucl. Phys. B* **2001**, *596*, 299–312. [CrossRef]
43. Bozzi, G.; Catani, S.; de Florian, D.; Grazzini, M. Transverse-momentum resummation and the spectrum of the Higgs boson at the LHC. *Nucl. Phys. B* **2006**, *737*, 73–120. [CrossRef]
44. Bozzi, G.; Catani, S.; Ferrera, G.; de Florian, D.; Grazzini, M. Transverse-momentum resummation: A Perturbative study of Z production at the Tevatron. *Nucl. Phys. B* **2009**, *815*, 174–197. [CrossRef]
45. Catani, S.; Grazzini, M. QCD transverse-momentum resummation in gluon fusion processes. *Nucl. Phys. B* **2011**, *845*, 297–323. [CrossRef]
46. Catani, S.; Grazzini, M. Higgs Boson Production at Hadron Colliders: Hard-Collinear Coefficients at the NNLO. *Eur. Phys. J. C* **2012**, *72*, 2013; Erratum in *Eur. Phys. J. C* **2012**, *72*, 2132. [CrossRef]
47. Catani, S.; Cieri, L.; de Florian, D.; Ferrera, G.; Grazzini, M. Universality of transverse-momentum resummation and hard factors at the NNLO. *Nucl. Phys. B* **2014**, *881*, 414–443. [CrossRef]

48. Catani, S.; de Florian, D.; Ferrera, G.; Grazzini, M. Vector boson production at hadron colliders: Transverse-momentum resummation and leptonic decay. *J. High Energy Phys.* **2015**, *12*, 047. [CrossRef]
49. Duhr, C.; Mistlberger, B.; Vita, G. Four-Loop Rapidity Anomalous Dimension and Event Shapes to Fourth Logarithmic Order. *Phys. Rev. Lett.* **2022**, *129*, 162001. [CrossRef] [PubMed]
50. Cieri, L.; Coradeschi, F.; de Florian, D. Diphoton production at hadron colliders: Transverse-momentum resummation at next-to-next-to-leading logarithmic accuracy. *J. High Energy Phys.* **2015**, *6*, 185. [CrossRef]
51. Alioli, S.; Broggio, A.; Gavardi, A.; Kallweit, S.; Lim, M.A.; Nagar, R.; Napoletano, D.; Rottoli, L. Precise predictions for photon pair production matched to parton showers in GENEVA. *J. High Energy Phys.* **2021**, *4*, 041. [CrossRef]
52. Becher, T.; Neumann, T. Fiducial q_T resummation of color-singlet processes at $N^3LL+NNLO$. *J. High Energy Phys.* **2021**, *3*, 199. [CrossRef]
53. Neumann, T. The diphoton q_T spectrum at $N^3LL' + NNLO$. *Eur. Phys. J. C* **2021**, *81*, 905. [CrossRef]
54. Ferrera, G.; Pires, J. Transverse-momentum resummation for Higgs boson pair production at the LHC with top-quark mass effects. *J. High Energy Phys.* **2017**, *2*, 139. [CrossRef]
55. Ju, W.-L.; Schönherr, M. The q_T and $\Delta\phi$ spectra in W and Z production at the LHC at $N^3LL'+N^2LO$. *J. High Energy Phys.* **2021**, *10*, 088. [CrossRef]
56. Monni, P.F.; Rottoli, L.; Torrielli, P. Higgs transverse momentum with a jet veto: A double-differential resummation. *Phys. Rev. Lett.* **2020**, *124*, 252001. [CrossRef] [PubMed]
57. Buonocore, L.; Grazzini, M.; Haag, J.; Rottoli, L. Transverse-momentum resummation for boson plus jet production at hadron colliders. *Eur. Phys. J. C* **2022**, *82*, 27. [CrossRef]
58. Wiesemann, M.; Rottoli, L.; Torrielli, P. The $Z\gamma$ transverse-momentum spectrum at NNLO+N^3LL. *Phys. Lett. B* **2020**, *809*, 135718. [CrossRef]
59. Ebert, M.A.; Michel, J.K.L.; Stewart, I.W.; Tackmann, F.J. Drell-Yan q_T resummation of fiducial power corrections at N^3LL. *J. High Energy Phys.* **2021**, *4*, 102. [CrossRef]
60. Re, E.; Rottoli, L.; Torrielli, P. Fiducial Higgs and Drell-Yan distributions at N^3LL'+NNLO with RadISH. *J. High Energy Phys.* **2021**, *9*, 108. [CrossRef]
61. Chen, X.; Gehrmann, T.; Glover, E.W.N.; Huss, A.; Monni, P.F.; Re, E.; Rottoli, L.; Torrielli, P. Third-Order Fiducial Predictions for Drell-Yan Production at the LHC. *Phys. Rev. Lett.* **2022**, *128*, 252001. [CrossRef]
62. Neumann, T.; Campbell, J. Fiducial Drell-Yan production at the LHC improved by transverse-momentum resummation at N^4LLp+N^3LO. *Phys. Rev. D* **2023**, *107*, L011506. [CrossRef]
63. Bizon, W.; Monni, P.F.; Re, E.; Rottoli, L.; Torrielli, P. Momentum-space resummation for transverse observables and the Higgs $p_\perp$ at $N^3LL+NNLO$. *J. High Energy Phys.* **2018**, *2*, 108. [CrossRef]
64. Billis, G.; Dehnadi, B.; Ebert, M.A.; Michel, J.K.L.; Tackmann, F.J. Higgs pT Spectrum and Total Cross Section with Fiducial Cuts at Third Resummed and Fixed Order in QCD. *Phys. Rev. Lett.* **2021**, *127*, 072001. [CrossRef] [PubMed]
65. Caola, F.; Chen, W.; Duhr, C.; Liu, X.; Mistlberger, B.; Petriello, F.; Vita, G.; Weinzierl, S. The Path forward to N^3LO. *arXiv* **2022**, arXiv:2203.06730.
66. Mueller, A.; Xiao, B.-W.; Yuan, F. Sudakov Resummation in Small-x Saturation Formalism. *Phys. Rev. Lett.* **2013**, *110*, 082301. [CrossRef] [PubMed]
67. Mueller, A.; Xiao, B.-W.; Yuan, F. Sudakov double logarithms resummation in hard processes in the small-x saturation formalism. *Phys. Rev. D* **2013**, *88*, 114010. [CrossRef]
68. Marzani, S. Combining Q_T and small-x resummations. *Phys. Rev. D* **2016**, *93*, 054047. . [CrossRef]
69. Mueller, A.; Szymanowski, L.; Wallon, S.; Xiao, B.-W.; Yuan, F. Sudakov Resummations in Mueller-Navelet Dijet Production. *J. High Energy Phys.* **2016**, *3*, 096. [CrossRef]
70. Xiao, B.-W.; Yuan, F. BFKL and Sudakov Resummation in Higgs Boson Plus Jet Production with Large Rapidity Separation. *Phys. Lett. B* **2018**, *782*, 28–33. [CrossRef]
71. Sterman, G.F. Summation of Large Corrections to Short Distance Hadronic Cross-Sections. *Nucl. Phys. B* **1987**, *281*, 310–364. [CrossRef]
72. Catani, S.; Trentadue, L. Resummation of the QCD Perturbative Series for Hard Processes. *Nucl. Phys. B* **1989**, *327*, 323–352. [CrossRef]
73. Catani, S.; Mangano, M.L.; Nason, P.; Trentadue, L. The Resummation of soft gluons in hadronic collisions. *Nucl. Phys. B* **1996**, *478*, 273–310. [CrossRef]
74. Bonciani, R.; Catani, S.; Mangano, M.L.; Nason, P. Sudakov resummation of multiparton QCD cross-sections. *Phys. Lett. B* **2003**, *575*, 268–278. [CrossRef]
75. de Florian, D.; Kulesza, A.; Vogelsang, W. Threshold resummation for high-transverse-momentum Higgs production at the LHC. *J. High Energy Phys.* **2006**, *2*, 047. [CrossRef]
76. Ahrens, V.; Becher, T.; Neubert, M.; Yang, L.L. Renormalization-Group Improved Prediction for Higgs Production at Hadron Colliders. *Eur. Phys. J. C* **2009**, *62*, 333–353. [CrossRef]
77. de Florian, D.; Grazzini, M. Higgs production at the LHC: Updated cross sections at $\sqrt{s} = 8$ TeV. *Phys. Lett. B* **2012**, *718*, 117–120. [CrossRef]

78. Forte, S.; Ridolfi, G.; Rota, S. Threshold resummation of transverse momentum distributions beyond next-to-leading log. *J. High Energy Phys.* **2021**, *8*, 110. [CrossRef]
79. Mukherjee, A.; Vogelsang, W. Threshold resummation for W-boson production at RHIC. *Phys. Rev. D* **2006**, *73*, 074005. [CrossRef]
80. Bolzoni, P. Threshold resummation of Drell-Yan rapidity distributions. *Phys. Lett. B* **2006**, *643*, 325–330. [CrossRef]
81. Becher, T.; Neubert, M. Threshold resummation in momentum space from effective field theory. *Phys. Rev. Lett.* **2006**, *97*, 082001. [CrossRef]
82. Becher, T.; Neubert, M.; Xu, G. Dynamical Threshold Enhancement and Resummation in Drell-Yan Production. *J. High Energy Phys.* **2008**, *7*, 030. [CrossRef]
83. Bonvini, M.; Forte, S.; Ridolfi, G. Soft gluon resummation of Drell-Yan rapidity distributions: Theory and phenomenology. *Nucl. Phys. B* **2011**, *847*, 93–159. [CrossRef]
84. Bonvini, M.; Marzani, S. Double resummation for Higgs production. *Phys. Rev. Lett.* **2018**, *120*, 202003. [CrossRef] [PubMed]
85. Ahmed, T.; Mandal, M.K.; Rana, N.; Ravindran, V. Higgs Rapidity Distribution in $b\bar{b}$ Annihilation at Threshold in N^3LO QCD. *J. High Energy Phys.* **2015**, *2*, 131. [CrossRef]
86. Banerjee, P.; Das, G.; Dhani, P.K.; Ravindran, V. Threshold resummation of the rapidity distribution for Drell-Yan production at NNLO+NNLL. *Phys. Rev. D* **2018**, *98*, 054018. [CrossRef]
87. Duhr, C.; Mistlberger, B.; Vita, G. Soft integrals and soft anomalous dimensions at N^3LO and beyond. *J. High Energy Phys.* **2022**, *9*, 155. [CrossRef]
88. Shi, Y.; Wang, L.; Wei, S.-Y.; Xiao, B.-W. Pursuing the Precision Study for Color Glass Condensate in Forward Hadron Productions. *Phys. Rev. Lett.* **2022**, *128*, 202302. [CrossRef] [PubMed]
89. Wang, L.; Chen, L.; Gao, Z.; Shi, Y.; Wei, S.-Y.; Xiao, B.-W. Forward inclusive jet productions in pA collisions. *Phys. Rev. D* **2023**, *107*, 016016. [CrossRef]
90. Moch, S.; Vogt, A. Higher-order soft corrections to lepton pair and Higgs boson production. *Phys. Lett. B* **2005**, *631*, 48–57. [CrossRef]
91. Idilbi, A.; Ji, X.-D.; Yuan, F. Resummation of threshold logarithms in effective field theory for DIS, Drell-Yan and Higgs production. *Nucl. Phys. B* **2006**, *753*, 42–68. [CrossRef]
92. Catani, S.; Cieri, L.; de Florian, D.; Ferrera, G.; Grazzini, M. Threshold resummation at N^3LL accuracy and soft-virtual cross sections at N^3LO. *Nucl. Phys. B* **2014**, *888*, 75–91. [CrossRef]
93. Ajjath, A.H.; Das, G.; Kumar, M.C.; Mukherjee, P.; Ravindran, V.; Samanta, K. Resummed Drell-Yan cross-section at N^3LL. *J. High Energy Phys.* **2020**, *10*, 153. [CrossRef]
94. Ajjath, A.H.; Mukherjee, P.; Ravindran, V.; Sankar, A.; Tiwari, S. Next-to-soft corrections for Drell-Yan and Higgs boson rapidity distributions beyond N^3LO. *Phys. Rev. D* **2021**, *103*, L111502. [CrossRef]
95. Ajjath, A.H.; Mukherjee, P.; Ravindran, V.; Sankar, A.; Tiwari, S. Next-to-soft-virtual resummed rapidity distribution for the Drell-Yan process to $NNLO + \overline{NNLL}$. *Phys. Rev. D* **2022**, *106*, 034005. [CrossRef]
96. Ahmed, T.; Ajjath, A.H.; Das, G.; Mukherjee, P.; Ravindran, V.; Tiwari, S. Soft-virtual correction and threshold resummation for n-colorless particles to fourth order in QCD: Part I. *arXiv* **2020**, arXiv:2010.02979.
97. Ajjath, A.H.; Mukherjee, P.; Ravindran, V.; Sankar, A.; Tiwari, S. Next-to SV resummed Drell–Yan cross section beyond leading-logarithm. *Eur. Phys. J. C* **2022**, *82*, 234. [CrossRef]
98. Kramer, M.; Laenen, E.; Spira, M. Soft gluon radiation in Higgs boson production at the LHC. *Nucl. Phys. B* **1998**, *511*, 523–549. [CrossRef]
99. Catani, S.; de Florian, D.; Grazzini, M.; Nason, P. Soft gluon resummation for Higgs boson production at hadron colliders. *J. High Energy Phys.* **2003**, *7*, 028. [CrossRef]
100. Bonvini, M.; Forte, S.; Ridolfi, G. The Threshold region for Higgs production in gluon fusion. *Phys. Rev. Lett.* **2012**, *109*, 102002. [CrossRef]
101. Bonvini, M.; Marzani, S. Resummed Higgs cross section at N^3LL. *J. High Energy Phys.* **2014**, *9*, 007. [CrossRef]
102. Bonvini, M.; Rottoli, L. Three loop soft function for N^3LL' gluon fusion Higgs production in soft-collinear effective theory. *Phys. Rev. D* **2015**, *91*, 051301. [CrossRef]
103. Bonvini, M.; Marzani, S.; Muselli, C.; Rottoli, L. On the Higgs cross section at N^3LO+N^3LL and its uncertainty. *J. High Energy Phys.* **2016**, *8*, 105. [CrossRef]
104. Beneke, M.; Garny, M.; Jaskiewicz, S.; Szafron, R.; Vernazza, L.; Wang, J. Leading-logarithmic threshold resummation of Higgs production in gluon fusion at next-to-leading power. *J. High Energy Phys.* **2020**, *1*, 094. [CrossRef]
105. Ajjath, A.H.; Mukherjee, P.; Ravindran, V.; Sankar, A.; Tiwari, S. On next to soft threshold corrections to DIS and SIA processes. *J. High Energy Phys.* **2021**, *4*, 131. [CrossRef]
106. Ajjath, A.H.; Mukherjee, P.; Ravindran, V.; Sankar, A.; Tiwari, S. Resummed Higgs boson cross section at next-to SV to $NNLO + \overline{NNLL}$. *Eur. Phys. J. C* **2022**, *82*, 774. [CrossRef]
107. de Florian, D.; Zurita, J. Soft-gluon resummation for pseudoscalar Higgs boson production at hadron colliders. *Phys. Lett. B* **2008**, *659*, 813–820. [CrossRef]
108. Schmidt, T.; Spira, M. Higgs Boson Production via Gluon Fusion: Soft-Gluon Resummation including Mass Effects. *Phys. Rev. D* **2016**, *93*, 014022. [CrossRef]

109. Ahmed, T.; Bonvini, M.; Kumar, M.C.; Mathews, P.; Rana, N.; Ravindran, V.; Rottoli, L. Pseudo-scalar Higgs boson production at N^3 LO_A +N^3 LL′. *Eur. Phys. J. C* **2016**, *76*, 663. [CrossRef] [PubMed]
110. Bhattacharya, A.; Mahakhud, M.; Mathews, P.; Ravindran, V. Two loop QCD amplitudes for di-pseudo scalar production in gluon fusion. *J. High Energy Phys.* **2020**, *2*, 121. [CrossRef]
111. Bhattacharya, A.; Kumar, M.C.; Mathews, P.; Ravindran, V. Next to SV resummed prediction for pseudoscalar Higgs boson production at NNLO+$\overline{\text{NNLL}}$. *Phys. Rev. D* **2022**, *105*, 116015. [CrossRef]
112. Bonvini, M.; Papanastasiou, A.S.; Tackmann, F.J. Matched predictions for the $b\bar{b}H$ cross section at the 13 TeV LHC. *J. High Energy Phys.* **2016**, *10*, 053. [CrossRef]
113. Ajjath, A.H.; Chakraborty, A.; Das, G.; Mukherjee, P.; Ravindran, V. Resummed prediction for Higgs boson production through $b\bar{b}$ annihilation at N^3LL. *J. High Energy Phys.* **2019**, *11*, 006. [CrossRef]
114. Moch, S.; Vermaseren, J.A.M.; Vogt, A. Higher-order corrections in threshold resummation. *Nucl. Phys. B* **2005**, *726*, 317–335. [CrossRef]
115. Das, G.; Moch, S.-O.; Vogt, A. Soft corrections to inclusive deep-inelastic scattering at four loops and beyond. *J. High Energy Phys.* **2020**, *3*, 116. [CrossRef]
116. Abele, M.; de Florian, D.; Vogelsang, W. Threshold resummation at N^3LL accuracy and approximate N^3LO corrections to semi-inclusive DIS. *Phys. Rev. D* **2022**, *106*, 014015. [CrossRef]
117. Das, G.; Kumar, M.C.; Samanta, K. Resummed inclusive cross-section in ADD model at N^3LL. *J. High Energy Phys.* **2020**, *10*, 161. [CrossRef]
118. Das, G.; Kumar, M.C.; Samanta, K. Resummed inclusive cross-section in Randall-Sundrum model at NNLO+NNLL. *J. High Energy Phys.* **2020**, *7*, 040. [CrossRef]
119. Muselli, C.; Forte, S.; Ridolfi, G. Combined threshold and transverse momentum resummation for inclusive observables. *J. High Energy Phys.* **2017**, *3*, 106. [CrossRef]
120. Bonvini, M.; Marzani, S.; Rojo, J.; Rottoli, L.; Ubiali, M.; Ball, R.D.; Bertone, V.; Carrazza, S.; Hartland, N.P. Parton distributions with threshold resummation. *J. High Energy Phys.* **2015**, *9*, 191. [CrossRef]
121. Nachtmann, O. Positivity constraints for anomalous dimensions. *Nucl. Phys. B* **1973**, *63*, 237–247. [CrossRef]
122. Georgi, H.; Politzer, H.D. Freedom at Moderate Energies: Masses in Color Dynamics. *Phys. Rev. D* **1976**, *14*, 1829. [CrossRef]
123. Barbieri, R.; Ellis, J.R.; Gaillard, M.K.; Ross, G.G. Mass Corrections to Scaling in Deep Inelastic Processes. *Nucl. Phys. B* **1976**, *117*, 50–76. [CrossRef]
124. Ellis, R.K.; Furmanski, W.; Petronzio, R. Power Corrections to the Parton Model in QCD. *Nucl. Phys. B* **1982**, *207*, 1–14. [CrossRef]
125. Ellis, R.K.; Furmanski, W.; Petronzio, R. Unraveling Higher Twists. *Nucl. Phys. B* **1983**, *212*, 29. [CrossRef]
126. Schienbein, I.; Radescu, V.A.; Zeller, G.P.; Eric Christy, M.; Keppel, C.E.; McFarland, K.S.; Melnitchouk, W.; Olness, F.I.; Reno, M.H.; Steffens, F.; et al. A Review of Target Mass Corrections. *J. Phys. G* **2008**, *35*, 053101. [CrossRef]
127. Accardi, A.; Qiu, J.-W. Collinear factorization for deep inelastic scattering structure functions at large Bjorken x(B). *J. High Energy Phys.* **2008**, *7*, 090. [CrossRef]
128. Accardi, A.; Melnitchouk, W. Target mass corrections for spin-dependent structure functions in collinear factorization. *Phys. Lett. B* **2008**, *670*, 114–118. [CrossRef]
129. Accardi, A. Large-x connections of nuclear and high-energy physics. *Mod. Phys. Lett. A* **2013**, *28*, 1330032. [CrossRef]
130. Accardi, A.; Anderle, D.P.; Ringer, F. Interplay of Threshold Resummation and Hadron Mass Corrections in Deep Inelastic Processes. *Phys. Rev. D* **2015**, *91*, 034008. [CrossRef]
131. Gribov, L.V.; Levin, E.M.; Ryskin, M.G. Semihard Processes in QCD. *Phys. Rept.* **1983**, *100*, 1–150. [CrossRef]
132. Celiberto, F.G. High-Energy Resummation in Semi-Hard Processes at the LHC. Ph.D. Thesis, Università della Calabria and INFN-Cosenza, Arcavacata di Rende, Cosenza, Italy, 2017. *arXiv* **2017**, arXiv:1707.04315.
133. Bolognino, A.D. From Semi-Hard Processes to the Unintegrated Gluon Distribution: A Phenomenological Path in the High-Energy Framework. Ph.D. Thesis, Università della Calabria and INFN-Cosenza, Arcavacata di Rende, Cosenza, Italy, 2021. *arXiv* **2021**, arXiv:2109.03033.
134. Mohammed, M.M.A. Hunting Stabilization Effects of the High-Energy Resummation at the LHC. Ph.D. Thesis, Università della Calabria and INFN-Cosenza, Arcavacata di Rende, Cosenza, Italy, 2022. *arXiv* **2022**, arXiv:2204.11606.
135. Fadin, V.S.; Kuraev, E.; Lipatov, L. On the Pomeranchuk Singularity in Asymptotically Free Theories. *Phys. Lett. B* **1975**, *60*, 50–52. [CrossRef]
136. Kuraev, E.A.; Lipatov, L.N.; Fadin, V.S. Multi-Reggeon Processes in the Yang-Mills Theory. *Sov. Phys. JETP* **1975**, *44*, 443–450.
137. Kuraev, E.; Lipatov, L.; Fadin, V.S. The Pomeranchuk Singularity in Nonabelian Gauge Theories. *Sov. Phys. JETP* **1977**, *45*, 199–204.
138. Balitsky, I.; Lipatov, L. The Pomeranchuk Singularity in Quantum Chromodynamics. *Sov. J. Nucl. Phys.* **1978**, *28*, 822–829.
139. Fadin, V.S. BFKL news. In *LAFEX International School on High-Energy Physics (LISHEP 98) Session A: Particle Physics for High School Teachers— Session B: Advanced School in HEP—Session C: Workshop on Diffractive Physics*; LISHEP: Rio de Janeiro, Brazil, 1998; pp. 742–776. Available online: http://arxiv.org/abs/hep-ph/9807528 (accessed on 18 June 2024).
140. Newton, R.G. Optical theorem and beyond. *Am. J. Phys.* **1976**, *44*, 639. [CrossRef]

141. Catani, S.; Ciafaloni, M.; Hautmann, F. Gluon Contributions to Small X Heavy Flavor Production. *Phys. Lett. B* **1990**, *242*, 97–102. [CrossRef]
142. Catani, S.; Ciafaloni, M.; Hautmann, F. High-energy factorization and small x heavy flavor production. *Nucl. Phys. B* **1991**, *366*, 135–188. [CrossRef]
143. Catani, S.; Ciafaloni, M.; Hautmann, F. High-energy factorization in QCD and minimal subtraction scheme. *Phys. Lett. B* **1993**, *307*, 147–153. [CrossRef]
144. Fadin, V.S.; Lipatov, L.N. BFKL pomeron in the next-to-leading approximation. *Phys. Lett. B* **1998**, *429*, 127–134. [CrossRef]
145. Ciafaloni, M.; Camici, G. Energy scale(s) and next-to-leading BFKL equation. *Phys. Lett. B* **1998**, *430*, 349–354. [CrossRef]
146. Fadin, V.S.; Fiore, R.; Papa, A. The Quark part of the nonforward BFKL kernel and the 'bootstrap' for the gluon Reggeization. *Phys. Rev. D* **1999**, *60*, 074025. [CrossRef]
147. Fadin, V.S.; Gorbachev, D.A. Nonforward color octet BFKL kernel. *JETP Lett.* **2000**, *71*, 222–226. [CrossRef]
148. Fadin, V.S.; Gorbachev, D.A. Nonforward color-octet kernel of the Balitsky-Fadin-Kuraev-Lipatov equation. *Phys. Atom. Nucl.* **2000**, *63*, 2157–2172. [CrossRef]
149. Fadin, V.S.; Fiore, R. Non-forward BFKL pomeron at next-to-leading order. *Phys. Lett. B* **2005**, *610*, 61–66; Erratum in *Phys. Lett. B* **2005**, *621*, 320. [CrossRef]
150. Fadin, V.S.; Fiore, R. Non-forward NLO BFKL kernel. *Phys. Rev. D* **2005**, *72*, 014018. [CrossRef]
151. Caola, F.; Chakraborty, A.; Gambuti, G.; von Manteuffel, A.; Tancredi, L. Three-Loop Gluon Scattering in QCD and the Gluon Regge Trajectory. *Phys. Rev. Lett.* **2022**, *128*, 212001. [CrossRef]
152. Falcioni, G.; Gardi, E.; Maher, N.; Milloy, C.; Vernazza, L. Disentangling the Regge Cut and Regge Pole in Perturbative QCD. *Phys. Rev. Lett.* **2022**, *128*, 132001. [CrossRef]
153. Duca, V.D.; Marzucca, R.; Verbeek, B. The gluon Regge trajectory at three loops from planar Yang-Mills theory. *J. High Energy Phys.* **2022**, *1*, 149. [CrossRef]
154. Byrne, E.P.; Duca, V.D.; Dixon, L.J.; Gardi, E.; Smillie, J.M. One-loop central-emission vertex for two gluons in $\mathcal{N}$ = 4 super Yang-Mills theory. *J. High Energy Phys.* **2022**, *8*, 271. [CrossRef]
155. Fadin, V.S.; Fucilla, M.; Papa, A. One-loop Lipatov vertex in QCD with higher ϵ-accuracy. *J. High Energy Phys.* **2023**, *4*, 137. [CrossRef]
156. Byrne, E.P. One-loop five-parton amplitudes in the NMRK limit. *arXiv* **2023**, arXiv:2312.15051.
157. Fadin, V.S.; Fiore, R.; Kotsky, M.I.; Papa, A. The Gluon impact factors. *Phys. Rev. D* **2000**, *61*, 094005. [CrossRef]
158. Fadin, V.S.; Fiore, R.; Kotsky, M.I.; Papa, A. The Quark impact factors. *Phys. Rev. D* **2000**, *61*, 094006. [CrossRef]
159. Bartels, J.; Colferai, D.; Vacca, G.P. The NLO jet vertex for Mueller-Navelet and forward jets: The Quark part. *Eur. Phys. J. C* **2002**, *24*, 83–99. [CrossRef]
160. Bartels, J.; Colferai, D.; Vacca, G.P. The NLO jet vertex for Mueller-Navelet and forward jets: The Gluon part. *Eur. Phys. J. C* **2003**, *29*, 235–249. [CrossRef]
161. Caporale, F.; Ivanov, D.Y.; Murdaca, B.; Papa, A.; Perri, A. The next-to-leading order jet vertex for Mueller-Navelet and forward jets revisited. *J. High Energy Phys.* **2012**, *2*, 101. [CrossRef]
162. Caporale, F.; Ivanov, D.Y.; Murdaca, B.; Papa, A. Mueller-Navelet small-cone jets at LHC in next-to-leading BFKL. *Nucl. Phys. B* **2013**, *877*, 73–94. [CrossRef]
163. Ivanov, D.Y.; Papa, A. The next-to-leading order forward jet vertex in the small-cone approximation. *J. High Energy Phys.* **2012**, *5*, 086. [CrossRef]
164. Colferai, D.; Niccoli, A. The NLO jet vertex in the small-cone approximation for kt and cone algorithms. *J. High Energy Phys.* **2015**, *4*, 071. [CrossRef]
165. Ivanov, D.Y.; Papa, A. Inclusive production of a pair of hadrons separated by a large interval of rapidity in proton collisions. *J. High Energy Phys.* **2012**, *7*, 045. [CrossRef]
166. Ivanov, D.Y.; Kotsky, M.I.; Papa, A. The Impact factor for the virtual photon to light vector meson transition. *Eur. Phys. J. C* **2004**, *38*, 195–213. [CrossRef]
167. Bartels, J.; Gieseke, S.; Qiao, C.F. The (gamma* —> q anti-q) Reggeon vertex in next-to-leading order QCD. *Phys. Rev. D* **2001**, *63*, 056014; Erratum in *Phys. Rev. D* **2002**, *65*, 079902. [CrossRef]
168. Bartels, J.; Gieseke, S.; Kyrieleis, A. The Process gamma*(L) + q —> (q anti-q g) + q: Real corrections to the virtual photon impact factor. *Phys. Rev. D* **2002**, *65*, 014006. [CrossRef]
169. Bartels, J.; Colferai, D.; Gieseke, S.; Kyrieleis, A. NLO corrections to the photon impact factor: Combining real and virtual corrections. *Phys. Rev. D* **2002**, *66*, 094017. [CrossRef]
170. Bartels, J.; Kyrieleis, A. NLO corrections to the gamma* impact factor: First numerical results for the real corrections to gamma*(L). *Phys. Rev. D* **2004**, *70*, 114003. [CrossRef]
171. Fadin, V.S.; Ivanov, D.Y.; Kotsky, M.I. Photon Reggeon interaction vertices in the NLA. *Phys. Atom. Nucl.* **2002**, *65*, 1513–1527. [CrossRef]
172. Balitsky, I.; Chirilli, G.A. Photon impact factor and k_T-factorization for DIS in the next-to-leading order. *Phys. Rev. D* **2013**, *87*, 014013. [CrossRef]

173. Hentschinski, M.; Kutak, K.; van Hameren, A. Forward Higgs production within high energy factorization in the heavy quark limit at next-to-leading order accuracy. *Eur. Phys. J. C* **2021**, *81*, 112; Erratum in *Eur. Phys. J. C* **2021**, *81*, 262. [CrossRef]
174. Celiberto, F.G.; Fucilla, M.; Ivanov, D.Y.; Mohammed, M.M.A.; Papa, A. The next-to-leading order Higgs impact factor in the infinite top-mass limit. *J. High Energy Phys.* **2022**, *8*, 092. [CrossRef]
175. Hentschinski, M. Forward Higgs production at NLO using Lipatov's high energy effective action. *SciPost Phys. Proc.* **2022**, *8*, 136. [CrossRef]
176. Fucilla, M. The Higgs Impact Factor at Next-to-leading Order. *Acta Phys. Polon. Suppl.* **2023**, *16*, 44. [CrossRef]
177. Hentschinski, M.; Salas, C. Forward Drell-Yan plus backward jet as a test of BFKL evolution. In Proceedings of the 20th International Workshop on Deep-Inelastic Scattering and Related Subjects, Bonn, Germany, 26–30 March 2012. [CrossRef]
178. Motyka, L.; Sadzikowski, M.; Stebel, T. Twist expansion of Drell-Yan structure functions in color dipole approach. *J. High Energy Phys.* **2015**, *5*, 087. [CrossRef]
179. Celiberto, F.G.; Ivanov, D.Y.; Murdaca, B.; Papa, A. High-energy resummation in heavy-quark pair photoproduction. *Phys. Lett. B* **2018**, *777*, 141–150. [CrossRef]
180. Bolognino, A.D.; Celiberto, F.G.; Fucilla, M.; Ivanov, D.Y.; Murdaca, B.; Papa, A. Inclusive production of two rapidity-separated heavy quarks as a probe of BFKL dynamics. *PoS DIS2019* **2019**, 067. [CrossRef]
181. Bolognino, A.D.; Celiberto, F.G.; Fucilla, M.; Ivanov, D.Y.; Papa, A. High-energy resummation in heavy-quark pair hadroproduction. *Eur. Phys. J. C* **2019**, *79*, 939. [CrossRef]
182. Boussarie, R.; Ducloué, B.; Szymanowski, L.; Wallon, S. Forward J/ψ and very backward jet inclusive production at the LHC. *Phys. Rev. D* **2018**, *97*, 014008. [CrossRef]
183. Boussarie, R.; Ducloué, B.; Szymanowski, L.; Wallon, S. Production of a forward J/psi and a backward jet at the LHC. In Proceedings of the International Conference on the Structure and Interactions of the Photon and 21st International Workshop on Photon-Photon Collisions and International Workshop on High Energy Photon Linear Colliders, Novosibirsk, Russia, 15–19 June 2015.
184. Boussarie, R.; Ducloue, B.; Szymanowski, L.; Wallon, S. Production of a forward J/ψ and a backward jet at the LHC. *arXiv* **2015**, arXiv:1511.02181. [CrossRef].
185. Boussarie, R.; Ducloué, B.; Szymanowski, L.; Wallon, S. QCD resummation effects in forward J/ψ and very backward jet inclusive production at the LHC. *arXiv* **2018**, arXiv:1709.02671. [CrossRef].
186. Diehl, M. Generalized parton distributions. *Phys. Rept.* **2003**, *388*, 41–277. [CrossRef]
187. Diehl, M. Introduction to GPDs and TMDs. *Eur. Phys. J. A* **2016**, *52*, 149. [CrossRef]
188. Müller, D.; Robaschik, D.; Geyer, B.; Dittes, F.M.; Hořejši, J. Wave functions, evolution equations and evolution kernels from light ray operators of QCD. *Fortsch. Phys.* **1994**, *42*, 101–141. [CrossRef]
189. Belitsky, A.V.; Radyushkin, A.V. Unraveling hadron structure with generalized parton distributions. *Phys. Rept.* **2005**, *418*, 1–387. [CrossRef]
190. Hentschinski, M.; Vera, A.S.; Salas, C. Hard to Soft Pomeron Transition in Small-x Deep Inelastic Scattering Data Using Optimal Renormalization. *Phys. Rev. Lett.* **2013**, *110*, 041601. [CrossRef] [PubMed]
191. Hentschinski, M.; Vera, A.S.; Salas, C. F_2 and F_L at small x using a collinearly improved BFKL resummation. *Phys. Rev. D* **2013**, *87*, 076005. [CrossRef]
192. Anikin, I.; Besse, A.; Ivanov, D.Y.; Pire, B.; Szymanowski, L.; Wallon, S. A phenomenological study of helicity amplitudes of high energy exclusive leptoproduction of the rho meson. *Phys. Rev. D* **2011**, *84*, 054004. [CrossRef]
193. Besse, A.; Szymanowski, L.; Wallon, S. Saturation effects in exclusive rhoT, rhoL meson electroproduction. *J. High Energy Phys.* **2013**, *11*, 062. [CrossRef]
194. Bolognino, A.D.; Celiberto, F.G.; Ivanov, D.Y.; Papa, A. Unintegrated gluon distribution from forward polarized ρ-electroproduction. *Eur. Phys. J. C* **2018**, *78*, 1023. [CrossRef]
195. Bolognino, A.D.; Celiberto, F.G.; Ivanov, D.Y.; Papa, A. ρ-meson leptoproduction as testfield for the unintegrated gluon distribution in the proton. *Frascati Phys. Ser.* **2018**, *67*, 76–82.
196. Bolognino, A.D.; Celiberto, F.G.; Ivanov, D.Y.; Papa, A. Leptoproduction of ρ-mesons as discriminator for the unintegrated gluon distribution in the proton. *Acta Phys. Polon. Suppl.* **2019**, *12*, 891. [CrossRef]
197. Bolognino, A.D.; Szczurek, A.; Schaefer, W. Exclusive production of ϕ meson in the $\gamma^* p \to \phi p$ reaction at large photon virtualities within k_T-factorization approach. *Phys. Rev. D* **2020**, *101*, 054041. [CrossRef]
198. Celiberto, F.G. Unraveling the Unintegrated Gluon Distribution in the Proton via ρ-Meson Leptoproduction. *Nuovo Cim. C* **2019**, *42*, 220. [CrossRef]
199. Bolognino, A.D.; Celiberto, F.G.; Ivanov, D.Y.; Papa, A.; Schäfer, W.; Szczurek, A. Exclusive production of ρ-mesons in high-energy factorization at HERA and EIC. *Eur. Phys. J. C* **2021**, *81*, 846. [CrossRef]
200. Bolognino, A.D.; Celiberto, F.G.; Ivanov, D.Y.; Papa, A. Exclusive emissions of rho-mesons and the unintegrated gluon distribution. *SciPost Phys. Proc.* **2022**, *8*, 089. [CrossRef]
201. Bolognino, A.D.; Celiberto, F.G.; Fucilla, M.; Ivanov, D.Y.; Papa, A.; Schäfer, W.; Szczurek, A. Hadron structure at small-x via unintegrated gluon densities. *Rev. Mex. Fis. Suppl.* **2022**, *3*, 0308109. [CrossRef]
202. Celiberto, F.G. Phenomenology of the hadronic structure at small-x. *arXiv* **2022**, arXiv:2202.04207.

203. Bolognino, A.D.; Celiberto, F.G.; Ivanov, D.Y.; Papa, A.; Schäfer, W.; Szczurek, A. Exclusive emissions of polarized ρ mesons at the EIC and the proton content at low x. In Proceedings of the 29th International Workshop on Deep-Inelastic Scattering and Related Subjects, Santiago de Compostela, Spain, 2–6 May 2022. *arXiv* **2022**, arXiv:2207.05726. [CrossRef]
204. Bautista, I.; Tellez, A.F.; Hentschinski, M. BFKL evolution and the growth with energy of exclusive J/ψ and Y photoproduction cross sections. *Phys. Rev. D* **2016**, *94*, 054002. [CrossRef]
205. Garcia, A.A.; Hentschinski, M.; Kutak, K. QCD evolution based evidence for the onset of gluon saturation in exclusive photoproduction of vector mesons. *Phys. Lett. B* **2019**, *795*, 569–575. [CrossRef]
206. Hentschinski, M.; Molina, E.P. Exclusive J/Ψ and $\Psi(2s)$ photo-production as a probe of QCD low x evolution equations. *Phys. Rev. D* **2021**, *103*, 074008. [CrossRef]
207. Peredo, M.A.; Hentschinski, M. Ratio of J/Ψ and $\Psi(2s)$ exclusive photoproduction cross-sections as an indicator for the presence of non-linear QCD evolution. *Phys. Rev. D* **2024**, *109*, 014032. [CrossRef]
208. Ducati, M.B.G.; Griep, M.T.; Machado, M.V.T. Exclusive photoproduction of J/psi and psi(2S) states in proton-proton collisions at the CERN LHC. *Phys. Rev. D* **2013**, *88*, 017504. [CrossRef]
209. Ducati, M.B.G.; Kopp, F.; Machado, M.V.T.; Martins, S. Photoproduction of Upsilon states in ultraperipheral collisions at the CERN Large Hadron Collider within the color dipole approach. *Phys. Rev. D* **2016**, *94*, 094023. [CrossRef]
210. Gonçalves, V.P.; Machado, M.V.T.; Moreira, B.D.; Navarra, F.S.; dos Santos, G.S. Color dipole predictions for the exclusive vector meson photoproduction in pp, pPb, and PbPb collisions at run 2 LHC energies. *Phys. Rev. D* **2017**, *96*, 094027. [CrossRef]
211. Gonçalves, V.P.; Navarra, F.S.; Spiering, D. Exclusive ρ and J/Ψ photoproduction in ultraperipheral pA collisions: Predictions of the gluon saturation models for the momentum transfer distributions. *Phys. Lett. B* **2019**, *791*, 299–304. [CrossRef]
212. Cepila, J.; Contreras, J.G.; Krelina, M. Coherent and incoherent J/ψ photonuclear production in an energy-dependent hot-spot model. *Phys. Rev. C* **2018**, *97*, 024901. [CrossRef]
213. Guzey, V.; Kryshen, E.; Strikman, M.; Zhalov, M. Nuclear suppression from coherent J/ψ photoproduction at the Large Hadron Collider. *Phys. Lett. B* **2021**, *816*, 136202. [CrossRef]
214. Jenkovszky, L.; Libov, V.; Machado, M.V.T. The reggeometric pomeron and exclusive production of J/ψ(2S) in ultraperipheral collisions at the LHC. *Phys. Lett. B* **2022**, *824*, 136836. [CrossRef]
215. Flore, C.; Lansberg, J.-P.; Shao, H.-S.; Yedelkina, Y. Large-P_T inclusive photoproduction of J/ψ in electron-proton collisions at HERA and the EIC. *Phys. Lett. B* **2020**, *811*, 135926. [CrossRef]
216. Serri, A.C.; Feng, Y.; Flore, C.; Lansberg, J.-P.; Ozcelik, M.A.; Shao, H.-S.; Yedelkina, Y. Revisiting NLO QCD corrections to total inclusive J/ψ and Y photoproduction cross sections in lepton-proton collisions. *Phys. Lett. B* **2022**, *835*, 137556. [CrossRef]
217. Brzeminski, D.; Motyka, L.; Sadzikowski, M.; Stebel, T. Twist decomposition of Drell-Yan structure functions: Phenomenological implications. *J. High Energy Phys.* **2017**, *1*, 005. [CrossRef]
218. Motyka, L.; Sadzikowski, M.; Stebel, T. Lam-Tung relation breaking in Z^0 hadroproduction as a probe of parton transverse momentum. *Phys. Rev.* **2017**, *D95*, 114025. [CrossRef]
219. Celiberto, F.G.; Gómez, D.G.; Vera, A.S. Forward Drell-Yan production at the LHC in the BFKL formalism with collinear corrections. *Phys. Lett.* **2018**, *B786*, 201–206. [CrossRef]
220. Chachamis, G.; Deak, M.; Hentschinski, M.; Rodrigo, G.; Vera, A.S. Single bottom quark production in k$_\perp$-factorisation. *J. High Energy Phys.* **2015**, *9*, 123. [CrossRef]
221. Bartels, J.; Vera, A.S.; Schwennsen, F. NLO inclusive jet production in k_T-factorization. *J. High Energy Phys.* **2006**, *11*, 051. [CrossRef]
222. Ball, R.D.; Forte, S. Summation of leading logarithms at small x. *Phys. Lett. B* **1995**, *351*, 313–324. [CrossRef]
223. Ball, R.D.; Forte, S. Asymptotically free partons at high-energy. *Phys. Lett. B* **1997**, *405*, 317–326. [CrossRef]
224. Altarelli, G.; Ball, R.D.; Forte, S. Factorization and resummation of small x scaling violations with running coupling. *Nucl. Phys. B* **2002**, *621*, 359–387. [CrossRef]
225. Altarelli, G.; Ball, R.D.; Forte, S. An Anomalous dimension for small x evolution. *Nucl. Phys. B* **2003**, *674*, 459–483. [CrossRef]
226. Altarelli, G.; Ball, R.D.; Forte, S. Perturbatively stable resummed small x evolution kernels. *Nucl. Phys. B* **2006**, *742*, 1–40. [CrossRef]
227. Altarelli, G.; Ball, R.D.; Forte, S. Small x Resummation with Quarks: Deep-Inelastic Scattering. *Nucl. Phys. B* **2008**, *799*, 199–240. [CrossRef]
228. White, C.; Thorne, R. A Global Fit to Scattering Data with NLL BFKL Resummations. *Phys. Rev. D* **2007**, *75*, 034005. [CrossRef]
229. Collins, J.C.; Ellis, R. Heavy quark production in very high-energy hadron collisions. *Nucl. Phys. B* **1991**, *360*, 3–30. [CrossRef]
230. Ball, R.D. Resummation of Hadroproduction Cross-sections at High Energy. *Nucl. Phys. B* **2008**, *796*, 137–183. [CrossRef]
231. Marzani, S.; Ball, R.D.; Duca, V.D.; Forte, S.; Vicini, A. Higgs production via gluon-gluon fusion with finite top mass beyond next-to-leading order. *Nucl. Phys. B* **2008**, *800*, 127–145. [CrossRef]
232. Caola, F.; Forte, S.; Marzani, S. Small x resummation of rapidity distributions: The Case of Higgs production. *Nucl. Phys. B* **2011**, *846*, 167–211. [CrossRef]
233. Caola, F.; Marzani, S. Finite fermion mass effects in pseudoscalar Higgs production via gluon-gluon fusion. *Phys. Lett. B* **2011**, *698*, 275–283. [CrossRef]

234. Forte, S.; Muselli, C. High energy resummation of transverse momentum distributions: Higgs in gluon fusion. *J. High Energy Phys.* **2016**, *3*, 122. [CrossRef]
235. Muselli, C.; Bonvini, M.; Forte, S.; Marzani, S.; Ridolfi, G. Top Quark Pair Production beyond NNLO. *J. High Energy Phys.* **2015**, *8*, 076. [CrossRef]
236. Silvetti, F.; Bonvini, M. Differential heavy quark pair production at small x. *Eur. Phys. J. C* **2023**, *83*, 267. [CrossRef]
237. Silvetti, F. Resummation Phenomenology and PDF Determination for Precision QCD at the LHC. Ph.D. Thesis, Rome U., Rome, Italy, 2023. *arXiv* **2024**, arXiv:2403.20315.
238. Ball, R.D.; Bertone, V.; Bonvini, M.; Marzani, S.; Rojo, J.; Rottoli, L. Parton distributions with small-x resummation: Evidence for BFKL dynamics in HERA data. *Eur. Phys. J.* **2018**, *C78*, 321. [CrossRef]
239. Abdolmaleki, H.; Bertone, V.; Britzger, D.; Camarda, S.; Cooper-Sarkar, A.; Giuli, F.; Glazov, A.; Kusina, A.; Luszczak, A.; Olness, F.; et al. Impact of low-x resummation on QCD analysis of HERA data. *Eur. Phys. J. C* **2018**, *78*, 621. [CrossRef]
240. Bonvini, M.; Giuli, F. A new simple PDF parametrization: Improved description of the HERA data. *Eur. Phys. J. Plus* **2019**, *134*, 531. [CrossRef]
241. Bacchetta, A.; Celiberto, F.G.; Radici, M.; Taels, P. Transverse-momentum-dependent gluon distribution functions in a spectator model. *Eur. Phys. J. C* **2020**, *80*, 733. [CrossRef]
242. Brodsky, S.J.; Fadin, V.S.; Kim, V.T.; Lipatov, L.N.; Pivovarov, G.B. High-energy QCD asymptotics of photon-photon collisions. *JETP Lett.* **2002**, *76*, 249–252. [CrossRef]
243. Chirilli, G.A.; Kovchegov, Y.V. $\gamma^*\gamma^*$ Cross Section at NLO and Properties of the BFKL Evolution at Higher Orders. *J. High Energy Phys.* **2014**, *5*, 099; Erratum in *J. High Energy Phys.* **2015**, *8*, 075. [CrossRef]
244. Ivanov, D.Y.; Murdaca, B.; Papa, A. The $\gamma^*\gamma^*$ total cross section in next-to-leading order BFKL and LEP2 data. *J. High Energy Phys.* **2014**, *10*, 058. [CrossRef]
245. Segond, M.; Szymanowski, L.; Wallon, S. Diffractive production of two rho0(L) mesons in e+e- collisions. *Eur. Phys. J. C* **2007**, *52*, 93–112. [CrossRef]
246. Ivanov, D.Y.; Papa, A. Electroproduction of two light vector mesons in the next-to-leading approximation. *Nucl. Phys. B* **2006**, *732*, 183–199. [CrossRef]
247. Ivanov, D.Y.; Papa, A. Electroproduction of two light vector mesons in next-to-leading BFKL: Study of systematic effects. *Eur. Phys. J. C* **2007**, *49*, 947–955. [CrossRef]
248. Colferai, D.; Schwennsen, F.; Szymanowski, L.; Wallon, S. Mueller Navelet jets at LHC - complete NLL BFKL calculation. *J. High Energy Phys.* **2010**, *12*, 026. [CrossRef]
249. Celiberto, F.G. Hunting BFKL in semi-hard reactions at the LHC. *Eur. Phys. J. C* **2021**, *81*, 691. [CrossRef]
250. Celiberto, F.G.; Ivanov, D.Y.; Mohammed, M.M.A.; Papa, A. High-energy resummed distributions for the inclusive Higgs-plus-jet production at the LHC. *Eur. Phys. J. C* **2021**, *81*, 293. [CrossRef]
251. Bolognino, A.D.; Celiberto, F.G.; Fucilla, M.; Ivanov, D.Y.; Papa, A. Inclusive production of a heavy-light dijet system in hybrid high-energy and collinear factorization. *Phys. Rev. D* **2021**, *103*, 094004. [CrossRef]
252. Celiberto, F.G. High-energy emissions of light mesons plus heavy flavor at the LHC and the Forward Physics Facility. *Phys. Rev. D* **2022**, *105*, 114008. [CrossRef]
253. Celiberto, F.G.; Fucilla, M. Diffractive semi-hard production of a J/ψ or a Y from single-parton fragmentation plus a jet in hybrid factorization. *Eur. Phys. J. C* **2022**, *82*, 929. [CrossRef]
254. Celiberto, F.G. Vector quarkonia at the LHC with JETHAD: A high-energy viewpoint. *Universe* **2023**, *9*, 324. [CrossRef]
255. Deak, M.; Hautmann, F.; Jung, H.; Kutak, K. Forward Jet Production at the Large Hadron Collider. *J. High Energy Phys.* **2009**, *9*, 121. [CrossRef]
256. van Hameren, A.; Kotko, P.; Kutak, K. Resummation effects in the forward production of Z_0+jet at the LHC. *Phys. Rev. D* **2015**, *92*, 054007. [CrossRef]
257. Deak, M.; van Hameren, A.; Jung, H.; Kusina, A.; Kutak, K.; Serino, M. Calculation of the Z+jet cross section including transverse momenta of initial partons. *Phys. Rev. D* **2019**, *99*, 094011. [CrossRef]
258. Van Haevermaet, H.; Van Hameren, A.; Kotko, P.; Kutak, K.; Van Mechelen, P. Trijets in k_{T}-factorisation: Matrix elements vs parton shower. *Eur. Phys. J. C* **2020**, *80*, 610. [CrossRef]
259. van Hameren, A.; Motyka, L.; Ziarko, G. Hybrid k_T-factorization and impact factors at NLO. *J. High Energy Phys.* **2022**, *11*, 103. [CrossRef]
260. Giachino, A.; van Hameren, A.; Ziarko, G. A new subtraction scheme at NLO exploiting the privilege of kT-factorization. *arXiv* **2023**, arXiv:2312.02808.
261. Guiot, B.; van Hameren, A. Examination of k_t-factorization in a Yukawa theory. *J. High Energy Phys.* **2024**, *4*, 085. [CrossRef]
262. Mueller, A.H.; Navelet, H. An Inclusive Minijet Cross-Section and the Bare Pomeron in QCD. *Nucl. Phys. B* **1987**, *282*, 727–744. [CrossRef]
263. Marquet, C.; Royon, C. Azimuthal decorrelation of Mueller-Navelet jets at the Tevatron and the LHC. *Phys. Rev. D* **2009**, *79*, 034028. [CrossRef]
264. Ducloué, B.; Szymanowski, L.; Wallon, S. Confronting Mueller-Navelet jets in NLL BFKL with LHC experiments at 7 TeV. *J. High Energy Phys.* **2013**, *5*, 096. [CrossRef]

265. Ducloué, B.; Szymanowski, L.; Wallon, S. Evidence for high-energy resummation effects in Mueller-Navelet jets at the LHC. *Phys. Rev. Lett.* **2014**, *112*, 082003. [CrossRef]
266. Caporale, F.; Murdaca, B.; Vera, A.S.; Salas, C. Scale choice and collinear contributions to Mueller-Navelet jets at LHC energies. *Nucl. Phys. B* **2013**, *875*, 134–151. [CrossRef]
267. Caporale, F.; Ivanov, D.Y.; Murdaca, B.; Papa, A. Mueller–Navelet jets in next-to-leading order BFKL: Theory versus experiment. *Eur. Phys. J. C* **2014**, *74*, 3084; Erratum in *Eur. Phys. J. C* **2015**, *75*, 535. [CrossRef]
268. Ducloué, B.; Szymanowski, L.; Wallon, S. Evaluating the double parton scattering contribution to Mueller-Navelet jets production at the LHC. *Phys. Rev. D* **2015**, *92*, 076002. [CrossRef]
269. Celiberto, F.G.; Ivanov, D.Y.; Murdaca, B.; Papa, A. Mueller–Navelet Jets at LHC: BFKL Versus High-Energy DGLAP. *Eur. Phys. J. C* **2015**, *75*, 292. [CrossRef]
270. Celiberto, F.G.; Ivanov, D.Y.; Murdaca, B.; Papa, A. Mueller–Navelet Jets at the LHC: Discriminating BFKL from DGLAP by Asymmetric Cuts. *Acta Phys. Polon. Suppl.* **2015**, *8*, 935. [CrossRef]
271. Caporale, F.; Ivanov, D.Y.; Murdaca, B.; Papa, A. Brodsky-Lepage-Mackenzie optimal renormalization scale setting for semihard processes. *Phys. Rev. D* **2015**, *91*, 114009. [CrossRef]
272. Celiberto, F.G.; Ivanov, D.Y.; Murdaca, B.; Papa, A. Mueller–Navelet jets at 13 TeV LHC: Dependence on dynamic constraints in the central rapidity region. *Eur. Phys. J. C* **2016**, *76*, 224. [CrossRef]
273. Celiberto, F.G.; Ivanov, D.Y.; Murdaca, B.; Papa, A. BFKL effects and central rapidity dependence in Mueller-Navelet jet production at 13 TeV LHC. *PoS DIS2016* **2016**, *256*, 176. [CrossRef]
274. Caporale, F.; Celiberto, F.G.; Chachamis, G.; Gómez, D.G.; Sabio Vera, A. Inclusive dijet hadroproduction with a rapidity veto constraint. *Nucl. Phys. B* **2018**, *935*, 412–434. [CrossRef]
275. de León, N.B.; Chachamis, G.; Sabio Vera, A. Average minijet rapidity ratios in Mueller–Navelet jets. *Eur. Phys. J. C* **2021**, *81*, 1019. [CrossRef]
276. Celiberto, F.G.; Papa, A. Mueller-Navelet jets at the LHC: Hunting data with azimuthal distributions. *Phys. Rev. D* **2022**, *106*, 114004. [CrossRef]
277. Egorov, A.I.; Kim, V.T. Next-to-leading BFKL evolution for dijets with large rapidity separation at different LHC energies. *Phys. Rev. D* **2023**, *108*, 014010. [CrossRef]
278. Khachatryan, V.; Sirunyan, A.M.; Tumasyan, A.; Adam, W.; Asilar, E.; Bergauer, T.; Brandstetter, J.; Brondolin, E.; Dragicevic, M.; Erö, J.; et al. Azimuthal decorrelation of jets widely separated in rapidity in pp collisions at $\sqrt{s} = 7$ TeV. *J. High Energy Phys.* **2016**, *8*, 139. [CrossRef]
279. Tumasyan, A. et al. [CMS Collaboration]. Study of dijet events with large rapidity separation in proton-proton collisions at $\sqrt{s}$ = 2.76 TeV. *J. High Energy Phys.* **2022**, *3*, 189. [CrossRef]
280. Celiberto, F.G.; Ivanov, D.Y.; Murdaca, B.; Papa, A. High energy resummation in dihadron production at the LHC. *Phys. Rev. D* **2016**, *94*, 034013. [CrossRef]
281. Celiberto, F.G.; Ivanov, D.Y.; Murdaca, B.; Papa, A. Dihadron Production at LHC: BFKL Predictions for Cross Sections and Azimuthal Correlations. *AIP Conf. Proc.* **2017**, *1819*, 060005. [CrossRef]
282. Celiberto, F.G.; Ivanov, D.Y.; Murdaca, B.; Papa, A. Dihadron production at the LHC: Full next-to-leading BFKL calculation. *Eur. Phys. J.* C **2017**, *77*, 382. [CrossRef]
283. Celiberto, F.G.; Ivanov, D.Y.; Murdaca, B.; Papa, A. Inclusive charged light di-hadron production at 7 and 13 TeV LHC in the full NLA BFKL approach. *arXiv* **2017**, arXiv:1709.01128.
284. Celiberto, F.G.; Ivanov, D.Y.; Murdaca, B.; Papa, A. Inclusive dihadron production at the LHC in NLA BFKL. In Proceedings of the 17th Conference on Elastic and Diffractive Scattering, Prague, Czech Republic, 26–30 June 2017. *arXiv* **2017**, arXiv:1709.04758.
285. Bolognino, A.D.; Celiberto, F.G.; Ivanov, D.Y.; Mohammed, M.M.A.; Papa, A. Hadron-jet correlations in high-energy hadronic collisions at the LHC. *Eur. Phys. J. C* **2018**, *78*, 772. [CrossRef]
286. Bolognino, A.D.; Celiberto, F.G.; Ivanov, D.Y.; Mohammed, M.M.A.; Papa, A. High-energy effects in forward inclusive dijet and hadron-jet production. *PoS DIS2019* **2019**, *352*, 049. [CrossRef]
287. Bolognino, A.D.; Celiberto, F.G.; Ivanov, D.Y.; Mohammed, M.M.A.; Papa, A. Inclusive hadron-jet production at the LHC. *Acta Phys. Polon. SuppL.* **2019**, *12*, 773. [CrossRef]
288. Celiberto, F.G.; Ivanov, D.Y.; Papa, A. Diffractive production of Λ hyperons in the high-energy limit of strong interactions. *Phys. Rev. D* **2020**, *102*, 094019. [CrossRef]
289. Celiberto, F.G. Emergence of high-energy dynamics from cascade-baryon detections at the LHC. *Eur. Phys. J. C* **2023**, *83*, 332. [CrossRef]
290. Caporale, F.; Chachamis, G.; Murdaca, B.; Sabio Vera, A. Balitsky-Fadin-Kuraev-Lipatov Predictions for Inclusive Three Jet Production at the LHC. *Phys. Rev. Lett.* **2016**, *116*, 012001. [CrossRef]
291. Caporale, F.; Celiberto, F.G.; Chachamis, G.; Sabio Vera, A. Multi-Regge kinematics and azimuthal angle observables for inclusive four-jet production. *Eur. Phys. J. C* **2016**, *76*, 165. [CrossRef]
292. Caporale, F.; Celiberto, F.G.; Chachamis, G.; Gómez, D.G.; Sabio Vera, A. BFKL azimuthal imprints in inclusive three-jet production at 7 and 13 TeV. *Nucl. Phys. B* **2016**, *910*, 374–386. [CrossRef]

293. Caporale, F.; Celiberto, F.G.; Chachamis, G.; Sabio Vera, A. Inclusive four-jet production: A study of Multi-Regge kinematics and BFKL observables. *PoS DIS2016* **2016**, *265*, 177. [CrossRef]
294. Caporale, F.; Celiberto, F.G.; Chachamis, G.; Gómez, D.G.; Sabio Vera, A. Inclusive Four-jet Production at 7 and 13 TeV: Azimuthal Profile in Multi-Regge Kinematics. *Eur. Phys. J. C* **2017**, *77*, 5. [CrossRef]
295. Celiberto, F.G. BFKL phenomenology: Resummation of high-energy logs in semi-hard processes at LHC. *Frascati Phys. Ser.* **2016**, *63*, 43–48.
296. Caporale, F.; Celiberto, F.G.; Chachamis, G.; Gómez, D.G.; Sabio Vera, A. Inclusive three- and four-jet production in multi-Regge kinematics at the LHC. *AIP Conf. Proc.* **2017**, *1819*, 060009. [CrossRef]
297. Caporale, F.; Celiberto, F.G.; Chachamis, G.; Gordo Gomez, D.; Murdaca, B.; Sabio Vera, A. High energy effects in multi-jet production at LHC. *arXiv* **2016**, arXiv:1610.04765.
298. Chachamis, G.; Caporale, F.; Celiberto, F.; Gomez Gordo, D.; Sabio Vera, A. Inclusive three jet production at the LHC for 7 and 13 TeV collision energies. *PoS DIS2016* **2016**, *265*, 178. [CrossRef]
299. Caporale, F.; Celiberto, F.G.; Chachamis, G.; Gordo Gómez, D.; Sabio Vera, A. Probing the BFKL dynamics in inclusive three jet production at the LHC. *EPJ Web Conf.* **2017**, *164*, 07027. [CrossRef]
300. Caporale, F.; Celiberto, F.G.; Chachamis, G.; Gordo Gómez, D.; Sabio Vera, A. Stability of Azimuthal-angle Observables under Higher Order Corrections in Inclusive Three-jet Production. *Phys. Rev. D* **2017**, *95*, 074007. [CrossRef]
301. Caporale, F.; Celiberto, F.G.; Gordo Gomez, D.; Sabio Vera, A.; Chachamis, G. Multi-jet production in the high energy limit at LHC. *arXiv* **2017**, arXiv:1801.00014.
302. Chachamis, G.; Caporale, F.; Celiberto, F.G.; Gordo Gomez, D.; Sabio Vera, A. Azimuthal-angle Observables in Inclusive Three-jet Production. *PoS DIS2017* **2018**, *297*, 067. [CrossRef]
303. Golec-Biernat, K.; Motyka, L.; Stebel, T. Forward Drell-Yan and backward jet production as a probe of the BFKL dynamics. *J. High Energy Phys.* **2018**, *12*, 091. [CrossRef]
304. Celiberto, F.G.; Ivanov, D.Y.; Mohammed, M.M.A.; Papa, A. High-energy resummation in inclusive hadroproduction of Higgs plus jet. *SciPost Phys. Proc.* **2022**, *8*, 039. [CrossRef]
305. Celiberto, F.G.; Fucilla, M.; Papa, A.; Ivanov, D.Y.; Mohammed, M.M.A. Higgs-plus-jet inclusive production as stabilizer of the high-energy resummation. *PoS EPS-HEP2021* **2022**, *398*, 589. [CrossRef]
306. Celiberto, F.G.; Fucilla, M.; Ivanov, D.Y.; Mohammed, M.M.A.; Papa, A. Higgs boson production in the high-energy limit of pQCD. *PoS PANIC2021* **2022**, *380*, 352. [CrossRef]
307. Celiberto, F.G.; Fucilla, M.; Ivanov, D.Y.; Mohammed, M.M.A.; Papa, A. BFKL phenomenology: Resummation of high-energy logs in inclusive processes. *SciPost Phys. Proc.* **2022**, *10*, 002. [CrossRef]
308. Bolognino, A.D.; Celiberto, F.G.; Fucilla, M.; Ivanov, D.Y.; Papa, A. Hybrid high-energy/collinear factorization in a heavy-light dijets system reaction. *SciPost Phys. Proc.* **2022**, *8*, 068. [CrossRef]
309. Celiberto, F.G.; Fucilla, M.; Ivanov, D.Y.; Papa, A. High-energy resummation in Λ_c baryon production. *Eur. Phys. J. C* **2021**, *81*, 780. [CrossRef]
310. Celiberto, F.G.; Fucilla, M.; Ivanov, D.Y.; Mohammed, M.M.A.; Papa, A. Bottom-flavored inclusive emissions in the variable-flavor number scheme: A high-energy analysis. *Phys. Rev. D* **2021**, *104*, 114007. [CrossRef]
311. Bolognino, A.D.; Celiberto, F.G.; Fucilla, M.; Ivanov, D.Y.; Papa, A. Heavy flavored emissions in hybrid collinear/high energy factorization. *PoS EPS-HEP2021* **2022**, *398*, 389. *arXiv* **2022**, arXiv:2110.12772. [CrossRef]
312. Celiberto, F.G. Stabilizing BFKL via Heavy-flavor and NRQCD Fragmentation. *Acta Phys. Polon. Suppl.* **2023**, *16*, 41. [CrossRef]
313. Bolognino, A.D.; Celiberto, F.G.; Fucilla, M.; Ivanov, D.Y.; Mohammed, M.M.A.; Papa, A. High-energy Signals from Heavy-flavor Physics. *Acta Phys. Polon. Suppl.* **2023**, *16*, 17. [CrossRef]
314. Celiberto, F.G. The high-energy spectrum of QCD from inclusive emissions of charmed B-mesons. *Phys. Lett. B* **2022**, *835*, 137554. [CrossRef]
315. Celiberto, F.G.; Fucilla, M.; Mohammed, M.M.A.; Papa, A. Ultraforward production of a charmed hadron plus a Higgs boson in unpolarized proton collisions. *Phys. Rev. D* **2022**, *105*, 114056. [CrossRef]
316. Celiberto, F.G.; Fucilla, M. Inclusive J/ψ and Y emissions from single-parton fragmentation in hybrid high-energy and collinear factorization. In Proceedings of the 29th International Workshop on Deep-Inelastic Scattering and Related Subjects, Santiago de Compostela, Spain, 2–6 May 2022. *arXiv* **2022**, arXiv:2208.07206. [CrossRef]
317. Celiberto, F.G. High-energy QCD dynamics from bottom flavor fragmentation at the Hi-Lumi LHC. *Eur. Phys. J. C* **2024**, *84*, 384. [CrossRef]
318. Celiberto, F.G.; Papa, A. A high-energy QCD portal to exotic matter: Heavy-light tetraquarks at the HL-LHC. *Phys. Lett. B* **2024**, *848*, 138406. [CrossRef]
319. Celiberto, F.G. Exotic tetraquarks at the HL-LHC with JETHAD: A high-energy viewpoint. *Symmetry* **2024**, *16*, 550. [CrossRef]
320. Celiberto, F.G.; Gatto, G.; Papa, A. Fully charmed tetraquarks from LHC to FCC: Natural stability from fragmentation. *arXiv* **2024**, arXiv:2405.14773.
321. Brodsky, S.J.; Hautmann, F.; Soper, D.E. Probing the QCD pomeron in e+ e- collisions. *Phys. Rev. Lett.* **1997**, *78*, 803–806; Erratum in *Phys. Rev. Lett.* **1997**, *79*, 3544. [CrossRef]

322. Brodsky, S.J.; Hautmann, F.; Soper, D.E. Virtual photon scattering at high-energies as a probe of the short distance pomeron. *Phys. Rev. D* **1997**, *56*, 6957–6979. [CrossRef]
323. Brodsky, S.J.; Fadin, V.S.; Kim, V.T.; Lipatov, L.N.; Pivovarov, G.B. The QCD pomeron with optimal renormalization. JETP Lett. **1999**, *70*, 155–160. [CrossRef]
324. Celiberto, F.G.; Papa, A. The high-energy QCD dynamics from Higgs-plus-jet correlations at the FCC. *arXiv* **2023**, arXiv:2305.00962.
325. Celiberto, F.G.; Delle Rose, L.; Fucilla, M.; Gatto, G.; Papa, A. High-energy resummed Higgs-plus-jet distributions at NLL/NLO* with POWHEG+JETHAD. In Proceedings of the 57th Rencontres de Moriond on QCD and High Energy Interactions, La Thuile, Italy, 25 March–1 April 2023. *arXiv* **2023**, arXiv:2305.05052.
326. Celiberto, F.G.; Delle Rose, L.; Fucilla, M.; Gatto, G.; Papa, A. NLL/NLO$^-$ studies on Higgs-plus-jet production with POWHEG+JETHAD. *PoS RADCOR2023* **2024**, *432*, 389. [CrossRef]
327. Celiberto, F.G.; Delle Rose, L.; Fucilla, M.; Gatto, G.; Papa, A. Towards high-energy Higgs+jet distributions at NLL matched to NLO. *PoS EPS-HEP2023* **2024**, *449*, 390. [CrossRef]
328. Celiberto, F.G.; Fucilla, M.; Ivanov, D.Y.; Mohammed, M.M.A.; Papa, A. Higgs boson production at next-to-leading logarithmic accuracy. In Proceedings of the 57th Rencontres de Moriond on QCD and High Energy Interactions, La Thuile, Italy, 25 March–1 April 2023. *arXiv* **2023**, arXiv:2305.11760.
329. Celiberto, F.G.; Fucilla, M.; Mohammed, M.M.A.; Ivanov, D.Y.; Papa, A. High-energy resummation in Higgs production at the next-to-leading order. *PoS RADCOR2023* **2024**, *432*, 389. [CrossRef]
330. Celiberto, F.G.; Fucilla, M.; Papa, A. The high-energy limit of perturbative QCD: Theory and phenomenology. *EPJ Web Conf.* **2022**, *270*, 00001. [CrossRef]
331. Mele, B.; Nason, P. The Fragmentation function for heavy quarks in QCD. *Nucl. Phys. B* **1991**, *361*, 626–644; Erratum in *Nucl. Phys. B* **2017**, *921*, 841–842. [CrossRef]
332. Cacciari, M.; Greco, M. Large p_T hadroproduction of heavy quarks. *Nucl. Phys. B* **1994**, *421*, 530–544. [CrossRef]
333. Buza, M.; Matiounine, Y.; Smith, J.; van Neerven, W.L. Charm electroproduction viewed in the variable flavor number scheme versus fixed order perturbation theory. *Eur. Phys. J. C* **1998**, *1*, 301–320. [CrossRef]
334. Celiberto, F.G. Towards Quarkonium Fragmentation from NRQCD in a Variable-Flavor Number Scheme. In Proceedings of the 58th Rencontres de Moriond on QCD and High Energy Interactions, La Thuile, Italy, 31 March–7 April 2024. *arXiv* **2024**, arXiv:2405.08221.
335. Celiberto, F.G. Quarkonium fragmentation in a variable-flavor number scheme: Towards NRFF1.0. *arXiv* **2024**, arXiv:2406.10779.
336. Chiappetta, P.; Fergani, R.; Guillet, J.P. Production of two large p(T) hadrons from hadronic collisions. *Z. Phys. C* **1996**, *69*, 443–457. [CrossRef]
337. Owens, J.F. A Next-to-leading order study of dihadron production. *Phys. Rev. D* **2002**, *65*, 034011. [CrossRef]
338. Binoth, T.; Guillet, J.P.; Pilon, E.; Werlen, M. A next-to-leading order study of pion pair production and comparison with E706 data. *Eur. Phys. J. C* **2002**, *24*, 245–260. [CrossRef]
339. Binoth, T.; Guillet, J.P.; Pilon, E.; Werlen, M. A Next-to-leading order study of photon pion and pion pair hadro production in the light of the Higgs boson search at the LHC. *Eur. Phys. J. Direct* **2002**, *4*, 7. [CrossRef]
340. Almeida, L.G.; Sterman, G.F.; Vogelsang, W. Threshold Resummation for Di-hadron Production in Hadronic Collisions. *Phys. Rev. D* **2009**, *80*, 074016. [CrossRef]
341. Hinderer, P.; Ringer, F.; Sterman, G.F.; Vogelsang, W. Toward NNLL Threshold Resummation for Hadron Pair Production in Hadronic Collisions. *Phys. Rev. D* **2015**, *91*, 014016. [CrossRef]
342. Arakawa, J.; Feng, J.L.; Ismail, A.; Kling, F.; Waterbury, M. Neutrino detection without neutrino detectors: Discovering collider neutrinos at FASER with electronic signals only. *Phys. Rev. D* **2022**, *106*, 052011. [CrossRef]
343. Maciula, R.; Szczurek, A. Far-forward production of charm mesons and neutrinos at forward physics facilities at the LHC and the intrinsic charm in the proton. *Phys. Rev. D* **2023**, *107*, 034002. [CrossRef]
344. Bhattacharya, A.; Kling, F.; Sarcevic, I.; Stasto, A.M. Forward neutrinos from charm at the Large Hadron Collider. *Phys. Rev. D* **2024**, *109*, 014040. [CrossRef]
345. Fieg, M.; Kling, F.; Schulz, H.; Sjöstrand, T. Tuning pythia for forward physics experiments. *Phys. Rev. D* **2024**, *109*, 016010. [CrossRef]
346. Cruz-Martinez, J.M.; Fieg, M.; Giani, T.; Krack, P.; Mäkelä, T.; Rabemananjara, T.R.; Rojo, J. The LHC as a Neutrino-Ion Collider. *Eur. Phys. J. C* **2024**, *84*, 369. [CrossRef]
347. Buonocore, L.; Kling, F.; Rottoli, L.; Sominka, J. Predictions for Neutrinos and New Physics from Forward Heavy Hadron Production at the LHC. *Eur. Phys. J. C* **2024**, *84*, 363. [CrossRef]
348. Wilkinson, C.; Soto, A.G. Low-ν method with LHC neutrinos. *Phys. Rev. D* **2024**, *109*, 033010. [CrossRef]
349. Feng, J.L.; Hewitt, A.; Kling, F.; La Rocco, D. Simulating Heavy Neutral Leptons with General Couplings at Collider and Fixed Target Experiments. *arXiv* **2024**, arXiv:2405.07330.
350. Bardeen, W.A.; Buras, A.J.; Duke, D.W.; Muta, T. Deep-inelastic scattering beyond the leading order in asymptotically free gauge theories. *Phys. Rev. D* **1978**, *18*, 3998–4017. [CrossRef]

351. Kotikov, A.V.; Lipatov, L.N. NLO corrections to the BFKL equation in QCD and in supersymmetric gauge theories. *Nucl. Phys. B* **2000**, *582*, 19–43. [CrossRef]
352. Kotikov, A.V.; Lipatov, L.N. DGLAP and BFKL equations in the $N = 4$ supersymmetric gauge theory. *Nucl. Phys. B* **2003**, *661*, 19–61; Erratum in *Nucl. Phys. B* **2004**, *685*, 405–407. [CrossRef]
353. Webber, B.R. QCD power corrections from a simple model for the running coupling. *J. High Energy Phys.* **1998**, *10*, 012. [CrossRef]
354. Bartels, J.; Lotter, H. A Note on the BFKL pomeron and the 'hot spot' cross-section. *Phys. Lett. B* **1993**, *309*, 400–408. [CrossRef]
355. Caporale, F.; Chachamis, G.; Madrigal, J.D.; Murdaca, B.; Sabio Vera, A. A study of the diffusion pattern in N = 4 SYM at high energies. *Phys. Lett. B* **2013**, *724*, 127–132. [CrossRef]
356. Ross, D.A.; Sabio Vera, A. The Effect of the Infrared Phase of the Discrete BFKL Pomeron on Transverse Momentum Diffusion. *J. High Energy Phys.* **2016**, *8*, 071. [CrossRef]
357. Ball, R.D. et al. [NNPDF Collaboration]. An open-source machine learning framework for global analyses of parton distributions. *Eur. Phys. J. C* **2021**, *81*, 958.
358. Ball, R.D. et al. [NNPDF Collaboration]. The path to proton structure at 1% accuracy. *Eur. Phys. J. C* **2022**, *82*, 428. [CrossRef]
359. Bertone, V.; Carrazza, S.; Hartland, N.P.; Nocera, E.R.; Rojo, J. A determination of the fragmentation functions of pions, kaons, and protons with faithful uncertainties. *Eur. Phys. J. C* **2017**, *77*, 516. [CrossRef]
360. Bertone, V.; Hartland, N.P.; Nocera, E.R.; Rojo, J.; Rottoli, L. Charged hadron fragmentation functions from collider data. *Eur. Phys. J. C* **2018**, *78*, 651. [CrossRef] [PubMed]
361. de Florian, D.; Sassot, R.; Epele, M.; Hernández-Pinto, R.J.; Stratmann, M. Parton-to-Pion Fragmentation Reloaded. *Phys. Rev. D* **2015**, *91*, 014035. [CrossRef]
362. Moffat, E.; Melnitchouk, W.; Rogers, T.C.; Sato, N. Simultaneous Monte Carlo analysis of parton densities and fragmentation functions. *Phys. Rev. D* **2021**, *104*, 016015. [CrossRef]
363. Khalek, R.A.; Bertone, V.; Nocera, E.R. Determination of unpolarized pion fragmentation functions using semi-inclusive deep-inelastic-scattering data. *Phys. Rev. D* **2021**, *104*, 034007. [CrossRef]
364. Abdul Khalek, R.; Bertone, V.; Khoudli, A.; Nocera, E.R. Pion and kaon fragmentation functions at next-to-next-to-leading order. *Phys. Lett. B* **2022**, *834*, 137456. [CrossRef]
365. Soleymaninia, M.; Hashamipour, H.; Khanpour, H.; Spiesberger, H. Fragmentation Functions for $\Xi^-/\bar{\Xi}^+$ Using Neural Networks. *Nucl. Phys. A* **2022**, *2023*, 01. [CrossRef]
366. Soleymaninia, M.; Hashamipour, H.; Khanpour, H. Neural network QCD analysis of charged hadron fragmentation functions in the presence of SIDIS data. *Phys. Rev. D* **2022**, *105*, 114018. [CrossRef]
367. Kniehl, B.A.; Kramer, G.; Schienbein, I.; Spiesberger, H. Inclusive D*+- production in p anti-p collisions with massive charm quarks. *Phys. Rev. D* **2005**, *71*, 014018. [CrossRef]
368. Kniehl, B.A.; Kramer, G. D0, D+, D+(s), and Lambda+(c) fragmentation functions from CERN LEP1. *Phys. Rev. D* **2005**, *71*, 094013. [CrossRef]
369. Kniehl, B.A.; Kramer, G. Charmed-hadron fragmentation functions from CERN LEP1 revisited. *Phys. Rev. D* **2006**, *74*, 037502. [CrossRef]
370. Kneesch, T.; Kniehl, B.A.; Kramer, G.; Schienbein, I. Charmed-meson fragmentation functions with finite-mass corrections. *Nucl. Phys. B* **2008**, *799*, 34–59. [CrossRef]
371. Bowler, M.G. e+ e- Production of Heavy Quarks in the String Model. *Z. Phys. C* **1981**, *11*, 169. [CrossRef]
372. Kniehl, B.A.; Kramer, G.; Schienbein, I.; Spiesberger, H. Finite-mass effects on inclusive *B* meson hadroproduction. *Phys. Rev. D* **2008**, *77*, 014011. [CrossRef]
373. Kartvelishvili, V.G.; Likhoded, A.K. Structure Functions and Leptonic Widths of Heavy Mesons. *Yad. Fiz.* **1985**, *42*, 1306–1308.
374. Corcella, G.; Ferrera, G. Charm-quark fragmentation with an effective coupling constant. *J. High Energy Phys.* **2007**, *12*, 029. [CrossRef]
375. Anderle, D.P.; Kaufmann, T.; Stratmann, M.; Ringer, F.; Vitev, I. Using hadron-in-jet data in a global analysis of D^* fragmentation functions. *Phys. Rev. D* **2017**, *96*, 034028. [CrossRef]
376. Salajegheh, M.; Moosavi Nejad, S.M.; Soleymaninia, M.; Khanpour, H.; Atashbar Tehrani, S. NNLO charmed-meson fragmentation functions and their uncertainties in the presence of meson mass corrections. *Eur. Phys. J. C* **2019**, *79*, 999. [CrossRef]
377. Salajegheh, M.; Moosavi Nejad, S.M.; Delpasand, M. Determination of D_s^+ meson fragmentation functions through two different approaches. *Phys. Rev. D* **2019**, *100*, 114031. [CrossRef]
378. Soleymaninia, M.; Khanpour, H.; Moosavi Nejad, S.M. First determination of D^{*+}-meson fragmentation functions and their uncertainties at next-to-next-to-leading order. *Phys. Rev. D* **2018**, *97*, 074014. [CrossRef]
379. Binnewies, J.; Kniehl, B.A.; Kramer, G. Inclusive *B* meson production in e^+e^- and $p\bar{p}$ collisions. *Phys. Rev. D* **1998**, *58*, 034016. [CrossRef]
380. Kniehl, B.A.; Kramer, G.; Schienbein, I.; Spiesberger, H. Inclusive B-Meson Production at the LHC in the GM-VFN Scheme. *Phys. Rev. D* **2011**, *84*, 094026. [CrossRef]
381. Kniehl, B.A.; Kramer, G.; Moosavi Nejad, S.M. Bottom-Flavored Hadrons from Top-Quark Decay at Next-to-Leading order in the General-Mass Variable-Flavor-Number Scheme. *Nucl. Phys. B* **2012**, *862*, 720–736. [CrossRef]

382. Kramer, G.; Spiesberger, H. *b*-hadron production in the general-mass variable-flavour-number scheme and LHC data. *Phys. Rev. D* **2018**, *98*, 114010. [CrossRef]
383. Kramer, G.; Spiesberger, H. Λ_b^0-baryon production in pp collisions in the general-mass variable-flavour-number scheme and comparison with CMS and LHCb data, Chin. Phys. C **2018**, *42*, 083102. [CrossRef]
384. Salajegheh, M.; Moosavi Nejad, S.M.; Khanpour, H.; Kniehl, B.A.; Soleymaninia, M. *B*-hadron fragmentation functions at next-to-next-to-leading order from a global analysis of e^+e^- annihilation data. *Phys. Rev. D* **2019**, *99*, 114001. [CrossRef]
385. Kniehl, B.A.; Moosavi Nejad, S.M. Angular analysis of bottom-flavored hadron production in semileptonic decays of polarized top quarks. *Phys. Rev. D* **2021**, *103*, 034015. [CrossRef]
386. Kniehl, B.A.; Kramer, G.; Schienbein, I.; Spiesberger, H. $\Lambda_c^\pm$ production in pp collisions with a new fragmentation function. *Phys. Rev. D* **2020**, *101*, 114021. [CrossRef]
387. Delpasand, M.; Moosavi Nejad, S.M.; Soleymaninia, M. Λ_c^+ fragmentation functions from pQCD approach and the Suzuki model. *Phys. Rev. D* **2020**, *101*, 114022. [CrossRef]
388. Salam, G.P. A Resummation of large subleading corrections at small x. JHEP **1998**, *7*, 019. [CrossRef]
389. Ciafaloni, M.; Colferai, D.; Salam, G.P.; Stasto, A.M. Renormalization group improved small x Green's function. *Phys. Rev. D* **2003**, *68*, 114003. [CrossRef]
390. Ciafaloni, M.; Colferai, D.; Colferai, D.; Salam, G.P.; Stasto, A.M. Extending QCD perturbation theory to higher energies. *Phys. Lett. B* **2003**, *576*, 143–151. [CrossRef]
391. Ciafaloni, M.; Colferai, D.; Salam, G.P. On factorization at small x. *J. High Energy Phys.* **2000**, *7*, 054. [CrossRef]
392. Ciafaloni, M.; Colferai, D.; Salam, G.P. Renormalization group improved small x equation. *Phys. Rev. D* **1999**, *60*, 114036. [CrossRef]
393. Ciafaloni, M.; Colferai, D. The BFKL equation at next-to-leading level and beyond. *Phys. Lett. B* **1999**, *452*, 372–378. [CrossRef]
394. Vera, A.S. An 'All-poles' approximation to collinear resummations in the Regge limit of perturbative QCD. *Nucl. Phys. B* **2005**, *722*, 65–80. [CrossRef]
395. Barbieri, R.; d'Emilio, E.; Curci, G.; Remiddi, E. Strong Radiative Corrections to Annihilations of Quarkonia in QCD. *Nucl. Phys. B* **1979**, *154*, 535–546. [CrossRef]
396. Celmaster, W.; Gonsalves, R.J. Quantum-chromodynamics perturbation expansions in a coupling constant renormalized by momentum-space subtraction. *Phys. Rev. Lett.* **1979**, *42*, 1435–1438. [CrossRef]
397. Chatrchyan, S. et al. [CMS Collaboration]. Measurement of the Λ_b cross section and the $\bar{\Lambda}_b$ to Λ_b ratio with $J/\Psi\Lambda$ decays in pp collisions at $\sqrt{s} = 7$ TeV. *Phys. Lett. B* **2012**, *714*, 136–157. [CrossRef]
398. Andersen, J.R.; Duca, V.D.; Frixione, S.; Schmidt, C.R.; Stirling, W.J. Mueller-Navelet jets at hadron colliders. *J. High Energy Phys.* **2001**, *2*, 007. [CrossRef]
399. Fontannaz, M.; Guillet, J.P.; Heinrich, G. Is a large intrinsic k(T) needed to describe photon + jet photoproduction at HERA? *Eur. Phys. J. C* **2001**, *22*, 303–315. [CrossRef]
400. Ducloué, B.; Szymanowski, L.; Wallon, S. Violation of energy–momentum conservation in Mueller–Navelet jets production. *Phys. Lett. B* **2014**, *738*, 311–316. [CrossRef]
401. Liu, H.-Y.; Kang, Z.-B.; Liu, X. Threshold resummation for hadron production in the small-x region. *Phys. Rev. D* **2020**, *102*, 051502. [CrossRef]
402. Stasto, A.M.; Xiao, B.-W.; Zaslavsky, D. Towards the Test of Saturation Physics Beyond Leading Logarithm. *Phys. Rev. Lett.* **2014**, *112*, 012302. [CrossRef]
403. Cerci, S.; d'Enterria, D. Low-x QCD studies with forward jets in proton-proton collisions at s**(1/2) = 14-TeV. *AIP Conf. Proc.* **2009**, *1105*, 28–32. [CrossRef]
404. Vera, A.S. The Effect of NLO conformal spins in azimuthal angle decorrelation of jet pairs. *Nucl. Phys. B* **2006**, *746*, 1–14. [CrossRef]
405. Sabio Vera, A.; Schwennsen, F. The Azimuthal decorrelation of jets widely separated in rapidity as a test of the BFKL kernel. *Nucl. Phys. B* **2007**, *776*, 170–186. [CrossRef]
406. Sirunyan, A.M. et al. [CMS Collaboration]. Observation of Correlated Azimuthal Anisotropy Fourier Harmonics in pp and $p+Pb$ Collisions at the LHC. *Phys. Rev. Lett.* **2018**, *120*, 092301. [CrossRef] [PubMed]
407. Mace, M.; Skokov, V.V.; Tribedy, P.; Venugopalan, R. Initial state description of azimuthally collimated long range correlations in ultrarelativistic light-heavy ion collisions. *arXiv* **2019**, arXiv:1901.10506.
408. Sirunyan, A.M. et al. [CMS Collaboration]. Correlations of azimuthal anisotropy Fourier harmonics with subevent cumulants in pPb collisions at $\sqrt{s_{NN}} = 8.16$ TeV. *Phys. Rev. C* **2021**, *103*, 014902. [CrossRef]
409. Arslandok, M.; Bass, S.A.; Baty, A.A.; Bautista, I.; Beattie, C.; Becattini, F.; Bellwied, R.; Berdnikov, Y.; Berdnikov, A.; Bielcik, J.; et al. Hot QCD White Paper. *arXiv* **2023**, arXiv:2303.17254.
410. Ollitrault, J.Y. Measures of azimuthal anisotropy in high-energy collisions. *Eur. Phys. J. A* **2023**, *59*, 236. [CrossRef]
411. Acharya, S. et al. [ALICE Collaboration]. Measurements of long-range two-particle correlation over a wide pseudorapidity range in p−Pb collisions at $\sqrt{s_{\rm NN}} = 5.0$ TeV. *J. High Energy Phys.* **2024**, *1*, 199. [CrossRef]
412. Tumasyan, A. et al. [CMS Collaboration]. Study of azimuthal anisotropy of $\Upsilon(1S)$ mesons in pPb collisions at $\sqrt{s_{\rm NN}}$ = 8.16 TeV. *Phys. Lett. B* **2024**, *850*, 138518. [CrossRef]

413. Hayrapetyan, A. [CMS Collaboration]. Overview of high-density QCD studies with the CMS experiment at the LHC. *arXiv* **2024**, arXiv:2405.10785.
414. Cacciari, M.; Greco, M.; Nason, P. The p_T spectrum in heavy-flavour hadroproduction. *J. High Energy Phys.* **1998**, *5*, 007. [CrossRef]
415. Cacciari, M.; Frixione, S.; Houdeau, N.; Mangano, M.L.; Nason, P.; Ridolfi, G. Theoretical predictions for charm and bottom production at the LHC. *J. High Energy Phys.* **2012**, *10*, 137. [CrossRef]
416. Cacciari, M.; Frixione, S.; Nason, P. The p(T) spectrum in heavy flavor photoproduction. *J. High Energy Phys.* **2001**, *3*, 006. [CrossRef]
417. Cacciari, M.; Mangano, M.L.; Nason, P. Gluon PDF constraints from the ratio of forward heavy-quark production at the LHC at $\sqrt{S} = 7$ and 13 TeV. *Eur. Phys. J. C* **2015**, *75*, 610. [CrossRef]
418. Bacchetta, A.; Celiberto, F.G.; Radici, M. T-odd gluon distribution functions in a spectator model. *Eur. Phys. J. C* **2024**, *84*, 576. [CrossRef]
419. Celiberto, F.G. 3D tomography of the nucleon: Transverse-momentum-dependent gluon distributions. *Nuovo Cim. C* **2021**, *44*, 36. [CrossRef]
420. Bacchetta, A.; Celiberto, F.G.; Radici, M.; Taels, P. A spectator-model way to transverse-momentum-dependent gluon distribution functions. *SciPost Phys. Proc.* **2022**, *8*, 040. [CrossRef]
421. Bacchetta, A.; Celiberto, F.G.; Radici, M. Toward twist-2 T-odd transverse-momentum-dependent gluon distributions: The f-type Sivers function. *PoS EPS-HEP2021* **2022**, *398*, 376. [CrossRef]
422. Bacchetta, A.; Celiberto, F.G.; Radici, M. Toward twist-2 T-odd transverse-momentum-dependent gluon distributions: The f-type linearity function. *PoS EPS-HEP2021* **2022**, *380*, 378. [CrossRef]
423. Bacchetta, A.; Celiberto, F.G.; Radici, M. Towards Leading-twist T-odd TMD Gluon Distributions. *JPS Conf. Proc.* **2022**, *37*, 020124. [CrossRef]
424. Bacchetta, A.; Celiberto, F.G.; Radici, M. Unveiling the proton structure via transverse-momentum-dependent gluon distributions. *Rev. Mex. Fis. Suppl.* **2022**, *3*, 0308108. [CrossRef]
425. Bacchetta, A.; Celiberto, F.G.; Radici, M.; Signori, A. Phenomenology of gluon TMDs from $\eta_{b,c}$ production. In Proceedings of the 29th International Workshop on Deep-Inelastic Scattering and Related Subjects, Santiago de Compostela, Spain, 2–6 May 2022. *arXiv* **2022**, arXiv:2208.06252. [CrossRef]
426. Celiberto, F.G. A Journey into the Proton Structure: Progresses and Challenges. *Universe* **2022**, *8*, 661. [CrossRef]
427. Bacchetta, A.; Celiberto, F.G.; Radici, M. Spectator-model studies for spin-dependent gluon TMD PDFs at the LHC and EIC. *PoS EPS-HEP2023* **2024**, *449*, 247. [CrossRef]
428. Bacchetta, A.; Celiberto, F.G.; Radici, M. Proton 3D reconstruction with T-odd TMD gluon densities. *arXiv* **2024**, arXiv:2406.04893.
429. Hautmann, F.; Jung, H.; Lelek, A.; Radescu, V.; Zlebcik, R. Soft-gluon resolution scale in QCD evolution equations. *Phys. Lett. B* **2017**, *772*, 446–451. [CrossRef]
430. Hautmann, F.; Jung, H.; Lelek, A.; Radescu, V.; Zlebcik, R. Collinear and TMD Quark and Gluon Densities from Parton Branching Solution of QCD Evolution Equations. *J. High Energy Phys.* **2018**, *1*, 070. [CrossRef]
431. Monfared, S.T.; Hautmann, F.; Jung, H.; Schmitz, M. Extending parton branching TMDs to small x. *PoS DIS2019* **2019**, *352*, 136. [CrossRef]
432. Mukherjee, S.; Skokov, V.V.; Tarasov, A.; Tiwari, S. Unified description of DGLAP, CSS, and BFKL evolution: TMD factorization bridging large and small x. *Phys. Rev. D* **2024**, *109*, 034035. [CrossRef]
433. Boer, D.; Mulders, P.J. Time reversal odd distribution functions in leptoproduction. *Phys. Rev. D* **1998**, *57*, 5780–5786. [CrossRef]
434. Bacchetta, A.; Boer, D.; Diehl, M.; Mulders, P.J. Matches and mismatches in the descriptions of semi-inclusive processes at low and high transverse momentum. *J. High Energy Phys.* **2008**, *8*, 023. [CrossRef]
435. Barone, V.; Prokudin, A.; Ma, B.-Q. A Systematic phenomenological study of the cos 2 phi asymmetry in unpolarized semi-inclusive DIS. *Phys. Rev. D* **2008**, *78*, 045022. [CrossRef]
436. Barone, V.; Melis, S.; Prokudin, A. The Boer-Mulders effect in unpolarized SIDIS: An Analysis of the COMPASS and HERMES data on the cos 2 phi asymmetry. *Phys. Rev. D* **2010**, *81*, 114026. [CrossRef]
437. Gelis, F.; Iancu, E.; Jalilian-Marian, J.; Venugopalan, R. The Color Glass Condensate. *Ann. Rev. Nucl. Part. Sci.* **2010**, *60*, 463–489. [CrossRef]
438. Kovchegov, Y.V.; Levin, E. *Quantum Chromodynamics at High Energy*; Cambridge University Press: Cambridge, UK, 2012; Volume 33. [CrossRef]
439. Chirilli, G.A.; Xiao, B.-W.; Yuan, F. Inclusive Hadron Productions in pA Collisions. *Phys. Rev. D* **2012**, *86*, 054005. [CrossRef]
440. Boussarie, R.; Grabovsky, A.V.; Szymanowski, L.; Wallon, S. Impact factor for high-energy two and three jets diffractive production. *J. High Energy Phys.* **2014**, *9*, 026. [CrossRef]
441. Benic, S.; Fukushima, K.; Garcia-Montero, O.; Venugopalan, R. Probing gluon saturation with next-to-leading order photon production at central rapidities in proton-nucleus collisions. *J. High Energy Phys.* **2017**, *1*, 115. [CrossRef]

442. Benić, S.; Fukushima, K.; Garcia-Montero, O.; Venugopalan, R. Constraining unintegrated gluon distributions from inclusive photon production in proton–proton collisions at the LHC. *Phys. Lett. B* **2019**, *791*, 11–16. [CrossRef]
443. Roy, K.; Venugopalan, R. NLO impact factor for inclusive photon+dijet production in $e + A$ DIS at small x. *Phys. Rev. D* **2020**, *101*, 034028. [CrossRef]
444. Roy, K.; Venugopalan, R. Extracting many-body correlators of saturated gluons with precision from inclusive photon+dijet final states in deeply inelastic scattering. *Phys. Rev. D* **2020**, *101*, 071505. [CrossRef]
445. Beuf, G.; Hänninen, H.; Lappi, T.; Mäntysaari, H. Color Glass Condensate at next-to-leading order meets HERA data. *Phys. Rev. D* **2020**, *102*, 074028. [CrossRef]
446. Iancu, E.; Mueller, A.H.; Triantafyllopoulos, D.N. Probing Parton Saturation and the Gluon Dipole via Diffractive Jet Production at the Electron-Ion Collider. *Phys. Rev. Lett.* **2022**, *128*, 202001. [CrossRef]
447. Iancu, E.; Mueller, A.H.; Triantafyllopoulos, D.N.; Wei, S.Y. Probing gluon saturation via diffractive jets in ultra-peripheral nucleus-nucleus collisions. *Eur. Phys. J. C* **2023**, *83*, 1078. [CrossRef]
448. van Hameren, A.; Kakkad, H.; Kotko, P.; Kutak, K.; Sapeta, S. Searching for saturation in forward dijet production at the LHC. *Eur. Phys. J. C* **2023**, *83*, 947. [CrossRef]
449. Wallon, S. The QCD Shockwave Approach at NLO: Towards Precision Physics in Gluonic Saturation. *Acta Phys. Polon. Suppl.* **2023**, *16*, 26. [CrossRef]
450. Celiberto, F.G.; Jenkovszky, L.; Myronenko, V. Saturation effects in low-x DIS structure functions and related hadronic total cross sections. *EPJ Web Conf.* **2016**, *125*, 04012. [CrossRef]
451. Celiberto, F.G.; Fiore, R.; Jenkovszky, L. Collective Phenomena in pp and ep Scattering. *AIP Conf. Proc.* **2017**, *1819*, 030005. [CrossRef]
452. Hatta, Y.; Xiao, B.-W.; Yuan, F.; Zhou, J. Anisotropy in Dijet Production in Exclusive and Inclusive Processes. *Phys. Rev. Lett.* **2021**, *126*, 142001. [CrossRef] [PubMed]
453. Hatta, Y.; Xiao, B.-W.; Yuan, F.; Zhou, J. Azimuthal angular asymmetry of soft gluon radiation in jet production. *Phys. Rev. D* **2021**, *104*, 054037. [CrossRef]
454. Caucal, P.; Salazar, F.; Venugopalan, R. Dijet impact factor in DIS at next-to-leading order in the Color Glass Condensate. *J. High Energy Phys.* **2021**, *11*, 222. [CrossRef]
455. Caucal, P.; Salazar, F.; Schenke, B.; Venugopalan, R. Back-to-back inclusive dijets in DIS at small x: Sudakov suppression and gluon saturation at NLO. *J. High Energy Phys.* **2022**, *11*, 169. [CrossRef]
456. Taels, P.; Altinoluk, T.; Beuf, G.; Marquet, C. Dijet photoproduction at low x at next-to-leading order and its back-to-back limit. *J. High Energy Phys.* **2022**, *10*, 184. [CrossRef]
457. Fucilla, M.; Grabovsky, A.V.; Li, E.; Szymanowski, L.; Wallon, S. NLO computation of diffractive di-hadron production in a saturation framework. *J. High Energy Phys.* **2023**, *3*, 159. [CrossRef]
458. Kotko, P.; Kutak, K.; Marquet, C.; Petreska, E.; Sapeta, S.; van Hameren, A. Improved TMD factorization for forward dijet production in dilute-dense hadronic collisions. *J. High Energy Phys.* **2015**, *9*, 106. [CrossRef]
459. van Hameren, A.; Kotko, P.; Kutak, K.; Marquet, C.; Petreska, E.; Sapeta, S. Forward di-jet production in p+Pb collisions in the small-x improved TMD factorization framework. *J. High Energy Phys.* **2016**, *12*, 034; Erratum in *J. High Energy Phys.* **2019**, *2*, 158. [CrossRef]
460. Altinoluk, T.; Boussarie, R.; Marquet, C.; Taels, P. Photoproduction of three jets in the CGC: Gluon TMDs and dilute limit. *J. High Energy Phys.* **2020**, *7*, 143. [CrossRef]
461. Altinoluk, T.; Marquet, C.; Taels, P. Low-x improved TMD approach to the lepto- and hadroproduction of a heavy-quark pair. *J. High Energy Phys.* **2021**, *6*, 085. [CrossRef]
462. Boussarie, R.; Mäntysaari, H.; Salazar, F.; Schenke, B. The importance of kinematic twists and genuine saturation effects in dijet production at the Electron-Ion Collider. *J. High Energy Phys.* **2021**, *9*, 178. [CrossRef]
463. Caucal, P.; Salazar, F.; Schenke, B.; Stebel, T.; Venugopalan, R. Back-to-back inclusive dijets in DIS at small x: Gluon Weizsäcker-Williams distribution at NLO. *J. High Energy Phys.* **2023**, *8*, 062. [CrossRef]
464. Kang, Z.-B.; Ma, Y.-Q.; Venugopalan, R. Quarkonium production in high energy proton-nucleus collisions: CGC meets NRQCD. *J. High Energy Phys.* **2014**, *1*, 056. [CrossRef]
465. Ma, Y.-Q.; Venugopalan, R. Comprehensive Description of J/ψ Production in Proton-Proton Collisions at Collider Energies. *Phys. Rev. Lett.* **2014**, *113*, 192301. [CrossRef]
466. Ma, Y.-Q.; Venugopalan, R.; Zhang, H.-F. J/ψ production and suppression in high energy proton-nucleus collisions. *Phys. Rev. D* **2015**, *92*, 071901. [CrossRef]
467. Ma, Y.-Q.; Stebel, T.; Venugopalan, R. J/ψ polarization in the CGC+NRQCD approach. *J. High Energy Phys.* **2018**, *12*, 057. [CrossRef]
468. Stebel, T.; Watanabe, K. $J\psi$ polarization in high multiplicity pp and pA collisions: CGC + NRQCD approach. *Phys. Rev. D* **2021**, *104*, 034004. [CrossRef]
469. Mäntysaari, H.; Penttala, J. Exclusive heavy vector meson production at next-to-leading order in the dipole picture. *Phys. Lett. B* **2021**, *823*, 136723. [CrossRef]

470. Mäntysaari, H.; Penttala, J. Complete calculation of exclusive heavy vector meson production at next-to-leading order in the dipole picture. *J. High Energy Phys.* **2022**, *8*, 247. [CrossRef]
471. Binosi, D.; Collins, J.; Kaufhold, C.; Theussl, L. JaxoDraw: A Graphical user interface for drawing Feynman diagrams. Version 2.0 release notes. *Comput. Phys. Commun.* **2009**, *180*, 1709–1715. [CrossRef]

Disclaimer/Publisher's Note: The statements, opinions and data contained in all publications are solely those of the individual author(s) and contributor(s) and not of MDPI and/or the editor(s). MDPI and/or the editor(s) disclaim responsibility for any injury to people or property resulting from any ideas, methods, instructions or products referred to in the content.